

Electronic Thesis and Dissertation Repository

6-21-2018 2:30 PM

Sources of Glass Transition Temperature Variation in Poly(methyl methacrylate)/Cellulose Composites

Elena Mamycheva, *The University of Western Ontario*

Supervisor: Wood, Jeffrey T., *The University of Western Ontario*

A thesis submitted in partial fulfillment of the requirements for the Master of Engineering Science degree in Mechanical and Materials Engineering

© Elena Mamycheva 2018

Follow this and additional works at: <https://ir.lib.uwo.ca/etd>

 Part of the [Materials Science and Engineering Commons](#)

Recommended Citation

Mamycheva, Elena, "Sources of Glass Transition Temperature Variation in Poly(methyl methacrylate)/Cellulose Composites" (2018). *Electronic Thesis and Dissertation Repository*. 5418. <https://ir.lib.uwo.ca/etd/5418>

This Dissertation/Thesis is brought to you for free and open access by Scholarship@Western. It has been accepted for inclusion in Electronic Thesis and Dissertation Repository by an authorized administrator of Scholarship@Western. For more information, please contact wlsadmin@uwo.ca.

Abstract

Variation in glass transition temperature (T_g) measured by differential scanning calorimetry (DSC) is addressed, specifically for composites of poly(methyl methacrylate) (PMMA) and freeze-dried cellulose nanocrystals; mortar-and-pestle grinding use for creating solventless PMMA/cellulose nanocomposites is evaluated. Experimentally, solvent-containing and solventless PMMA and PMMA/cellulose composite samples (prepared using mortar-and-pestle grinding, melt-pressing, and acetone addition) were tested by DSC in hermetically-sealed pans using one of two maximum first heating scan temperatures; post-DSC samples were photographed. Mortar-and-pestle-ground cellulose was imaged by Field Emission Scanning Electron Microscopy (FE-SEM). Post-DSC samples had different shapes, some corresponding to greater increases in T_g from first to second heating, associated with T_g variation. A shape classification is proposed. Second heating T_g was affected by first heating peak temperature in solvent-containing samples. FE-SEM showed only low aspect ratio microscale cellulose particles. Visual analysis of samples after DSC testing is recommended; mortar-and-pestle grinding is found unsuitable for solventless PMMA/cellulose nanocomposite preparation.

Keywords

Glass transition temperature, differential scanning calorimetry, sample shape, hermetic, composite, cellulose, PMMA, acetone, polymer, mortar and pestle.

Acknowledgments

I would like to thank my supervisor, Dr. Jeff Wood; your strong leadership conducted with patience and personal example is something I aim to emulate.

I would also like to thank my supervisory committee, Dr. Klassen; thank you for your teachings, foresight, and support.

Thank yous also go to Dr. Charpentier for allowing me the use of his differential scanning calorimeter, to Chao Chen for conducting the DSC tests, to Surface Science Western for giving me access to the FE-SEM, and to Dr. Mark Biesinger and for conducting the FE-SEM tests. This work is built upon the data from these tests.

I would also like to thank Dr. Kamran Siddiqui, Claire Naudi, Joanna Blom, Chris Seres, the University of Western Ontario, and everyone else who supported me on this journey.

An overall final big thank you goes to everyone who taught me, formally and informally.

Abbreviations

PMMA = poly(methyl methacrylate)

T_g = glass transition temperature

DSC = differential scanning calorimetry

FE-SEM = field emission scanning electron microscopy

First heating peak temperature = the highest temperature during the first heating scan during a differential scanning calorimetry test

Table of Contents

Abstract	i
Acknowledgments.....	ii
Abbreviations	iii
Table of Contents	iv
List of Tables	vii
List of Figures	viii
List of Appendices	xxii
Chapter 1	1
1 Introduction	1
1.1 Purpose.....	3
1.2 Objectives	4
1.3 Hypotheses	4
Chapter 2.....	6
2 Literature Review.....	6
2.1 Introduction to Tg influences.....	6
2.1.1 Material conditions	6
2.1.2 Testing conditions	7
2.2 Review of Tg measurement, analysis, and reporting thereof for PMMA/cellulose composites and nanocomposites	8
2.2.1 Purge gas.....	9
2.2.2 Heating and cooling rates.....	9
2.2.3 Temperature and Tg determination method.....	9
2.2.4 DSC pans and samples.....	10
2.2.5 Result reporting and repeatability	10

2.2.6	Visual analysis after DSC testing	10
2.2.7	Interpretation of Tg results.....	10
2.2.8	Commentary on insufficient reporting.....	13
2.3	Recent advancements in Tg measuring and analysis techniques based on visual information	13
Chapter 3	16
3	Methodology	16
3.1	Materials and Equipment	18
3.2	Study 1	19
3.2.1	Sample preparation	19
3.2.2	Differential scanning calorimetry	23
3.3	Study 2	26
3.3.1	Sample preparation	26
3.3.2	Differential scanning calorimetry	27
3.3.3	Field emission scanning electron microscopy	28
3.4	Study 3	29
3.4.1	Sample preparation	29
3.4.2	Differential scanning calorimetry	30
3.5	Open pan heating	31
Chapter 4	32
4	Results	32
4.1	Sample appearance.....	33
4.2	Study 1	34
4.2.1	Differential scanning calorimetry	34
4.2.2	Visual analysis of samples after DSC testing	46
4.2.3	Selective Tg analysis based on visual data	63

4.3 Study 2	66
4.3.1 Differential scanning calorimetry	66
4.3.2 Visual analysis of samples after DSC testing	73
4.3.3 Field Emission Scanning Electron Microscopy	80
4.4 Study 3	84
4.4.1 Differential scanning calorimetry	84
4.4.2 Visual analysis of samples after DSC testing	93
4.4.3 Selective Tg analysis based on visual data	98
4.5 Open pan heating	99
Chapter 5	102
5 Discussion	102
5.1 Evaluation of mortar-and-pestle grinding	102
5.2 Influences on glass transition temperature.....	102
5.2.1 First heating vs. second heating	102
5.2.2 First heating peak temperature.....	103
5.2.3 Sample geometry	104
5.2.4 Composite vs. PMMA	107
5.2.5 Leakage and yellowing	108
5.3 Study limitations	109
Chapter 6.....	112
6 Conclusions	112
References.....	114
Appendices.....	124
Curriculum Vitae	173

List of Tables

Table 1. General overview of performed studies. (The open-pan heating study is omitted in this overview.)	17
Table 2. Summary of experimental conditions from Study 1 and Study 3.....	19
Table 3. Overview of DSC conditions in Study 2. Each checkmark indicates the use of both a solventless and a solvent-containing sample in that condition. Thus, two checkmarks indicates that two solventless samples and two solvent-containing samples were used. Only one of each sample were used in the 4 mg condition (because that mass was already looked at in Study 1).....	26
Table A4. Glass transition temperatures and shapes from Study 1.	124
Table A5. Glass transition temperatures and shapes from Study 2.	125
Table A6. Glass transition temperatures from Study 3. “MC Capsule” means multi-compartment capsule. “SC Capsule” means single compartment capsule.	148

List of Figures

Figure 1. Powder on aluminum foil, on a metal disc, that would later be covered with another piece of aluminum foil before being transferred to the melt press.	20
Figure 2. Melt-pressing set-up. The sample powder being pressed is located between two pieces of aluminum foil.	21
Figure 3. Example of a baking tray compartment sealed with aluminum foil and duct tape. The compartment contains a sample of PMMA or composite together with acetone. A small hole is present in the middle of this makeshift lid to allow for acetone evaporation.....	23
Figure 4. Overview of differential scanning calorimetry settings. One experimental condition (solid grey line) has a first heating peak temperature of 160 °C. The other experimental condition (dashed black line) has a first heating peak temperature of 200 °C. All heating rates are 10 °C/min, all cooling rates are -10 °C/min. The maximum temperature (160 °C or 200 °C) and minimum temperature (0 °C) are both held for 2 minutes. Glass transition temperature was measured from both first heating and second heating.....	24
Figure 5. Examples of isolated solventless samples from Study 1 (left column) and Study 3 (right column) after melt pressing. In each image, the sample on the left is PMMA and the sample on the right is the composite. On a light background (top photos), the composite looks very similar to the neat PMMA sample; the samples from Study 3 appear darker than the samples from Study 1. On the black background (bottom photos), under certain lighting, white spots can be seen on the composite samples; these spots are smaller and more uniform in the composite from Study 3. Photographs from Study 1 were taken with a different camera than those from Study 3.	33
Figure 6. Solvent-containing PMMA (left) and solvent-containing composite (right) samples from Study 3; no images from Study 1 are available but they appeared similar. The composite sample looks very similar to the PMMA sample.	34

Figure 7. Outlier in differential scanning calorimetry results. Heat flow curve for outlier is shown in red; other heat flow curves from Study 1 are shown in black. 36

Figure 8. Glass transition temperature results from first heating of Study 1, including outlier in the P160 condition, where it results in a large error bar..... 38

Figure 9. Glass transition temperature results from first heating of Study 1, excluding outlier in the P160 condition. No significant differences are seen between samples designated for the 160 °C and the 200 °C first heating peak temperature, which is expected because these results are from the first heating scan (i.e. from before that peak temperature was reached). Error bars are generally small. 38

Figure 10. Glass transition temperature results from first heating, with data from 160 °C and 200 °C conditions combined; the outlier in the P condition is included, resulting in a large error bar..... 39

Figure 11. Glass transition temperature results from first heating, with data from 160 °C and 200 °C conditions combined; the outlier in the P condition is excluded. Solvent-containing samples have a significant lower T_g than solventless samples; no significant difference is seen between equivalent composite and PMMA samples. 39

Figure 12. Glass transition temperature results from second heating of Study 1, including outlier in the P160 condition, resulting in a large error bar. 41

Figure 13. Glass transition temperature results from second heating of Study 1, excluding outlier in the P160 condition. Error bars in the solvent-containing conditions are significantly greater compared to the solventless conditions and compared to the results from first heating (Figure 9). The T_g of the P160 condition is significantly lower than that of the P200 condition; otherwise, no significant differences are seen between the 160 °C and 200 °C first heating peak temperature conditions. No significant differences are seen between composite and PMMA conditions. 41

Figure 14. Comparisons of increases in measured glass transition temperature from first heating to second heating, with outlier included, resulting in a large error bar..... 44

Figure 15. Comparisons of increases in measured glass transition temperature from first heating to second heating, with outlier excluded. Increases in T_g are significantly greater than 0 °C with the 200 °C first heating peak temperature but not with the 160 °C first heating peak temperature. The P200 condition has a significantly greater increase in T_g than the P160 condition.44

Figure 16. Comparison of increases in measured glass transition temperature from first heating to second heating between solvent-containing and solventless conditions, with outlier included, resulting in a large error bar.....45

Figure 17. Comparison of increases in measured glass transition temperature from first heating to second heating between solvent-containing and solventless conditions, with outlier excluded. Increase in T_g is significantly greater in solvent-containing samples than in solventless samples; in the latter, no significant increase in T_g is seen.46

Figure 18. Top view of opened DSC pan of the outlier sample (P160 condition; Sample ID #11 in Appendix A). The sample is convex, with minimal contact with the pan floor.48

Figure 19. Examples from the CS160 condition of the “floor-based” sample shape, with the sample touching the wall (A; Sample ID #2 in Appendix A) and centered on the pan floor (B; Sample ID #9 in Appendix A).49

Figure 20. Examples of the “coated walls” sample shape, with a clear sample from the PS200 condition (A; Sample ID #14 in Appendix A) and a yellowed sample from the CS200 condition (B; Sample ID #18 in Appendix A).49

Figure 21. “Pillar” shape of sample in DSC pan after testing, in the PS160 condition (A; Sample ID #8 in Appendix A) and in the CS160 condition (B; Sample ID #1 in Appendix A).50

Figure 22. Stacked bar chart of the total number of samples belonging to each shape category in Study 1; solventless samples are distinguished from solvent-containing samples. Both solventless and solvent-containing samples are represented in the floor-based shape category. Aside from the outlier, all solventless samples have a floor-based

shape. Only solvent-containing samples were seen to have a coated walls or pillar shape.
..... 51

Figure 23. Comparison of measured glass transition temperatures from first and second heating in solvent-containing samples with different shape classifications. Samples with pillar and coated walls shapes have a significantly greater Tg measured from second heating compared to samples with the floor-based shape, despite having had significantly lower or not significantly different Tg when measured from first heating, respectively. 52

Figure 24. Increase in glass transition temperature from first to second heating of solvent-containing samples with different shape classifications. There is a significant increase in measured Tg from first to second heating in pillar-shaped and coated walls-shaped samples but not in samples with the floor-based shape. 53

Figure 25. Photographs from the PS160 condition. Although Tg from first heating (H1 Tg) is similar for all samples, Tg from second heating (H2 Tg) is much higher in the pillar-shaped sample compared to the samples with the floor-based shape. 55

Figure 26. Photographs from the CS160 condition. The pillar-shaped sample again has a higher Tg from second heating (H2 Tg) than the samples with the floor-based shape. The floor-based shape samples have H2 Tg values very similar to each other despite having had a larger difference in their Tg from first heating (H1 Tg) and one being more yellow than the other..... 56

Figure 27. Photographs from the PS200 condition. The samples with the coated walls shape have higher Tg values than the sample with the floor-based shape. The sample with the bubbly coated walls has higher Tg values than the sample with the smooth coated walls..... 57

Figure 28. Photographs from the CS200 condition. The samples with the coated walls shape have higher Tg values than the sample with the floor-based shape. The sample with the large-bubbled, white coated walls has higher Tg values than the sample with the smaller-bubbled, yellowed coated walls. The third sample has greatly non-uniform yellowing/browning. 58

Figure 29. Photographs from the P160 condition. The two floor-based samples have similar T_g values both from first heating (H1 T_g) and from second heating (H2 T_g), despite one being in the form of two clumps instead of one. The outlier, having both T_g values greatly different from the other samples, has a clump located primarily against the pan wall, with very little contact with the pan floor, and only a very small separate clump on the pan floor. 59

Figure 30. Photographs from the C160 condition. All samples have a floor-based shape, similar T_g values from first heating (H1 T_g), and somewhat similar T_g values from second heating (H2 T_g)..... 60

Figure 31. Photographs from the P200 condition. All samples have a floor-based shape; the large-bubbled samples have larger T_g values than the small-bubbled sample. One of the samples has a small clump on the pan wall in addition to the main clump on the pan floor..... 61

Figure 32. Photographs from the C200 condition. All samples have a floor-based shape. Clear samples with large bubbles have higher T_g values than the yellowed sample with small bubbles. 62

Figure 33. Selective comparison of solvent-containing experimental conditions based on glass transition temperatures from first and second heating using only floor-based-shaped samples. The number of samples in each condition is indicated; only one sample was available in the CS200 and PS200 conditions. C160 but not P160 samples has a significantly greater second heating T_g compared to first heating. 63

Figure 34. Comparison of first heating peak temperatures based on T_g from first and second heating using only solvent-containing samples with a floor-based shape. Although there is no significant difference between the two sample groups on first heating, the T_g obtained from second heating is significantly greater when measured using a first heating peak temperature of 200 °C compared to 160 °C. 65

Figure 35. Comparison of first heating peak temperatures based on increase in T_g from first to second heating using only solvent-containing samples with a floor-based shape. Samples subjected to a first heating peak temperature of 200 °C have a significantly

greater increase in Tg from first to second heating compared to samples subjected to a first heating peak temperature of 160 °C. 66

Figure 36. Effect of grinding time on measured Tg in solventless, 10 mg samples. A general trend of increased Tg with increasing grinding time is seen; see text. 68

Figure 37. Effect of grinding time on measured Tg in solvent-containing, 10 mg samples. In contrast to the solventless samples (Figure 36), a general trend of decreasing Tg with increasing grinding time is seen; see text. The error bar in the first heating 30-minute condition is too small to be seen. 69

Figure 38. Effect of grinding time on measured glass transition temperature in 10 mg samples. Variation, as seen with error bars, is least with 60 minutes of grinding time.... 71

Figure 39. Effect of sample mass in DSC pan on measured glass transition temperature using samples subjected to 30 minutes of grinding time. The 4 mg condition has no error bars because only one solvent-containing and solventless sample was used in that condition. The other conditions had two of each kind of sample. In the 10 mg condition, one error bar is too small to be seen. Variation as shown by error bars is generally lower in the 10 mg condition than in the 15 mg condition. 72

Figure 40. Example of the “capsule” sample shape, intact (A) and after the top was pushed in to reveal the hollow center (B); shown sample is Sample ID #13B..... 74

Figure 41. Examples of the “vertical half” (A; Sample ID #7B) and “seemingly full” (B; Sample ID #25B) sample shape..... 74

Figure 42. A sample with both a capsule and vertical half shape, intact (A) and after the top was pushed in to reveal the hollow half inside (B); shown sample is Sample ID #24B. 75

Figure 43. Shape distribution in Study 2. Most solventless samples have a floor-based shape. Most solvent-containing samples have a capsule shape. 76

Figure 44. Examples of small (A; Sample ID #22B) and large (B; Sample ID #24B) leakage from DSC pans. 76

Figure 45. Photographs of the 4 mg condition, without solvent (left) and with solvent (right). The sample with the pillar shape has a much larger Tg from second heating than the sample with the floor-based shape, despite the former having had a much smaller Tg from first heating than the latter..... 77

Figure 46. Samples 13B (left of vertical line) and 14B (right of vertical line), which comprise the 15-minute ground, solvent-containing, 10 mg condition. For sample 13B, the leakage (top left), intact sample (top center), and pressed-in-roof sample (bottom left) are shown. For sample 14B, the intact sample (top right) and pressed-in-roof sample (bottom right) are shown. Despite similar Tg values from first heating, sample 13B with the leakage has higher Tg from second heating..... 78

Figure 47. Samples 21B (left) and 22B (right), which comprise the 30-minute ground, solvent-containing, 10 mg condition. Both have mild leakage, but the leakage is greater in sample 21B. Despite identical Tg values from first heating, sample 21B with the greater leakage has somewhat higher Tg after second heating..... 79

Figure 48. FE-SEM image of the 60-minute ground cellulose powder with indicated dimensions. Only microscale, low aspect ratio particles are seen. 81

Figure 49. FE-SEM image of cellulose powder after mortar-and-pestle grinding for 3 minutes (left) and 15 minutes (right). A noticeable decrease in particle size and greater particle uniformity is seen with 15 minutes of grinding compared to 3 minutes of grinding 82

Figure 50. FE-SEM image of cellulose powder after mortar-and-pestle grinding for 30 minutes (left) and 60 minutes (right). Although these greater grinding times have smaller particles and greater particle uniformity compared to the smaller grinding times (Figure 49), a plateau appears to have been reached after 30 minutes of grinding. 83

Figure 51. Comparison of experimental conditions based on Tg measured from the first heating scan. No significant difference is seen between samples designated for the different first heating peak temperatures, as expected because these results are from before the first heating peak temperature has been reached. Error bars are relatively small..... 85

Figure 52. Comparison of Study 3 experimental materials based on T_g measured from the first heating scan. Solventless samples have a significantly greater T_g than solvent-containing samples; no significant difference is seen between equivalent composite and PMMA samples. 86

Figure 53. Comparison of Study 3 experimental materials based on T_g measured from the second heating scan, after a first heating peak of either 160 °C or 200 °C. A significant difference between the 200 °C and the 160 °C condition is seen among the solvent-containing composite samples. No such difference is seen among the solvent-containing PMMA samples or among the solventless samples. 87

Figure 54. Comparison of differences between T_g measured from the second heating scan and T_g measured from the first heating scan. The increase in T_g from first to second heating is significantly greater in the 200 °C condition than in the 160 °C condition for solvent-containing composite samples but not for solvent-containing PMMA samples. See text. 88

Figure 55. Comparison of solvent-containing and solventless samples based on differences between T_g measured from first heating and from second heating. Solvent-containing samples had a significant increase in T_g whereas solventless samples had a significant decrease in T_g from first to second heating. 90

Figure 56. Comparison of PMMA-cellulose composites' glass transition temperatures from first heating relative to a fixed PMMA value. Solventless samples can be seen to be significantly closer in T_g to the fixed T_g value than the solvent-containing samples. No significant difference between the solvent-containing composite samples designated for the two different first heating peak temperatures is seen if using T_g measured from first heating. 91

Figure 57. Comparison of PMMA-cellulose composites' glass transition temperatures from second heating relative to a fixed PMMA value. Solventless samples are still significantly closer in T_g to the fixed value than the solvent-containing samples. However, the solvent-containing composite tested using a first heating peak temperature of 200 °C has a significantly closer T_g to the fixed value (by approximately 9 °C)

compared to the solvent-containing composite tested using a first heating peak temperature of 160 °C, despite them both being samples of the same material. 92

Figure 58. Examples of capsule shapes seen in Study 3: capsule with one single compartment (top left), capsule with two compartments (top right), capsule with three compartments (bottom left), and capsule with two unequally-sized compartments (bottom right). All photos were taken after the roof of the sample was removed by gentle pressing to show the inner hollowness. 95

Figure 59. Shape distribution in Study 3. All solventless samples had a floor-based shape. Most solvent-containing samples had a multi-compartment capsule shape. 96

Figure 60. Comparison of the single-compartment and multi-compartment capsule shapes based on increase in Tg measured from the first heating scan to the second heating scan and using a first heating peak temperature of either 160 °C or 200 °C. The number of samples in each category is indicated. The single-compartment capsule shape is associated with a significantly greater increase in Tg from first to second heating compared to the multi-compartment capsule shape. 96

Figure 61. Comparison of solvent-containing experimental conditions based on Tg from first and second heating and using only samples with the multi-compartment capsule shape. Number of samples in each condition is indicated. Composite samples have a significantly greater Tg than PMMA samples as measured from second heating when tested using a first heating peak temperature of 200 °C. See text. 99

Figure 62. Samples before heating. On the left is a sample of neat PMMA without solvent; on the right is a solvent-containing composite sample. 100

Figure 63. Samples at the same time partway through heating. On the left is neat PMMA without solvent; on the right is the solvent-containing composite. The latter is seen to have expanded. 100

Figure 64. Samples after heating for the same amount of time. On the left is neat PMMA without solvent; on the right is the solvent-containing composite. Both samples have a concave shape. Such a shape was not seen in the current work's DSC samples, which

were sealed hermetic lids. These samples are too concave for the floor-based shape and do not have as much wall contact as the coated walls shape. 101

Figure 65. Photograph of Sample 4B. This sample has a floor-based shape..... 126

Figure 66. Photograph of Sample 5B. This sample has a floor-based shape..... 127

Figure 67. Photograph of Sample 6B. This sample has a floor-based shape..... 128

Figure 68. Photograph of Sample 7B. This sample has a “vertical half” shape. 129

Figure 69. Photograph of Sample 8B. This sample has a “vertical half” shape. 130

Figure 70. Photograph of Sample 9B. This sample has a floor-based shape..... 131

Figure 71. Photograph of Sample 10B. This sample has a floor-based shape..... 132

Figure 72. Photograph of Sample 11B, with its roof pushed in to reveal a hollow center. This sample has a capsule shape. 133

Figure 73. Photographs of Sample 12B, showing intact structure (top) and structure after pressing in roof to reveal hollow center (bottom). This sample has a capsule shape. 134

Figure 74. Photographs of Sample 13B, showing pan leakage (top left), intact structure (top right), and structure after pressing in roof to reveal hollow center (bottom). This sample has a capsule shape. 135

Figure 75. Photographs of Sample 14B, showing intact structure (top) and structure after pressing in roof to reveal hollow center (bottom). This sample has a capsule shape. 136

Figure 76. Photograph of Sample 15B. This sample has a floor-based shape..... 137

Figure 77. Photograph of Sample 16B. This sample has a floor-based shape..... 138

Figure 78. Photographs of Sample 17B, showing intact structure (top) and structure after pressing in roof to reveal hollow center (bottom). This sample has a capsule shape. 139

Figure 79. Photographs of Sample 18B, showing intact structure (top) and structure after pressing in roof to reveal hollow center (bottom). This sample has a capsule shape. 140

Figure 80. Photograph of Sample 19B. This sample has a floor-based shape..... 141

Figure 81. Photograph of Sample 20B. This sample has a floor-based shape..... 142

Figure 82. Photographs of Sample 21B, showing pan leakage (top left), intact structure (top right), and structure after pressing in roof to reveal hollow center (bottom). This sample has a capsule shape. 143

Figure 83. Photographs of Sample 22B, showing pan leakage (top left), intact structure (top right), and structure after pressing in roof to reveal hollow center (bottom). This sample has a capsule shape. 144

Figure 84. Photograph of Sample 23B, which has a pillar shape. 145

Figure 85. Photographs of Sample 24B, showing pan leakage (top left), intact structure (top right), and structure after pressing in roof to reveal hollow center (bottom). This sample appears to have both a “capsule” and “vertical half” shape. 146

Figure 86. Photograph of Sample 25B, which has a “seemingly full” shape. 147

Figure 87. Photographs of Sample 1C, after originally being put into the DSC pan (left), after testing when the lid was removed (center), and after pressing in the roof of the structure to reveal the hollowness inside (right). This sample has a multi-compartment capsule shape. 149

Figure 88. Photographs of Sample 2C, after originally being put into the DSC pan (left), after testing when the lid was removed (center), and after pressing in the roof of the structure to reveal the hollowness inside (right). This sample has a single compartment capsule shape. 150

Figure 89. Photographs of Sample 3C, after originally being put into the DSC pan (left), after testing when the lid was removed (center), and after pressing in the roof of the

structure to reveal the hollowness inside (right). This sample has a multi-compartment capsule shape. 151

Figure 90. Photographs of Sample 4C, after originally being put into the DSC pan (left), after testing when the lid was removed (center), and after pressing in the roof of the structure to reveal the hollowness inside (right). This sample has a multi-compartment capsule shape. 152

Figure 91. Photographs of Sample 5C, after originally being put into the DSC pan (left top), after testing before the lid was removed – leakage is seen (left bottom), after the lid was removed (center), and after pressing in the roof of the structure to reveal the hollowness inside (right). This sample has a single compartment capsule shape. 153

Figure 92. Photographs of Sample 6C, after originally being put into the DSC pan (left) and after testing when the lid was removed (right). This sample has a coated walls shape. 154

Figure 93. Photographs of Sample 7C, after originally being put into the DSC pan (left) and after testing when the lid was removed (right). This sample has a floor-based shape. 155

Figure 94. Photographs of Sample 8C, after originally being put into the DSC pan (left) and after testing when the lid was removed (right). This sample has a floor-based shape. 156

Figure 95. Photographs of Sample 9C, after originally being put into the DSC pan (left) and after testing when the lid was removed (right). This sample has a floor-based shape. 157

Figure 96. Photographs of Sample 10C, after originally being put into the DSC pan (left) and after testing when the lid was removed (right). This sample has a floor-based shape. 158

Figure 97. Photographs of Sample 11C, after originally being put into the DSC pan (left) and after testing when the lid was removed (right). This sample has a floor-based shape.

..... 159

Figure 98. Photographs of Sample 12C, after originally being put into the DSC pan (left) and after testing when the lid was removed (right). This sample has a floor-based shape.

..... 160

Figure 99. Photographs of Sample 13C, after originally being put into the DSC pan (left top), after testing before the lid was removed – a dent is seen (left bottom), after the lid was removed (center), and after pressing in the roof of the structure to reveal the hollowness inside (right). This sample has a multi-compartment capsule shape. 161

Figure 100. Photographs of Sample 14C, after originally being put into the DSC pan (left), after testing when the lid was removed (center), and after pressing in the roof of the structure to reveal the hollowness inside (right). This sample exhibits yellowing and a multi-compartment capsule shape..... 162

Figure 101. Photographs of Sample 15C, after originally being put into the DSC pan (left), after testing when the lid was removed (center), and after pressing in the roof of the structure to reveal the hollowness inside (right). This sample exhibits yellowing and a multi-compartment capsule shape..... 163

Figure 102. Photographs of Sample 16C, after originally being put into the DSC pan (left), after testing when the lid was removed (center), and after pressing in the roof of the structure to reveal the hollowness inside (right). This sample has a single compartment capsule shape. 164

Figure 103. Photographs of Sample 17C, after originally being put into the DSC pan (left), after testing when the lid was removed (center), and after pressing in the roof of the structure to reveal the hollowness inside (right). This sample has a multi-compartment capsule shape. 165

Figure 104. Photographs of Sample 18C, after originally being put into the DSC pan (left), after testing when the lid was removed (center), and after pressing in the roof of

the structure to reveal the hollowness inside (right). This sample has a multi-compartment capsule shape. 166

Figure 105. Photographs of Sample 19C, after originally being put into the DSC pan (left) and after testing when the lid was removed (right). This sample exhibits slight yellowing and a floor-based shape..... 167

Figure 106. Photographs of Sample 20C, after originally being put into the DSC pan (left) and after testing when the lid was removed (right). This sample exhibits slight yellowing and a floor-based shape..... 168

Figure 107. Photographs of Sample 21C, after originally being put into the DSC pan (left) and after testing when the lid was removed (right). This sample exhibits yellowing and a floor-based shape..... 169

Figure 108. Photographs of Sample 22C, after originally being put into the DSC pan (left) and after testing when the lid was removed (right). This sample has a floor-based shape. 170

Figure 109. Photographs of Sample 23C, after originally being put into the DSC pan (left) and after testing when the lid was removed (right). This sample has a floor-based shape. 171

Figure 110. Photographs of Sample 24C, after originally being put into the DSC pan (left) and after testing when the lid was removed (right). This sample has a floor-based shape. 172

List of Appendices

Appendix A: Data from Study 1	124
Appendix B: Data from Study 2	125
Appendix C: Data from Study 3	148

Chapter 1

1 Introduction

Throughout all of history, people have been conducting research. Throughout all fields of research, people have been conducting analyses and conveying their results to other people. It can be said that this superb ability to analyze and communicate are some of the fundamental things that make us human. Researching humans often use standards such as the ASTM standards to help them be mindful of various sources of error in their testing, help them aid others in accurate reproduction of their tests, and help make their testing more amenable to comparison and analysis among other studies. It is into this noble effort of supporting researchers with such help that this current work primarily fits in.

Specifically, the current work aims to help in materials-related research, on polymers and their composites, by improving the procedure for and interpretation of a certain thermal analysis: the determination of glass transition temperature by differential scanning calorimetry.

The glass transition temperature (T_g) is a material property that represents the temperature at which the material, such as a polymer, transitions from a stiff, brittle, and glass-like state to a rubbery state [1]. This transition actually occurs over a range of temperatures, but systematic methods are in place to identify one specific temperature in the middle of this range to represent the whole transition [2]. Structurally speaking, at temperatures below T_g , atoms in polymer chains remain mostly fixed in their positions relative to other atoms, with polymer chain mobility limited to chain vibration and to side chain rotation. Above T_g , however, the polymer chain backbone can undergo rotation, allowing the chains to move [3]. As this structural transition occurs, the material exhibits changes in a wide variety of properties, including stiffness, density, electrical properties, coefficient of thermal expansion, refractive index, and heat capacity [4][5][6]. Given this importance of T_g to a variety of properties, T_g is an important determinant of a material's applications [7]. Efforts to increase various materials' T_g are underway. In one study, a T_g increase of 4 °C was described as a slight increase; in another study, an approximately

10 °C increase was described as substantial; and, in a third study, an increase of 29 °C was described as exceptional [8][9][10].

Given the effect of Tg on multiple properties, multiple properties can be monitored to help detect the Tg of a material. The most common instrument used for measuring Tg, the differential scanning calorimeter (DSC), relies on a material's change in heat capacity to detect Tg [7]. There are two main types of DSCs – the power compensation DSC and the heat flux DSC. The former heats the tested sample and a reference sample using separate heaters and measures the difference in power input required to get these two samples to the same temperatures. The latter increases the temperature of the tested sample while subjecting the reference sample to the same heater and measures the heat differential between the tested sample and the reference sample [11]. In both cases, the DSC heats the tested sample and a reference sample, and outputs the heat flow required for the tested sample to acquire these changes in temperature [12]. From the resulting chart, called a thermogram, gradual change in heat capacity can be seen as the sample transitions from its rigid to its rubbery state; in approximately the middle of that range of gradual change is the Tg value [13]. Two common approaches of finding that middle (i.e. the Tg value) are by finding the midpoint temperature and by finding the inflection temperature, as described in ASTM E1356 [13].

Currently, explanations for increases or decreases in Tg of composites relative to neat polymer tend to be combinations of only a few constantly encountered ideas; the use of the same idea in different contexts can lead to contradictions that make it difficult to evaluate composites [14][15]. In many studies, variation in Tg tends to be assumed to be solely the result of the tested materials' components and the interactions within them. Possible influences of the Tg-measuring testing procedure and changes to samples as a result of this procedure tend not to be discussed, beyond those influences that were discovered long ago, such as heating and cooling rate during testing. Furthermore, Tg values can be difficult to compare due to differences in Tg measurement [16]. The current work aims to reveal more of the factors that influence Tg variation as well as provide a method through which these factors or additional factors can be further studied.

The chosen materials upon which these sources of variation are demonstrated in the current study are poly(methyl methacrylate) (PMMA) and its composite with cellulose. PMMA is a clear, thermoplastic polymer with diverse applications, ranging from dentures to automotive tail-light covers, and has been extensively investigated in T_g-related studies; cellulose, which can be found in plant cell walls, is the most abundant biopolymer on earth and has been the focus of much composite-related research due to being biodegradable, strong, and light [7], [17]–[21].

Most PMMA/cellulose composites to date have involved the use of a solvent. However, the current work requires a comparison between a solventless and solvent-containing condition. Therefore, a solventless method of composite preparation followed by solvent addition has been used. In the literature, solventless methods of preparing such composites consist primarily of melt-mixing, which involves exposure to high temperatures for relatively long time periods and can result in discoloration [22]. Therefore, this opportunity was used to investigate a different method of creating solventless PMMA/cellulose composites, possibly nanocomposites: by grinding PMMA and cellulose powders together in a mortar and pestle and then subjecting the resulting composite powder to melt-pressing to make solventless composite samples. Addition of solvent to some of the samples later was used to make solvent-containing samples. PMMA samples without cellulose were similarly prepared for comparison.

A potential source of variation in T_g investigated in the current work is the DSC setting of maximum temperature assigned for the first heating scan (from here on referred to as the first heating peak temperature). Additionally, samples after DSC testing were photographed and visually examined to see whether additional sources of variation could be found.

1.1 Purpose

The primary purpose of the current work is to provide a method of finding potential reasons for T_g variation and extracting more informatic use from a DSC test.

The secondary purpose of the current work is to identify previously unconsidered sources of variation in T_g, measured by DSC. In addition to providing possible alternative explanations for some T_g findings, this information is meant to help with the design of studies and the reporting of experimental information that would make comparisons of T_g findings between studies easier and more valid.

The final additional purpose is to provide an evaluation on the use of a certain mixing tool – the mortar and pestle – for creating solventless PMMA/cellulose nanocomposites.

1.2 Objectives

The current work has the following objectives:

1. To determine whether analytically useful information for T_g comparison can be extracted from photographs taken of samples after DSC testing.
2. To determine whether T_g results from DSC testing are affected by the first heating peak temperature used in DSC testing.
3. To determine whether mortar-and-pestle grinding is a suitable technique for preparing solventless PMMA/cellulose nanocomposites.
4. To determine whether solventless and solvent-containing PMMA/cellulose composite and PMMA samples have different T_g tendencies in response to different first heating peak temperatures being used in DSC testing.
5. To determine whether mortar-and-pestle grinding yields solventless and solvent-containing PMMA/cellulose composites with greater T_g values compared to similarly prepared solventless and solvent-containing PMMA.
6. To determine whether the first heating scan or the second heating scan of DSC testing produces more reliable T_g results for solventless and solvent-containing PMMA/cellulose composites.
7. To determine unconsidered potential sources of variation in T_g.

1.3 Hypotheses

The following hypotheses are tested in the current work:

1. Visual data collected by photographs of samples after DSC testing contains information about a source or sources of variation in T_g.
2. DSC test samples exposed to a higher first heating peak temperature during testing ultimately have higher measured T_g values from second heating.
3. Mortar-and-pestle grinding is a suitable technique for preparing solventless PMMA/cellulose nanocomposites.
4. Solvent-containing samples are more sensitive to differences in first heating peak temperatures used in DSC testing than are solventless samples.
5. Solventless and solvent-containing PMMA/cellulose composites have greater T_g values compared to similarly prepared solventless and solvent-containing PMMA.
6. The first heating scan of DSC testing produces more reliable T_g results than the second heating scan for solvent-containing but not solventless PMMA/cellulose composites.
7. Sample shape change during DSC testing and first heating peak temperature during DSC testing are sources of variation in T_g.

Chapter 2

2 Literature Review

This review introduces the reader to some of the main known factors that affect Tg measurement; compares, contrasts, and analyzes available PMMA/cellulose studies based on their Tg measurement, analysis, and reporting thereof; and summarizes the most recent advancements related to Tg measurement techniques.

2.1 Introduction to Tg influences

Glass transition temperature may be affected by two main categories of factors: factors related to the material being tested, and factors related to the testing procedure itself.

2.1.1 Material conditions

Generally, factors that reduce the mobility of polymer chains tend to increase Tg. Some factors that have been reported as responsible for reducing mobility of polymer chains, and consequently increasing Tg, have been increased crosslinking, increased crystallinity, and increased molecular weight [23]–[26].

The addition of various particles to polymers can also modify Tg. No large increases in Tg are generally found with addition of low aspect ratio particles, such as spheres [15]. With large aspect ratios, there is potential for Tg to be increased; however, adequate dispersal of filler in the matrix is required, as well as sufficiently strong interactions between filler and matrix [27][14]. A recent study has shown that strength of interactions between filler and matrix can be affected by temperature [28].

Solvent is commonly used in polymer nanocomposite preparation and, generally, residual solvent in polymers is known to act as a plasticizer, decreasing Tg [15]. (In addition to solvent, plasticization has also been reported to arise from moisture due to humidity, gas when testing under high pressures, and the filler in composites [29]–[32].) This plasticization effect, however, can depend on the solvent-polymer pair, as the solvent *N,N*-dimethylformamide (DMF) has been found to actually increase Tg of PMMA while

other solvents such as toluene and chloroform decrease T_g of PMMA [33]. The solvent-caused increase in T_g in this study was attributed to bonding between DMF and PMMA [33]. The extent of solvent retention in a material varies depending on the material's preparation. Polymers with larger molecular weights retain more solvent and, when solution cast onto a dish, most of the residual solvent tends to be found at the interface between the dish and the bottom of the sample; more solvent is retained in thicker polymer films [34].

Also related to material preparation is thermal history, which is the locking in of a structure into the polymer chains that is reflective of the temperature at which that material was processed [35]. In addition to processing, thermal history can be affected by factors related to where the material has been stored, including sunlight [36]. The ASTM standard recommends annealing in order to erase thermal history prior to conducting the heating scan from which the T_g will be measured. The standard recommends avoiding grinding samples as friction may impart heat and differences in thermal history [37].

2.1.2 Testing conditions

Many of the known influences due to testing conditions are related to thermal lag, which refers to the delay in distribution of heat through the sample, resulting in a difference between the sample's average temperature and the sensor temperature [38]. Although T_g is a material property and should, therefore, be independent of sample size, the T_g value as measured by DSC can be affected by thermal lag, which is affected by sample size. Test sample sizes that are large tend to result in increased thermal lag, which can manifest itself as greater measured T_g values; consequently, lower sample masses are recommended for DSC testing [39]–[42]. However, measured T_g of very small specimens, such as thin films, can be different from that of the bulk sample [43]. For example, T_g of thin free-standing films decreases with film thickness; this phenomenon is due to the surface of the film being a place where movement of polymer chains is easier than on the inside. The thinner the film, the larger the portion of the polymer's chains that the surface of the film accounts for and, consequently, the greater the polymer chain mobility and the lower the T_g [15]. In supported films, a variety of findings have been observed; for PMMA, decreased thickness generally yielded higher T_g values [15].

Differences between samples due to thermal lag tend to be reduced by performing testing on samples of similar size and shape, as shape also has an effect of thermal lag; however, the shape of a sample can change when the sample is heated, so a risk of thermal lag remains [41], [44]–[46]. In addition to change in shape, a sample can also lose mass during heating, affecting heat capacity and, consequently, DSC results [42].

When measuring T_g by DSC, the heating and cooling rate settings have been shown to affect T_g [47]. Higher rates of heating and cooling yield higher measured T_g values, due to thermal lag [47]. However, higher heating rates also improve signal detectability in DSC; therefore, optimal heating and cooling rates should be chosen [13].

With regard to first heating peak temperature, the ASTM does not mention its influence on T_g. However, the ASTM does state that if the polymer undergoes degradation at the annealing temperature (i.e. the first heating peak temperature), then the annealing time can be decreased as long as it is reported [37]. In the field of food science, a study on cooked rice noodles found measured T_g to generally increase with first heating peak temperature, with some exceptions [48]. However, this case is quite different from the current study, not only because of the tested material but also because of the temperature ranges: both the T_g values and the first heating peak temperatures in that study were under 0 °C. Overall, little information is available on the influence of the first heating peak temperature on T_g.

2.2 Review of T_g measurement, analysis, and reporting thereof for PMMA/cellulose composites and nanocomposites

Measurement and analysis of T_g, and reporting thereof, in PMMA/cellulose composites and nanocomposites is compared in this section based on fourteen studies from 2010 to 2018 [8], [49]–[61]. Based on the analysis of the reported T_g measurement techniques in these studies, it can be seen that many aspects are often left unreported. The relevance of these previous studies to the current work is described.

2.2.1 Purge gas

In these studies, the purge gas was nitrogen, with reported flow rates ranging from 20 mL/min to 50 mL/min; in many studies, flow rate of nitrogen was not reported; in some cases, neither purge gas nor its flow rate was reported. In the current work, nitrogen with a flow rate of 50 mL/min is used.

2.2.2 Heating and cooling rates

Heating rates were most often 10 °C/min, although some studies had heating rates of 20 °C/min or 7 °C/min. Reported cooling rates were often -10 °C/min and sometimes -40 °C/min; in some cases, cooling rate was not reported. In the current work, the most common of these rates (10 °C/min for heating and -10 °C/min for cooling) are used.

2.2.3 Temperature and Tg determination method

Maximum and minimum DSC temperatures were always reported. Maximum temperatures ranged from 160 °C to 300 °C, and minimum temperatures ranged from -40 °C to 40 °C. However, of the fourteen studies, half reported using the second heating scan to determine Tg and the other half did not report which heating scan was used to determine Tg. Therefore, in some cases it could not be determined whether the maximum temperature used was the maximum first heating scan temperature (i.e. the maximum temperature to which the sample would be exposed before having its Tg measured in the second heating scan). It may be possible that some solvent would evaporate at these maximum temperatures and that cellulose may begin to brown or degrade [62][63]. In the current work, the effect of first heating peak temperature (maximum temperature to which the sample is exposed before second heating) on measured Tg in second heating is investigated.

Two studies indicated that the midpoint was used for Tg determination [55][49], one study indicated that the inflection point was used for Tg determination [56], and the rest of the studies did not indicate what method of Tg determination they used. In the current work, the inflection point is used for Tg determination because it is found to allow for less variation depending on chosen range of Tg onset to Tg end during analysis.

2.2.4 DSC pans and samples

None of the studies indicated whether their DSC pans had hermetic lids or regular lids. When reported, sample size ranged from 5 mg to 10 mg; sample size was most often not reported. In the current work, DSC pans with hermetic lids are used and sample size is varied between 4 mg to 15 mg.

2.2.5 Result reporting and repeatability

One study indicated that results were averaged based on three samples and provided a graph with error bars [52]; in another study, results were also averaged based on at least three samples but only average values with neither standard deviations nor error bars were given [8]. In all of the other studies, however, the number of sample repetitions was not indicated, and results did not provide any error bars or standard deviations; results were instead expressed as single values or single heat flow curves.

Therefore, I question the repeatability of these results. In the studies that provided results based on averages of three samples, composite T_g results were either lower or only slightly higher than those of PMMA, whereas a few of the other studies reported great increases in PMMA. In the current work, results are provided as averages on graphs with error bars, and possibilities of occasional high T_g measurements due to certain sample shapes in the DSC pan are investigated.

2.2.6 Visual analysis after DSC testing

None of these studies reported opening DSC pans after testing and visually analyzing them. In the current work, pans after DSC testing are opened and the samples inside are photographed and visually compared.

2.2.7 Interpretation of T_g results

Explanations for magnitude of composite T_g relative to PMMA T_g were generally one or a combination of five types. For reduction in T_g, the following explanations have been given:

1. Small amount of filler acts as a plasticizer, reducing T_g [51][52].

2. Residual solvent acts as a plasticizer, reducing Tg [58][60].
3. Filler agglomeration reduces Tg [57][52].

For increases in Tg, the following explanations have been given:

1. Interactions (generally hydrogen bonding) between filler and polymer led to restricted mobility of polymer chains, increasing Tg [8], [50], [55]–[61], [64].
2. Molecular weight of polymer chains was increased by in situ polymerization, increasing Tg [61][50][49].

These explanations will be discussed below. In all cases, Tg appears to have been assumed to be the result solely of the components of the material and the interactions between them; sample shape during testing has not been considered. Contributions to Tg findings from DSC settings were not commented on. In the current work, the contribution to Tg of DSC settings and sample shape are investigated, potentially providing additional explanations for Tg-related findings.

2.2.7.1 Reduction in Tg

The explanation that low filler amounts reduce Tg by acting as plasticizers comes from studies where the lowest filler concentrations were 0.3 wt% and 0.5 wt% [51][52]. This explanation is inconsistent with another study, where a slight increase in Tg was found in composites relative to PMMA despite low filler concentrations of 0.25 wt% and 0.5 wt% [8].

An alternative explanation for one of the studies [51], in which an in situ polymerized composite sample was compared with an in situ polymerized PMMA sample, may be that the two instances of in situ polymerization produced different molecular weights. Perhaps this difference may have been due to viscosity differences from nanoparticle addition, as time required for the reacting medium to reach a critical viscosity corresponding to prepolymerization has been found to be affected by nanoparticle amount in a study on in situ polymerized PMMA/calcium carbonate nanocomposites [65]. In the PMMA/cellulose study mentioning low filler content acting as a plasticizer, no mixing time adjustments to compensate for such possible effects were mentioned; the PMMA

samples were indicated to be “prepared by the same suspension polymerization technique” [51]. Another source of variation may be the high DSC temperature (250 °C) used in the study [51]; some material degradation may have begun during testing and the extent of this degradation may have differed due to the different material composition. However, it should be noted that the obtained T_g values were still relatively high, both for PMMA and the composite sample (123 °C and 115 °C, respectively), suggesting that extreme degradation was unlikely.

In the other study mentioning low filler content acting as a plasticizer [52], not only composites with low filler content but all composites were found to have lower T_g than PMMA. It was reported that “addition of [cellulose] lowered the glass transition temperature of PMMA at all compositions”. I question the accuracy of this statement because the composites were prepared using a solvent in addition to the cellulose and the study does not indicate whether the T_g of composites is compared against the T_g of similarly solvent-containing PMMA samples or against solventless PMMA. It may have been that the addition of solvent, rather than cellulose, lowered the T_g of PMMA; residual solvent in PMMA has been shown to act as a plasticizer, reducing its T_g [15]. Regarding variation in T_g among the composites, the study provides an explanation based on network formation between the cellulose particles that requires an optimum amount of cellulose [52]. However, a cellulose network would be expected to raise T_g to a value greater than that of PMMA by trapping PMMA chains in place and, if no clearly equivalent solvent-containing PMMA condition is provided for comparison, this explanation of a cellulose network is difficult to judge.

2.2.7.2 Increases in T_g

Generally, whenever an increase in T_g has been seen in PMMA/cellulose composites compared to PMMA, this increase has been attributed to favourable interactions between the cellulose filler and the PMMA matrix. In studies involving situ polymerization, contributions of higher molecular weights due to the polymerization procedure were also acknowledged. No sources of T_g variation unrelated to the contents of the tested material have been considered in these studies. As mentioned previously, I question the repeatability of some of these obtained T_g values because, most often, no standard

deviations were reported, and no reporting was made of the number of samples used. It may be possible that some high T_g values were obtained not due to drastically improved interactions between PMMA and cellulose but simply due to the shape of the sample in the DSC pan, as is investigated in the current work.

Of note, a different PMMA/cellulose study [66], that did not do any T_g-related testing but found great increases in mechanical and chemical properties in composites with high transparency compared to PMMA did not attribute these great increases to interactions between PMMA and cellulose. They found hydrogen bonding to be solely among cellulose chains. They instead attributed their findings to good dispersion of cellulose.

2.2.8 Commentary on insufficient reporting

The above review has mentioned many times that one or another quantity or factor was not reported in a study or studies. Incomplete reporting can lead to difficulty in reproducing experimental materials [67]. Proper reporting of findings has been stated as particularly important for advancing emerging research areas; in the review paper in which this statement was found, some literature was deemed to be unusable due to factors such as insufficient details about studied particles and methodology, suggesting that these problems are widespread [68]. Reporting of variance is also important for meta-analyses, so that variance-based weighting does not come at a cost of losing much data, as has been the case in a recent meta-analysis [69]. A recent review of nanofilled/nanohybrid composite performance in the clinical setting indicated an “unclear or high” risk of bias of reviewed studies and encouraged the reader to use caution when interpreting the review’s findings, which is unfortunate given that research progress relies on building on each other’s findings [70]. I therefore urge researchers to be more open and thorough in their explanations of research procedures and findings.

2.3 Recent advancements in T_g measuring and analysis techniques based on visual information

Primary recent advancements in improving the measurement and analysis of T_g have come in the form of deviation from DSC testing; related recent advancements have been in predicting T_g based on polymer structure [71]. Because many aspects of a material can

change after it passes through its T_g range, such as Young's modulus, thermal expansion coefficient, as well as some visual data as discussed here, there are many ways to detect this transition [72][73][7].

One recently proposed technique has involved using the change in a polymer's refractive index to detect T_g [6]. In this technique, a microsphere of a polymer is immersed into a liquid medium with a known refractive index and set on a temperature-controlled surface under a microscope; light is shone down on the microsphere, resulting in a circular band to be seen; from the dimensions of this circular band, the refractive index of the microsphere relative to the liquid medium can be calculated and its variation with temperature detected. Claimed advantages of this method are reduced error due to thermal lag because of the microscopic sample size, reduced variation due to cooling and heating rate, and increased sensitivity relative to conventional T_g-measuring techniques; limitations of this technique are limited allowable temperature range (which is based on the liquid medium) and required microsphere preparation [6].

Another new T_g measurement technique, also visual in nature, has involved the addition of fluorescent probes based on aggregation induced emission (AIE) luminogens [74][75]. These probes strongly emit light when they are in an aggregated state and light emission is reduced when they are farther apart from each other. Consequently, as the temperature of a material is increased, and intramolecular motion is less restricted while free volume is increased, the light emission of the probes is seen to decrease. These AIE probes can be added to polymers by solution blending followed by solution casting [74][75]. However, I question the applicability of this technique for T_g measurement because processing methods required to add the AIE probes may affect the material's T_g; for example, residual solvent from solution blending for AIE probe addition may act as a plasticizer, reducing measured T_g [15].

Yet another visual-based T_g measurement technique has been introduced for conjugated polymers, which have shifts in their light wavelength absorbance patterns depending on temperature [76]. An advantage of this technique is that it can be performed on very thin films and requires relatively widely available equipment: a hot plate, spin coater,

glovebox, and UV–vis spectrometer. A disadvantage of this technique is that it is limited in the materials for which it can be applied [76].

Like these recent advancements, the current work aims to improve Tg measurement and analysis through visual information; one main difference of the current work, however, is that it aims to add to the existing DSC technique rather than replace it. The current DSC technique for measuring Tg has not changed much recently, as evidenced by the ASTM standards related to measurement and analysis of Tg by DSC testing having remained the same in the past few years. The ASTM standard “Standard Test Method for Assignment of the Glass Transition Temperatures by Differential Scanning Calorimetry” (E1365) has not recently undergone any changes; the current version is simply the 2008 version that was reapproved in 2014 [13]. The ASTM standard “Standard Test Method for Transition Temperatures and Enthalpies of Fusion and Crystallization of Polymers by Differential Scanning Calorimetry” (D3418) was changed from its 2012 version in 2015 to include a table showing the effect of heating rate on measured transition temperatures, including glass transition temperature [37]. If the current work provides sufficient evidence that photographic data after DSC testing can prove useful to Tg-related analyses, then this addition will likely become a feature of a future standard on using DSC for Tg measurement.

Chapter 3

3 Methodology

The current study was composed of three stages, which will be referred to as Study 1, Study 2, and Study 3. These studies are summarized below and in Table 1.

Study 1 was the initial experiment, consisting of glass transition temperature (T_g) measurements of a neat and composite material using different differential scanning calorimetry (DSC) temperature settings, followed by visual analysis of these samples after opening their DSC pans post-testing.

In efforts to reduce variation in measured T_g values, Study 2 was performed, which involved manipulating an aspect of the material manufacturing method (grinding time) as well as sample mass put into DSC pans for testing.

Based on results from Study 2, Study 3 was performed; Study 3 was essentially a repeat of Study 1 except with modifications based on Study 2 results.

Finally, to uncover a limitation of the present work, an additional, smaller-scale study was performed, which involved visually examining a sample as it was heated on a hot plate in a DSC pan without a lid.

Table 1. General overview of performed studies. (The open-pan heating study is omitted in this overview.)

	Study 1	Study 2		Study 3
Brief description	Original study	Investigation of ways to improve repeatability of measured Tg		Modified Study 1 based on results of Study 2
Characterization method	DSC	DSC	FE-SEM	DSC
Materials	PMMA vs. composite	PMMA	Cellulose	PMMA vs. composite
Independent variables	<ul style="list-style-type: none"> - PMMA vs. composite - Solvent vs. no solvent - Peak temperature of first heating in DSC (160 °C vs. 200 °C) 	<ul style="list-style-type: none"> - Grinding time - Solvent vs. no solvent - Mass in DSC pan 	<ul style="list-style-type: none"> - Grinding time 	<ul style="list-style-type: none"> - PMMA vs. composite - Solvent vs. no solvent - Peak temperature of first heating in DSC (160 °C vs. 200 °C)
Dependent variables	<ul style="list-style-type: none"> - Measured Tg from 1st and 2nd heating - Appearance of sample after DSC testing - Tg repeatability 	<ul style="list-style-type: none"> - Measured Tg from 1st and 2nd heating - Appearance of sample after DSC testing - Tg repeatability 	<ul style="list-style-type: none"> - Particle size, aspect ratio, and uniformity 	<ul style="list-style-type: none"> - Measured Tg from 1st and 2nd heating - Appearance of sample after DSC testing - Tg repeatability

3.1 Materials and Equipment

Poly(methyl methacrylate) powder (PMMA) was purchased from Sigma-Aldrich; the average molecular weight by GPC of the PMMA powder was reported as ~15,000; the glass transition temperature by DSC of the PMMA powder was reported to be 105 °C.

Freeze-dried cellulose nanocrystals (in dry form), which were purchased from Cellulose Lab (Fredericton, New Brunswick, Canada). These freeze-dried cellulose nanocrystals, which will be referred to simply as cellulose from here on, were indicated to contain between 0 to 2 percent sulfur by weight.

Acetone was used as solvent.

PMMA and cellulose powders were ground using mortars and pestles (United Scientific Supplies, model JMD400). A non-commercial melt press at the University of Western Ontario was used to create experimental samples from the PMMA and cellulose powders. The melt press' temperature was controlled with a digital controller; pressure was controlled with a manual hydraulic pump and a pressure gauge. Addition of solvent to melt-pressed samples was performed in a non-stick mini muffin baking tray, with compartments covered using aluminum foil and duct tape.

Glass transition temperatures were obtained from analyses using TA Universal Analysis Software based on measurements obtained using a differential scanning calorimeter (TA Instruments, Q200) at the University of Western Ontario. Samples were contained in aluminum Tzero hermetic lid and pan sets during DSC testing; the lids were crimped using a Tzero Sample Press Kit. Open pan sample heating was performed using those same pans but without the hermetic lid. Samples after DSC testing were photographed using a digital camera; specifically, in Study 1, a Canon PowerShot SD400 Digital ELPH camera was used; in Studies 2 and 3, a Canon PowerShot ELPH 180 camera was used.

Imaging of cellulose powder particles was performed using a field emission scanning electron microscope (FE-SEM) at Surface Science Western (London, Ontario, Canada).

3.2 Study 1

In this initial study, measured glass transition temperatures of prepared solventless and solvent-containing neat PMMA and PMMA/cellulose composite samples were compared. Measurement of glass transition temperature was performed using different DSC settings (specifically, using different peak temperatures on first heating, to see whether glass transition temperature measured from the second heating scan was affected). After DSC testing, DSC pans were opened and the samples therein were photographed and analyzed. A summary of the experimental conditions is available in the table below.

Table 2. Summary of experimental conditions from Study 1 and Study 3.

Condition label	PMMA or composite	Solvent or no solvent	DSC first peak temperature
P160	PMMA	No solvent	160 °C
PS160	PMMA	Solvent	160 °C
C160	Composite	No solvent	160 °C
CS160	Composite	Solvent	160 °C
P200	PMMA	No solvent	200 °C
PS200	PMMA	Solvent	200 °C
C200	Composite	No solvent	200 °C
CS200	Composite	Solvent	200 °C

3.2.1 Sample preparation

Four different types of samples were prepared: neat PMMA without solvent, neat PMMA with solvent, PMMA/cellulose composite without solvent, and PMMA/cellulose composite with solvent. Briefly, PMMA was ground using a mortar and pestle with or without cellulose; then, the resulting powders were melt-pressed. To create solvent-containing samples, some of the resulting melt-pressed samples were left to soak in acetone until the acetone mostly evaporated and the samples appeared dry but some acetone remained.

3.2.1.1 Grinding

A mortar and pestle were used to grind the following materials, by hand, for 5 minutes. For pure PMMA specimens, ~2.4 g of PMMA was ground. For composite specimens, a separate mortar and pestle was used and ~2.28 g of PMMA was ground together with ~0.12 g of cellulose, resulting in a powder that was ~5% cellulose by weight.

3.2.1.2 Melt pressing

Melt pressing was performed separately for the PMMA sample and the composite sample in the following manner. The powder obtained by mortar and pestle grinding was poured onto an aluminum foil sheet, which lay on a large, flat metal disc, as shown in the figure below. The disc was used to minimize movement of the aluminum foil during transportation to the melt press.



Figure 1. Powder on aluminum foil, on a metal disc, that would later be covered with another piece of aluminum foil before being transferred to the melt press.

The powder was then covered by another sheet of aluminum foil. Thus, the ground powder was sandwiched between aluminum foil sheets that lay upon a large, flat metal disc. This arrangement was then transferred to a preheated melt-press; the melt-pressing set-up is shown in the figure below. The melt press was then manually controlled by a hydraulic pump and a pressure gauge to provide a displayed pressure of 100 kg/cm^2 for 3 minutes. Because much of the sample was found to remain in powdered form after these 3 minutes, the samples were then subjected to a pressure of 120 kg/cm^2 for an additional 3 minutes. During the first pressure period, the temperature display of the melt press indicated that the temperature was constantly varying, reaching a minimum of $100 \text{ }^\circ\text{C}$ and a maximum of $109 \text{ }^\circ\text{C}$. During the second pressure period, the variation in temperature reached a minimum of $106 \text{ }^\circ\text{C}$ and a maximum of $114 \text{ }^\circ\text{C}$.



Figure 2. Melt-pressing set-up. The sample powder being pressed is located between two pieces of aluminum foil.

After melt-pressing, the arrangement of the metal disc, aluminum foil, and sandwiched powder was placed on a table at room temperature. The top sheet of aluminum foil was removed; underneath, the sample was in the form of a transparent, flat piece of plastic that had an irregular border of brittle whiteness that was further surrounded by powder (suggesting that these areas at the edges were not fully melt-pressed, possibly due to the differences in the powder hill's height in the center compared to its edges). The sample was broken by hand to isolate only fully melt-pressed, flat, transparent sample pieces; the rest was discarded. Some of the isolated sample was put into a resealable plastic bag to be used as samples without solvent. Another part of the isolated sample (~0.2 g) was further used to make solvent-containing samples.

3.2.1.3 Solvent addition

The neat PMMA and composite isolated melt-pressed samples that were designated for solvent addition were put into separate compartments of a non-stick mini muffin baking tray. Thus, two compartments of the tray were used: one for neat PMMA and one for the composite. Approximately 10 mL of acetone was poured on top of the samples in the compartments. The compartments were then promptly covered and sealed with aluminum foil and duct tape as shown in Figure 3. A pinhole was punctured in the center of this makeshift lid, with the intent that evaporated solvent escape through it.



Figure 3. Example of a baking tray compartment sealed with aluminum foil and duct tape. The compartment contains a sample of PMMA or composite together with acetone. A small hole is present in the middle of this makeshift lid to allow for acetone evaporation.

Thus covered, the compartments were left for several days, after which they were put into resealable plastic bags. Thus, by this time, there were four types of samples: PMMA without solvent (P), neat PMMA with solvent (PS), composite without solvent (C), and composite with solvent (CS).

3.2.2 Differential scanning calorimetry

Prepared test samples were put into pans, sealed with a hermetic lid, and subjected to DSC testing involving one of two heating procedures, differing in their first heating peak temperatures and illustrated in Figure 4. Glass transition temperatures (T_g) were obtained from the first and second heating scans, to see whether measured T_g from second heating

would be affected by differences in the first heating peak temperature that samples were exposed to earlier. Samples after testing were also examined visually.

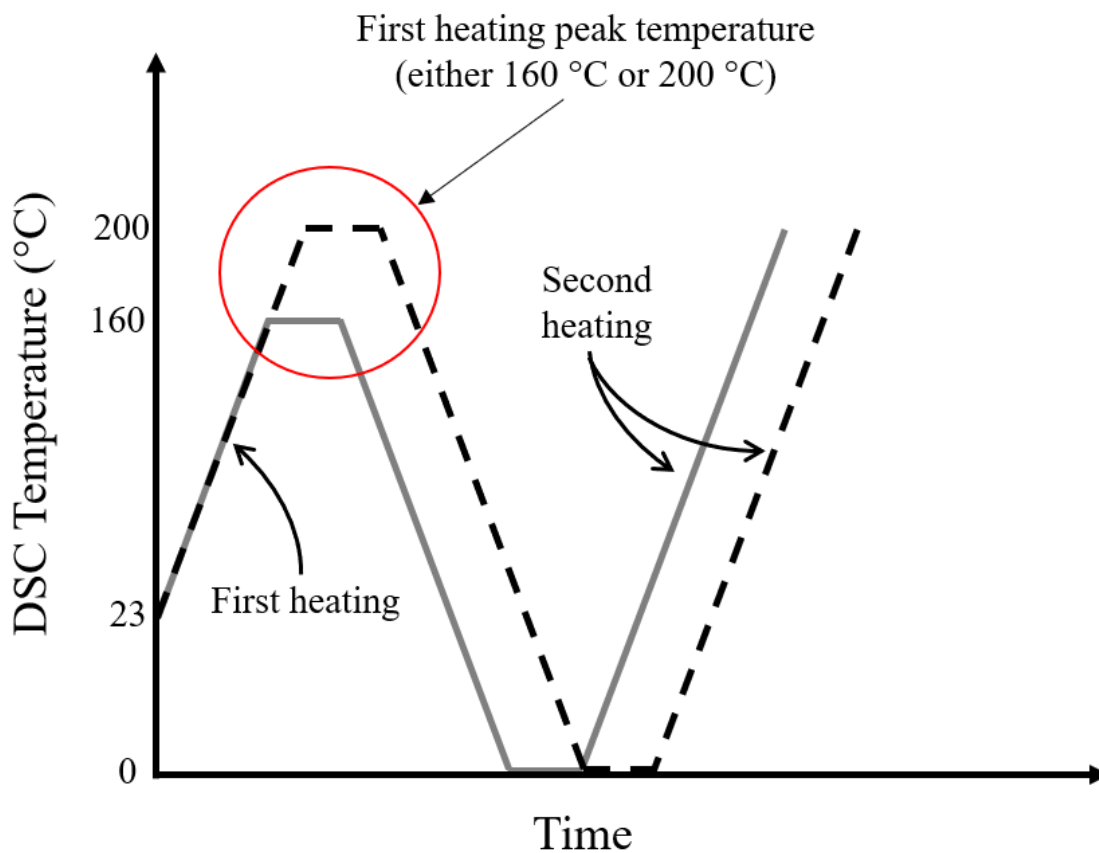


Figure 4. Overview of differential scanning calorimetry settings. One experimental condition (solid grey line) has a first heating peak temperature of 160 °C. The other experimental condition (dashed black line) has a first heating peak temperature of 200 °C. All heating rates are 10 °C/min, all cooling rates are -10 °C/min. The maximum temperature (160 °C or 200 °C) and minimum temperature (0 °C) are both held for 2 minutes. Glass transition temperature was measured from both first heating and second heating.

3.2.2.1 DSC pan preparation

Samples within plastic bags were broken by hand into small fragments, which were put in DSC pans. Specifically, approximately 4 mg of each sample type was put into separate pans, covered with hermetic lids, and crimped. Six such DSC pans were prepared for

each sample type, of which half were designated for a first heating peak temperature of 160 °C and the other half were designated for a first heating peak temperature of 200 °C.

3.2.2.2 DSC testing

The DSC pans were loaded into the differential scanning calorimeter, which had an autosampler. A nitrogen flow rate of 50 mL/min was used. An empty DCS pan was used as a reference. The following heat treatment program (illustrated in Figure 4) was used:

1. Samples were first heated from room temperature to a designated first heating peak temperature (either 160 °C or 200 °C, depending on sample designation) at a rate of 10 °C/min.
2. Samples were then held isothermally at that peak temperature for 2 minutes.
3. Samples were then cooled down to 0 °C at a rate of -10 °C/min.
4. At 0 °C, the samples were held isothermally for 2 minutes.
5. Finally, all samples were heated to 200 °C at a rate of 10 °C/min.

Thus, in this study there were eight compared conditions, with three samples designated for each of those conditions to observe repeatability. These eight conditions are summarized in Table 2.

3.2.2.3 Analyses

After the DSC testing was complete, the sample pans were collected. Later, the sample pans were opened (by cutting along the edge of the lid with scissors) and photographs of the samples were taken to allow for a visual analysis of samples following DSC testing.

Analysis of DSC data was performed using TA Universal Analysis software; the inflection point was used as glass transition temperature (T_g). A comparison was made between T_g values obtained from first heating and second heating.

3.3 Study 2

After results from Study 1 were analyzed and much variability in measured T_g was found, Study 2 was performed in an effort to find ways of reducing variability. Specifically, in Study 2, T_g variability in response to different sample grinding times (during sample preparation) and different DSC pan loadings was investigated. Only neat PMMA samples (no composites) and only a first heating peak temperature of 200 °C (not 160 °C) were used in the DSC-involving portion of this study. The conditions from the DSC portion of Study 2 are summarized in the table below. The second portion of this study involved using an FE-SEM to image cellulose powder particles that were subjected to the same investigated grinding times.

Table 3. Overview of DSC conditions in Study 2. Each checkmark indicates the use of both a solventless and a solvent-containing sample in that condition. Thus, two checkmarks indicates that two solventless samples and two solvent-containing samples were used. Only one of each sample were used in the 4 mg condition (because that mass was already looked at in Study 1).

		Mortar-and-Pestle Grinding Time			
		3 min	15 min	30 min	60 min
Mass of Sample Put into the DSC pan	4 mg			✓	
	10 mg	✓✓	✓✓	✓✓	✓✓
	15 mg			✓✓	

3.3.1 Sample preparation

New samples were created for this study, much in the same manner as in Study 1, with some exceptions, as described below.

3.3.1.1 Grinding

Grinding occurred as in Study 1 except only neat PMMA was used (no composite samples were made) and grinding time was varied. Four powders were made based on four grinding times: 3 minutes, 15 minutes, 30 minutes, and 60 minutes. Thus, at this

time, there were four types of samples, labeled 3P, 15P, 30P, and 60P, where the number represents the minutes of grinding time and the letter P stands for neat PMMA.

3.3.1.2 Melt pressing

Melt pressing was performed as in Study 1, with the following exceptions. As in Study 1, the melt pressing was performed in two stages; however, these melt-pressing stages now occurred for different durations and involved sample rearrangement after the first stage. Specifically, in the first stage, the sample was first subjected to a pressure of 110 kg/cm^2 for 1 minute. Then, after this initial melt pressing, the sample was removed and re-piled into a new hill on the aluminum foil (to make sure that the thin edges of the sample are put near the center to be better incorporated in the melt pressing). Finally, after this rearrangement, the sample was then melt pressed again at a pressure of 110 kg/cm^2 , this time for 2 minutes. The pressure was the same as in Study 1. The temperature on the indicator was again seen to vary, this time reaching a minimum of $96 \text{ }^\circ\text{C}$ and a maximum of $108 \text{ }^\circ\text{C}$.

3.3.1.3 Solvent addition

As before, part of the sample was put away to be used without solvent; ~ 0.5 grams of sample in each grinding condition was subjected to solvent addition as in Study 1. Thus, at this time there were 8 types of samples, which varied in grinding time and presence or absence of solvent.

3.3.2 Differential scanning calorimetry

In contrast to Study 1, DSC testing in Study 2 involved different sample loadings in DSC pans and only one first heating peak temperature.

3.3.2.1 DSC pan preparation

Whereas in Study 1 sample mass in DSC pans was kept at approximately 4 mg, in Study 2 sample mass in DSC pans was varied. Specifically, sample mass was varied for the samples that were ground for 30 minutes; for the other samples, the mass was kept consistent at 10 mg. With the 30-minute grinding samples, DSC pans containing a low (4

mg), medium (10 mg), and high (15 mg) amount of sample were prepared. Thus, at this time there were 12 conditions, listed below. The first number represents grinding time in minutes; P represents PMMA without solvent while PS represents PMMA with solvent; and the last number represents DSC loading.

3P-10mg	15P-10mg	30P-4mg	60P-10mg
3PS-10mg	15PS-10mg	30PS-4mg	60PS-10mg
		30P-10mg	
		30PS-10mg	
		30P-15mg	
		30PS-15mg	

Two DSC pans were prepared for each condition except with the 4 mg samples, which were kept at a single DSC pan per condition; the mass of 4 mg was used in Study 1.

3.3.2.2 DSC testing

Only a peak temperature of 200 °C was in Study 2. Otherwise, DSC testing occurred in the same fashion and with the same settings as in Study 1.

3.3.2.3 Analyses

Samples were photographed after DSC testing as in Study 1, with some additional photos taken, such as when leakage from pans was noticed or to show a certain aspect of the sample shape. Specifically, some samples had a capsule structure and a finger was used to press in their “roof”, revealing the hollowness inside, which was then photographed. It should be noted though that instances of leakage from pans were noticed only partway through the visual analysis, after some pans were already opened; therefore, some instances of leakage may have been missed. Measured T_g values were obtained as in Study 1.

3.3.3 Field emission scanning electron microscopy

Whereas the DSC portion of Study 2 only used neat PMMA, the FE-SEM portion of Study 2 only used cellulose, without PMMA. Cellulose powders were prepared using the

same grinding times as investigated above. These cellulose powders were then imaged with an FE-SEM to see the effect of those grinding times on the cellulose powder particles' size, aspect ratio, and uniformity.

3.3.3.1 Grinding

Cellulose powders were prepared by grinding 0.5 grams of cellulose using a mortar and pestle; no PMMA was included. Samples of resulting cellulose powder in the mortar were periodically removed during grinding – after 3 minutes, 15 minutes, 30 minutes, and 60 minutes to obtain four types of samples: cellulose powder that was 3-minute ground, 15-minute ground, 30-minute ground, and 60-minute ground.

3.3.3.2 Imaging and analysis

Those differently ground cellulose powders were sputter-coated with platinum and then imaged with an FE-SEM. In the resulting images, selected particle dimensions were measured and aspect ratios were calculated. The images were also compared based on particle uniformity in shape and size.

3.4 Study 3

Study 3 was essentially a repeat of Study 1 but with procedural modifications applied based on Study 2 to hopefully yield reduced Tg variation within experimental conditions and see results more clearly. The main differences from Study 1 involved using DSC pan sample loadings of 10 mg, grinding times of 60 minutes, and the melt-pressing technique from Study 2. Experimental conditions were the same as are summarized in Table 2.

3.4.1 Sample preparation

As in Study 1, both composite and neat PMMA samples were created. Grinding time and melt-pressing technique were changed based on Study 2 findings.

3.4.1.1 Grinding

Grinding was performed as in Study 1, except it was performed for the much longer period of 60 minutes. Material amounts were slightly different but the percentage of

cellulose by weight in the composite sample remained approximately the same. Specifically, one mortar and pestle set was used to grind ~3 grams of neat PMMA, and another mortar and pestle set was used to prepare the composite powder from ~2.88 grams of PMMA together with ~0.15 grams of cellulose, resulting in a mixture containing ~5% cellulose by weight.

3.4.1.2 Melt pressing

The resulting powders were melt-pressed as described in Study 2. The temperature display on the melt press indicated that the temperature varied within a range of 98 °C to 110 °C during melt pressing.

3.4.1.3 Solvent addition

Approximately 0.25 g of melt-pressed composite and neat PMMA material were subjected to solvent addition in the same manner as in Studies 1 and 2.

3.4.2 Differential scanning calorimetry

Other than differences to pan loading, DSC testing was mostly performed as in Study 1 and photographs of samples were taken similarly to Study 2. Additional photographs were taken of the samples before DSC testing.

3.4.2.1 DSC pan preparation

Sample mass in the DSC pans was kept at 10 mg for all conditions. Before sealing the pans, photos of the samples in pans were taken to show that the original sample shapes before DSC testing were comparable.

3.4.2.2 DSC testing

Settings for DSC testing were the same as in Study 1.

3.4.2.3 Analyses

DSC pans after testing were first inspected for leakage and any leakage was photographed. Then the DSC pans were opened and the samples therein were

photographed in the same way as in Study 2. Measured Tg values were obtained in the same way as in Studies 1 and 2.

3.5 Open pan heating

A final additional study was later performed to see whether a different sample shape would emerge if samples were heated without a lid.

Two samples – a solventless PMMA sample and a solvent-containing composite sample (that were both extras from Study 3) – were heated on a hot plate in open DSC pans (i.e. the same pans as previously but without the lid). Both pans were heated on the same hot plate at the same time. The pans (and the samples therein) were photographed periodically, at approximately the same time, as they were heated. The shape of the samples in the pans was observed.

Chapter 4

4 Results

This chapter first shows what the experimental samples looked like, and then describes what results those samples yielded when tested. The results are organized based on the experimental progression described in the previous chapter.

In Study 1, much variation in glass transition temperature (T_g) is found and the photographs of samples after DSC testing reveal unexpected shapes, some of which appear to be associated with higher measured T_g values in second heating; a shape classification is offered and a selective T_g comparison using only samples with similar shapes is presented. In this study, an outlier was also identified based on both DSC data and visual data.

In Study 2, the effects of grinding time and sample mass in DSC pans on measured T_g and on the variation of measured T_g are presented. Through the photographs, new shapes are found and additional categories for shape classification are offered. Visual data suggesting reasons for observed variation in measured T_g is presented. Results from FE-SEM image of cellulose powder are presented, with commentary on particle size, aspect ratio, and uniformity.

In Study 3, which is a modified version of Study 1, measured T_g between the experimental conditions is again compared and, this time, less variation in values within experimental conditions is found. Again, both a comprehensive comparison based on the entire DSC data and a selective comparison informed by photographs is presented.

In the Open Pan Heating study, photographs of the sample shape before, partway through, and at the end of heating are presented. The shape from heating in an open pan is seen to be different from those found in Studies 1, 2, and 3, which involved heating samples in a pan sealed with a hermetic lid.

For all graphs, error bars represent the average plus and minus a standard deviation.

4.1 Sample appearance

Samples obtained directly from melt pressing were different from those that had also undergone solvent addition. Examples of melt-pressed samples from Study 1 and Study 3 are shown in the figure below. Composite samples are more easily distinguished from neat PMMA samples on a black background; composite samples can be seen to have white marks, which are smaller and more uniform in the sample from Study 3.

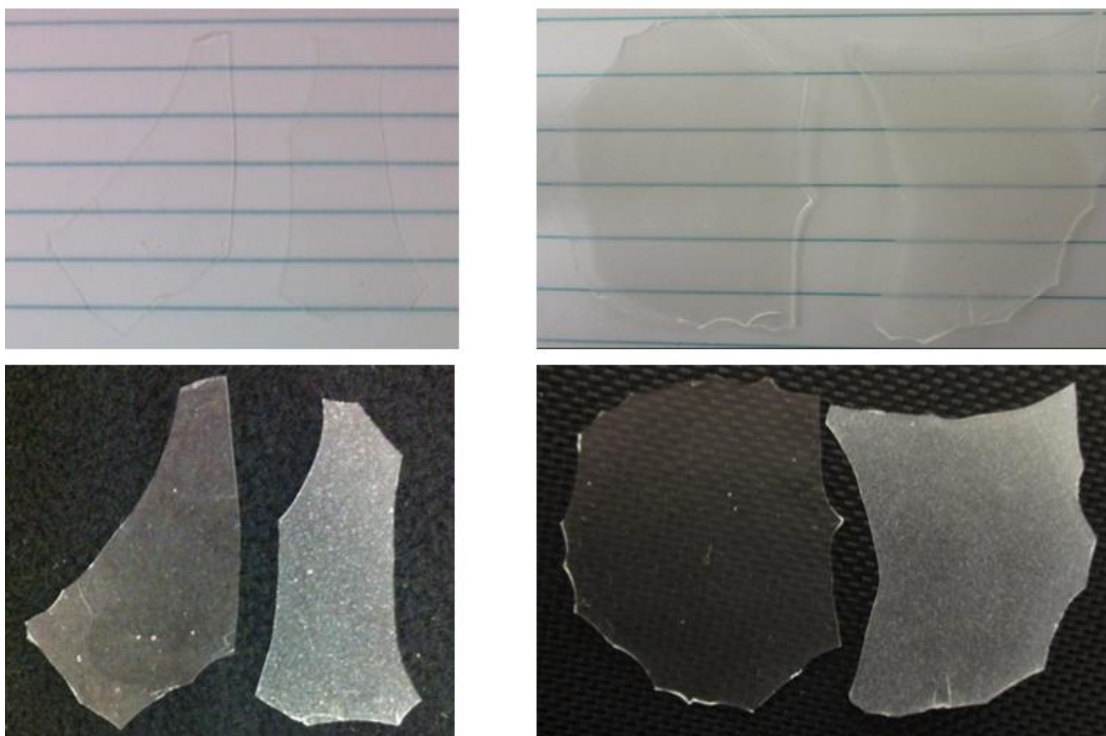


Figure 5. Examples of isolated solventless samples from Study 1 (left column) and Study 3 (right column) after melt pressing. In each image, the sample on the left is PMMA and the sample on the right is the composite. On a light background (top photos), the composite looks very similar to the neat PMMA sample; the samples from Study 3 appear darker than the samples from Study 1. On the black background (bottom photos), under certain lighting, white spots can be seen on the composite samples; these spots are smaller and more uniform in the composite from Study 3. Photographs from Study 1 were taken with a different camera than those from Study 3.



Figure 6. Solvent-containing PMMA (left) and solvent-containing composite (right) samples from Study 3; no images from Study 1 are available but they appeared similar. The composite sample looks very similar to the PMMA sample.

The solvent-containing samples were very fragile; they would break when picked up so the figure above shows them when they were still in the tray after solvent addition. Unlike the solventless samples that were transparent or translucent, the solvent-containing samples appeared white and full of tiny bubbles. Solvent-containing composite samples appeared indistinguishable from the solvent-containing PMMA samples.

4.2 Study 1

Results of the first study are comprised of glass transition temperature (T_g) comparisons from DSC data, photographic comparisons of samples after DSC testing, and analyses that combine DSC data with photographic data.

4.2.1 Differential scanning calorimetry

In this section, comparisons based on the following measurements are presented: T_g measured from the first heating scan, T_g measured from the second heating scan, and increases in T_g from the first to the second heating scan. Comparisons are also presented based on the following factors: presence of solvent vs. absence of solvent;

PMMA/cellulose composite vs. PMMA; and a first heating peak temperature of 200 °C vs. 160 °C.

These comparisons are presented with and without a certain outlier. This outlier was clearly seen not only from its T_g that greatly deviated from the others obtained in this study but also from the shape of the its whole heat flow curve. The figure on the next page presents the heat flow data of the outlier compared to that of the other Study 1 samples.

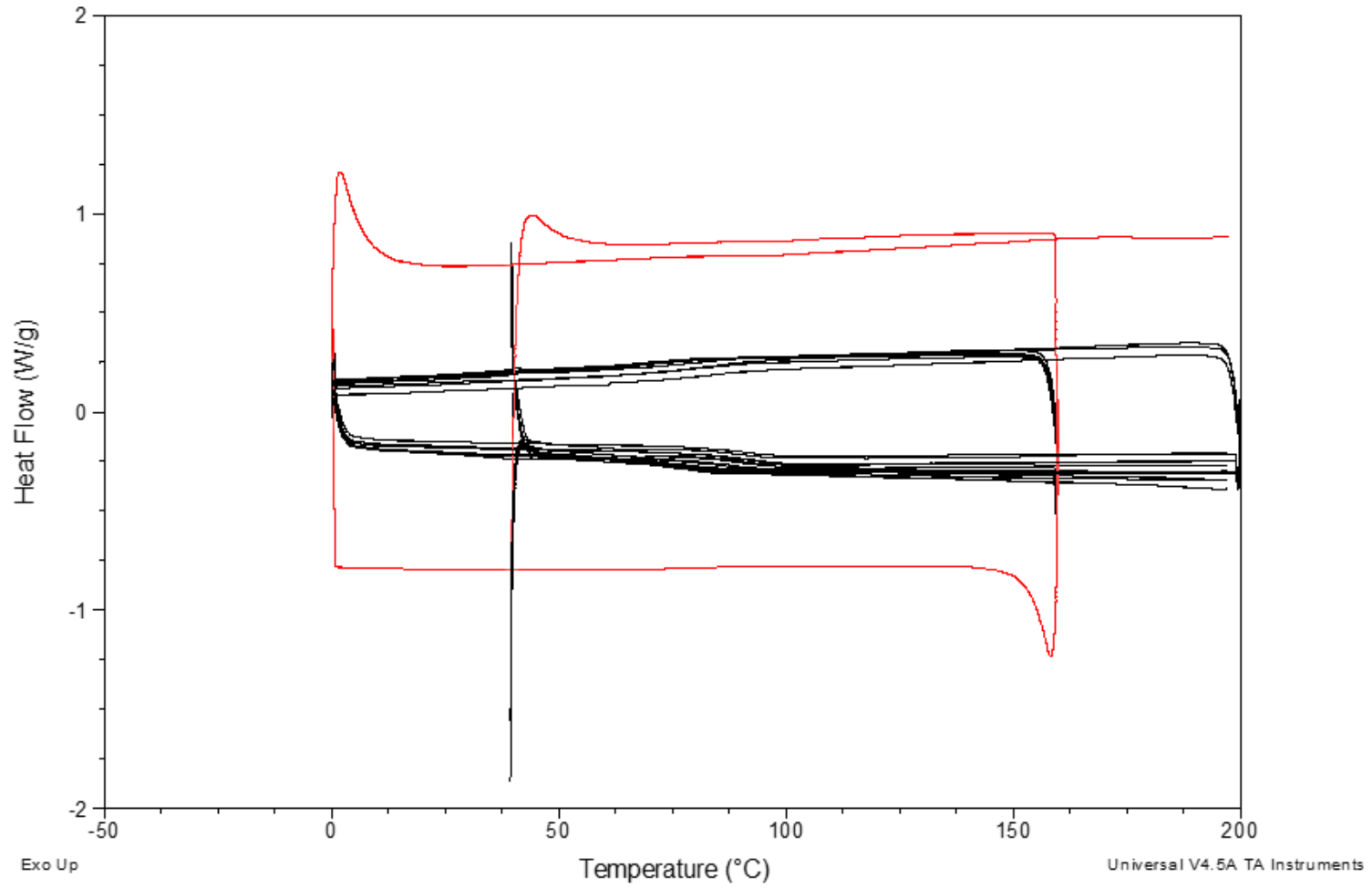


Figure 7. Outlier in differential scanning calorimetry results. Heat flow curve for outlier is shown in red; other heat flow curves from Study 1 are shown in black.

4.2.1.1 Glass transition temperature from first heating

A summary of the measured T_g values from first heating for the different experimental conditions is given with and without the aforementioned outlier in Figures 8 and 9.

No significant differences are seen between the 160 °C and 200 °C conditions, which is expected because these T_g values are from first heating, before the samples were exposed to those peak temperatures. Because these conditions are thus identical in the case of first heating T_g, their results have been grouped and summarized, with and without the outlier, in Figures 10 and 11.

4.2.1.1.1 Solvent vs. no solvent

If the outlier is omitted, a significant difference in T_g is seen between the solvent-containing and solventless conditions; the latter are seen to have greater T_g values. With the outlier included, the condition of which the outlier was part does not follow this trend.

4.2.1.1.2 Composite vs. PMMA

No significant difference is seen between measured T_g of composite samples compared to PMMA samples in the solvent-containing condition.

Figure 10 shows that, in the solventless condition, where the outlier is removed, a significant difference is seen between the C160 and P160 condition, with the former having a higher measured T_g from first heating. However, no significant difference is seen between the C200 and P200 condition, which are the same types of materials exposed to the same conditions during first heating as C160 and P160. Figure 12, which therefore groups the 160 °C and 200 °C conditions, shows that solventless composite samples are not significantly different from solventless PMMA in terms of their measured T_g from first heating.

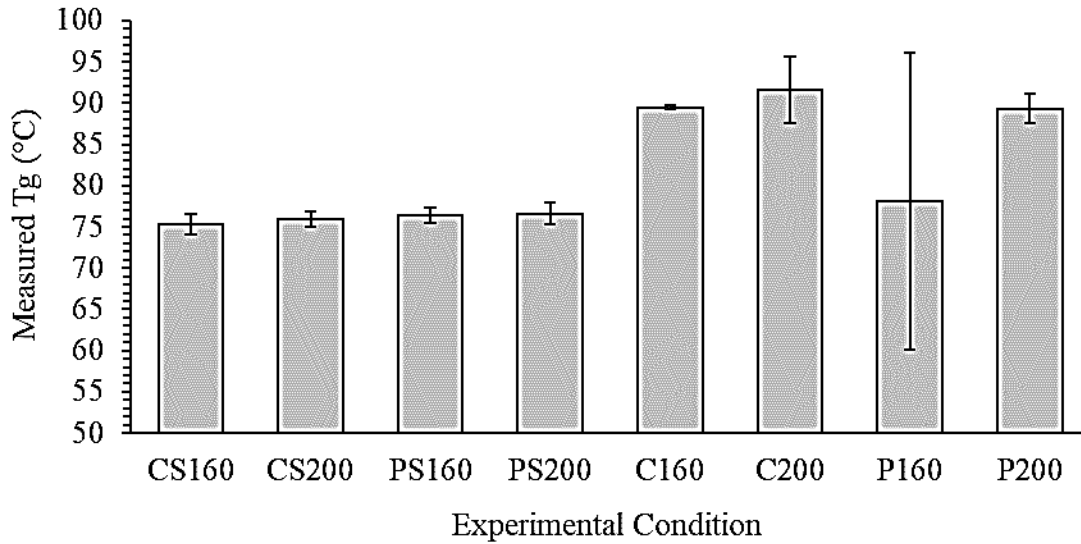


Figure 8. Glass transition temperature results from first heating of Study 1, including the outlier in the P160 condition, where it results in a large error bar.

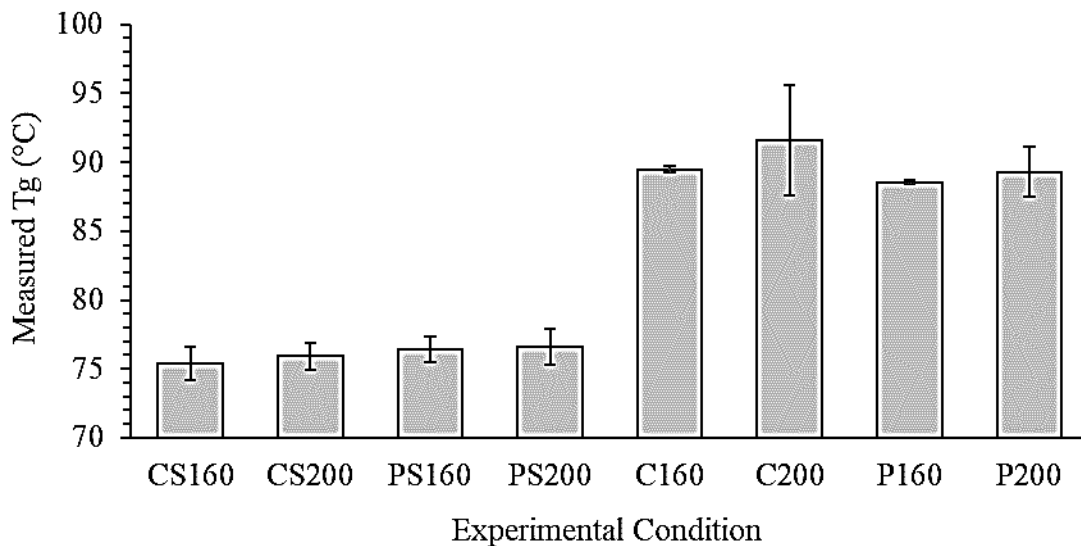


Figure 9. Glass transition temperature results from first heating of Study 1, excluding outlier in the P160 condition. No significant differences are seen between samples designated for the 160 °C and the 200 °C first heating peak temperature, which is expected because these results are from the first heating scan (i.e. from before that peak temperature was reached). Error bars are generally small.

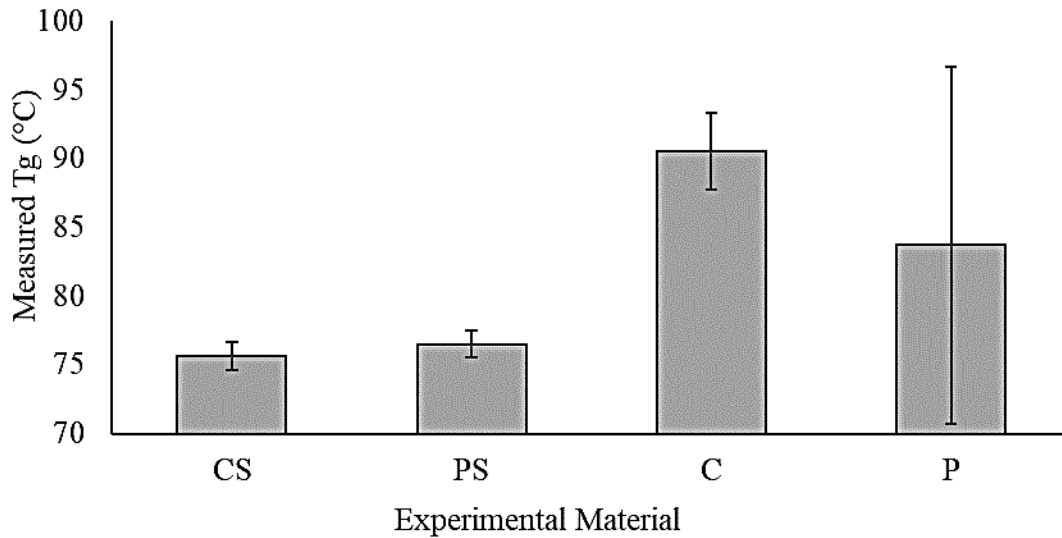


Figure 10. Glass transition temperature results from first heating, with data from 160 °C and 200 °C conditions combined; the outlier in the P condition is included, resulting in a large error bar.

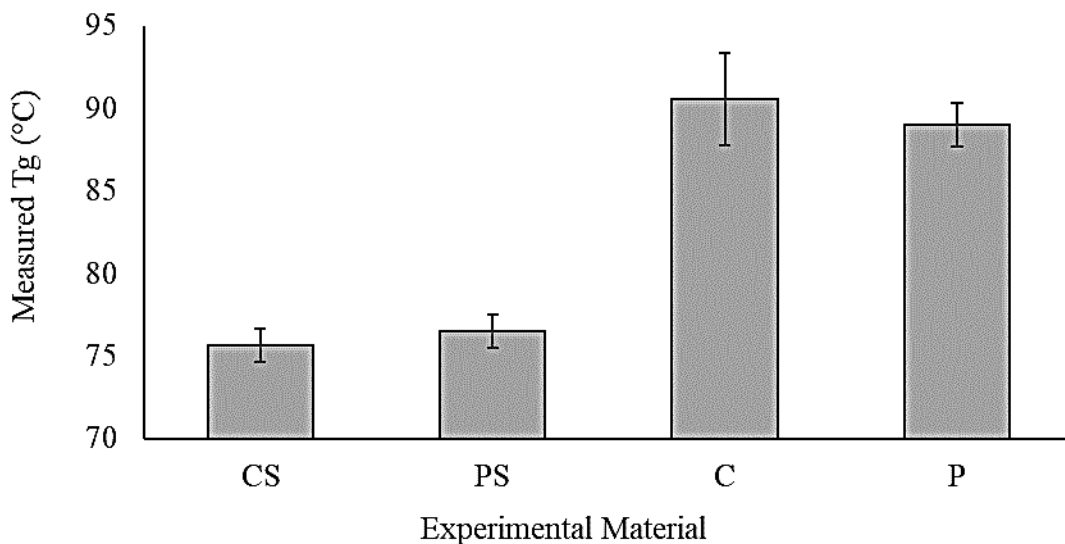


Figure 11. Glass transition temperature results from first heating, with data from 160 °C and 200 °C conditions combined; the outlier in the P condition is excluded. Solvent-containing samples have a significantly lower T_g than solventless samples; no significant difference is seen between composite and PMMA samples, neither with nor without solvent.

4.2.1.2 Glass transition temperature from second heating

A summary of the measured T_g values for the different experimental conditions is given with and without the aforementioned outlier in Figures 12 and 13.

4.2.1.2.1 Solvent vs. no Solvent

Unlike the results from first heating, the results from second heating show no significant difference between measured T_g from solventless and solvent-containing samples, even without the outlier.

However, without the outlier, it can be seen that the error bars for the solvent-containing conditions are greater than for solventless conditions. The standard deviation of measured T_g for solvent-containing samples is significantly greater than that of solventless samples. With the outlier included, no such significant difference is seen.

4.2.1.2.2 Composite vs. PMMA

As in the results from first heating, no significant differences are seen between the composite and PMMA samples, neither in the solventless condition nor in the solvent-containing condition.

4.2.1.2.3 160 °C vs. 200 °C

If the outlier is omitted, the measured T_g of the P160 condition is seen to be significantly less than that of the P200 condition. Otherwise, no significant differences are seen between the 160 °C and 200 °C conditions. No significant difference is seen if the outlier is included.

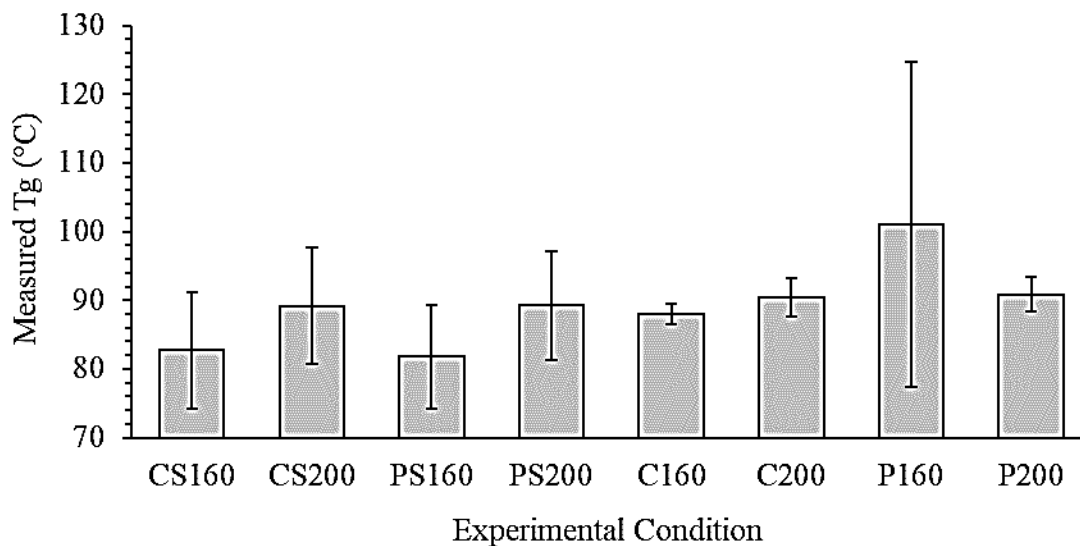


Figure 12. Glass transition temperature results from second heating of Study 1, including the outlier in the P160 condition, resulting in a large error bar.

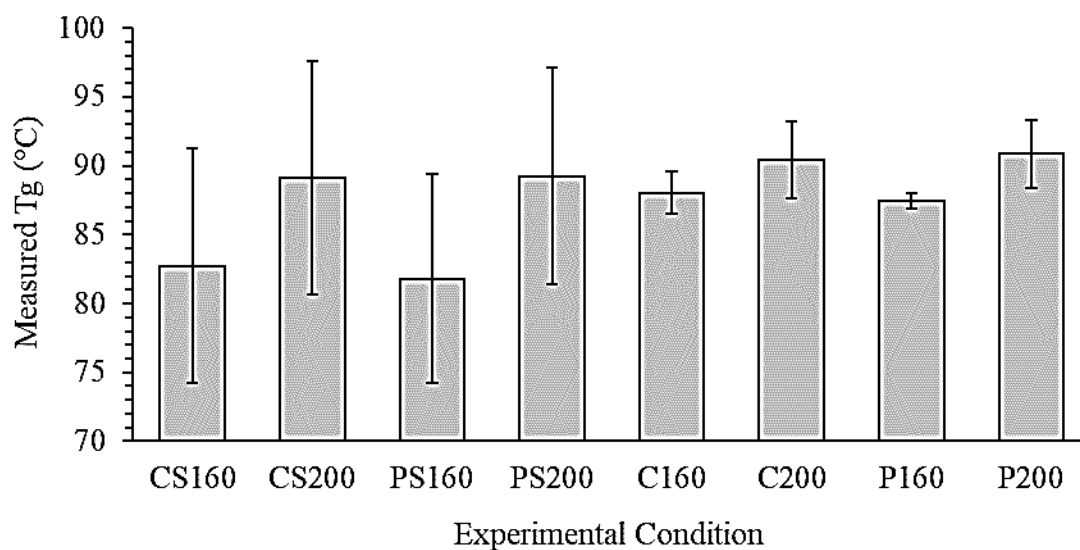


Figure 13. Glass transition temperature results from second heating of Study 1, excluding outlier in the P160 condition. Error bars in the solvent-containing conditions are significantly greater compared to the solventless conditions and compared to the results from first heating (Figure 9). The Tg of the P160 condition is significantly lower than that of the P200 condition; otherwise, no significant differences are seen between the 160 °C and 200 °C first heating peak temperature

conditions. No significant differences are seen between composite and PMMA conditions.

4.2.1.3 Increase in glass transition temperature from first to second heating

A summary of the increase in measured T_g from first to second heating for the different experimental conditions is given with and without the aforementioned outlier in Figures 14 and 15.

4.2.1.3.1 Solvent vs. no solvent

With the outlier omitted, a significant difference in T_g increase from first to second heating is seen between the solventless samples and the solvent-containing samples in the 200 °C condition, with the latter having the larger increase.

With the outlier omitted, a significant difference in T_g increase from first to second heating is also seen between the CS160 and P160 conditions, with the former have a larger increase than the latter, which had a decrease.

No significant difference in T_g increase from first to second heating is seen between the solventless samples and the PS160 condition.

As can be seen from the error bars Figure 15, significantly more variation is seen in the T_g increases from first to second heating in the solvent-containing samples compared to the solventless samples. This significant difference is only seen when the outlier is omitted.

When all solvent-containing samples are grouped and compared with a group of all solventless samples, then the former group is seen to have a significantly greater increase in T_g from first to second heating than the latter group, but only if the outlier is omitted, as seen in Figures 16 and 17.

4.2.1.3.2 Composite vs. PMMA

No significant difference is seen in T_g increase from first to second heating between composite and PMMA samples in the solvent-containing samples.

In the solventless samples, no significant difference is seen in T_g increase from first to second heating between composite and PMMA samples in the same temperature condition. However, if comparing between temperature conditions, a significant difference is seen between the C160 and P200 condition; the latter condition has a significantly larger increase in T_g from first to second heating.

4.2.1.3.3 160 °C vs. 200 °C

If the outlier is omitted, the measured T_g of the P160 condition is seen to be significantly less than that of the P200 condition. Otherwise, no significant differences are seen between the 160 °C and 200 °C conditions.

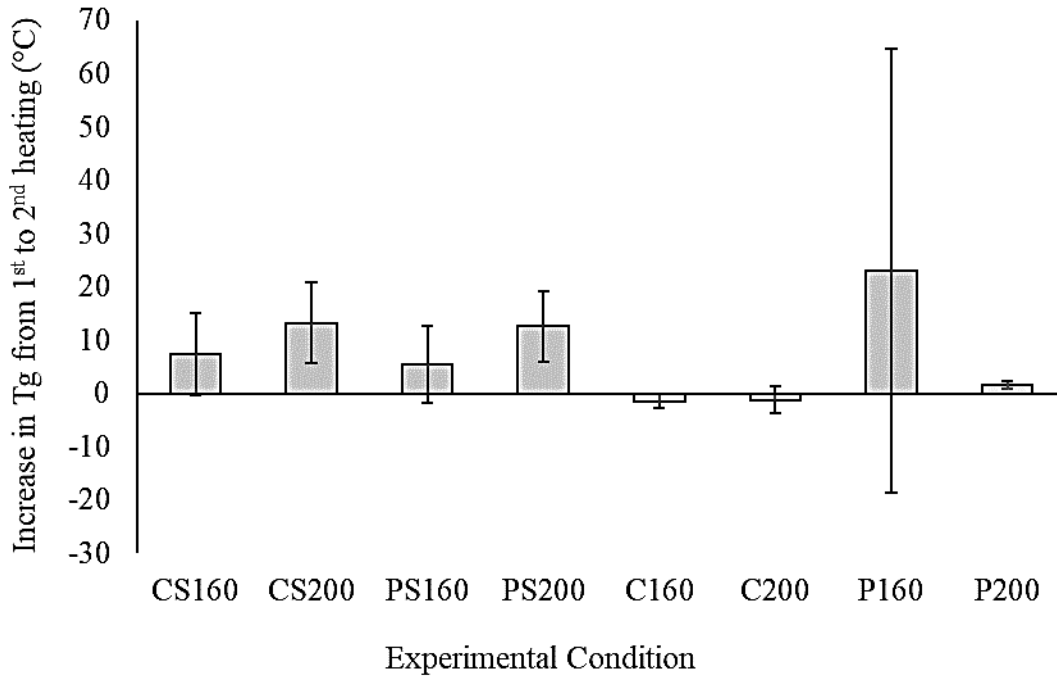


Figure 14. Comparisons of increases in measured glass transition temperature from first heating to second heating, with outlier included, resulting in a large error bar.

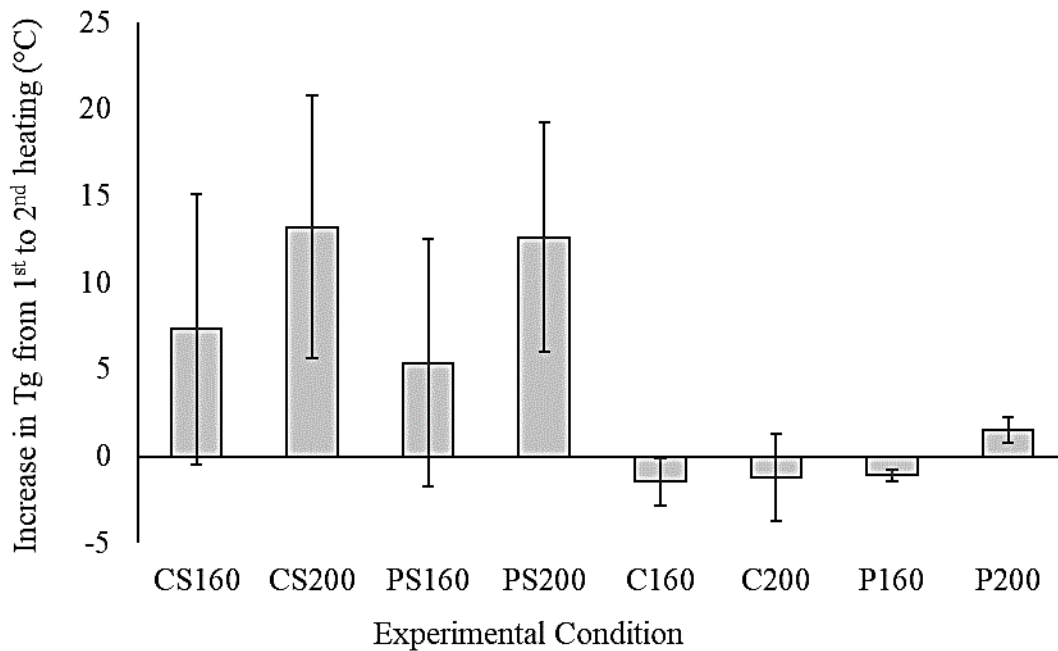


Figure 15. Comparisons of increases in measured glass transition temperature from first heating to second heating, with outlier excluded. Increases in Tg are

significantly greater than 0 °C with the 200 °C first heating peak temperature but not with the 160 °C first heating peak temperature. The P200 condition has a significantly greater increase in T_g than the P160 condition.

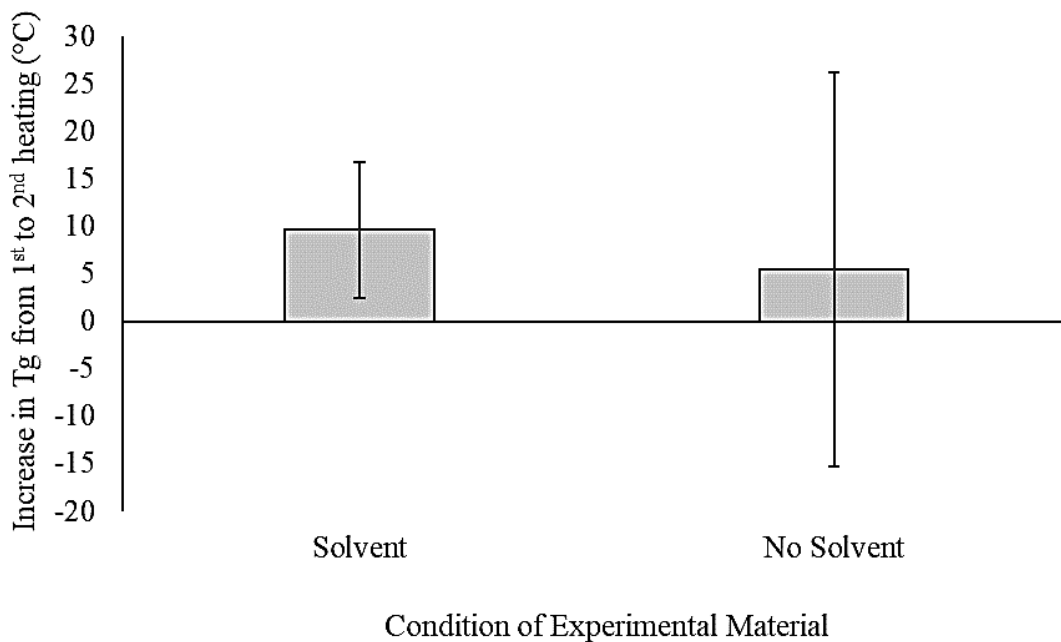


Figure 16. Comparison of increases in measured glass transition temperature from first heating to second heating between solvent-containing and solventless conditions, with outlier included, resulting in a large error bar.

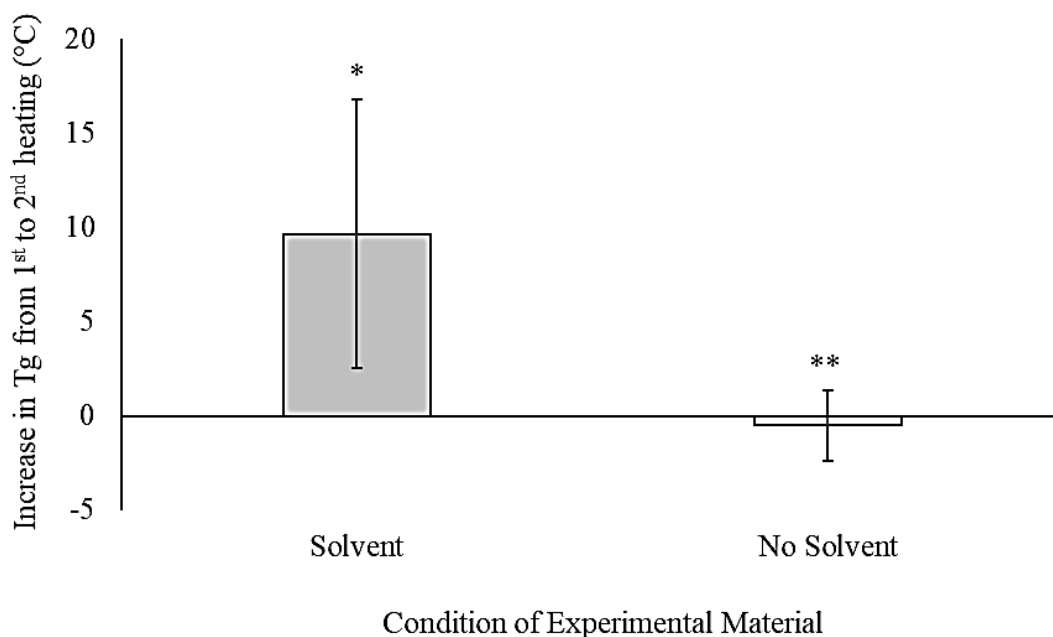


Figure 17. Comparison of increases in measured glass transition temperature from first heating to second heating between solvent-containing and solventless conditions, with outlier excluded. Increase in Tg is significantly greater in solvent-containing samples than in solventless samples; in the latter, no significant increase in Tg is seen.

4.2.2 Visual analysis of samples after DSC testing

As it can be difficult to say what causes variation in DSC results simply by looking at the heat flow curves, an additional visual analysis was performed. Simply, DSC pans after testing were opened and the samples were inspected and photographed. In this section, the outlier from the previous section can be seen to correspond to a sample with an irregular shape, the other samples are classified based on their shape, and the different shape classifications are compared based on their Tg-related trends.

4.2.2.1 Outlier

The sample corresponding to the outlier described in the previous section was examined visually. A photograph of this outlier sample is shown Figure 18. Most of the sample can be seen to be a clump leaning on the pan wall with little contact with the floor of the pan.

Only a small droplet of sample is present entirely on the pan floor. This sample has less contact with the floor than all of the other Study 1 samples, which are described next.

4.2.2.2 Shape classification

Sample shapes seen upon visual examination following DSC testing were mostly irregular; none of the samples had a shape that simply evenly covered the floor of the DSC pan. Although there were 24 samples, trends appeared to emerge and, excluding the outlier, all samples were classified into the following proposed classifications:

- **Floor-based shape**, pictured in Figure 19. This shape has most of its contact with the floor of the pan and has a convex shape.
- **Coated walls shape**, pictured in Figure 20. With this shape, the sample appears to be climbing up the walls from the pan floor, in most directions. It can be distinguished from the floor-based shape by its lack of convexity and its range of wall contact around the pan floor and up the wall.
- **Pillar shape**, pictured in Figure 21. This shape is like a pillar that grew from the pan floor and supports the lid of the pan. This pillar appears to have an approximately circular region of flatness right under the pan lid.



Figure 18. Top view of opened DSC pan of the outlier sample (P160 condition; Sample ID #11 in Appendix A). The sample is convex, with minimal contact with the pan floor.

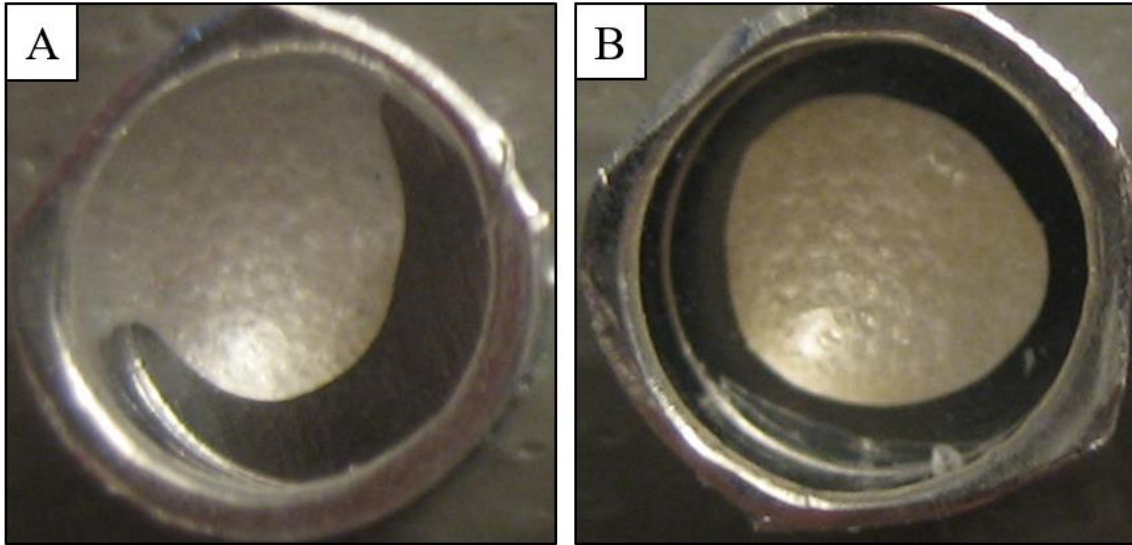


Figure 19. Examples from the CS160 condition of the “floor-based” sample shape, with the sample touching the wall (A; Sample ID #2 in Appendix A) and centered on the pan floor (B; Sample ID #9 in Appendix A).

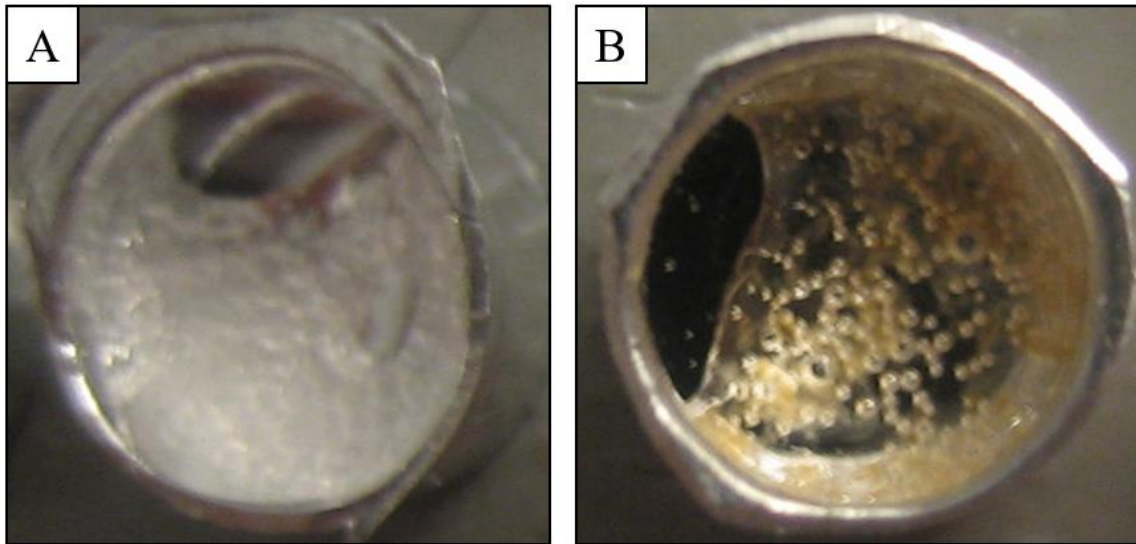


Figure 20. Examples of the “coated walls” sample shape, with a clear sample from the PS200 condition (A; Sample ID #14 in Appendix A) and a yellowed sample from the CS200 condition (B; Sample ID #18 in Appendix A).

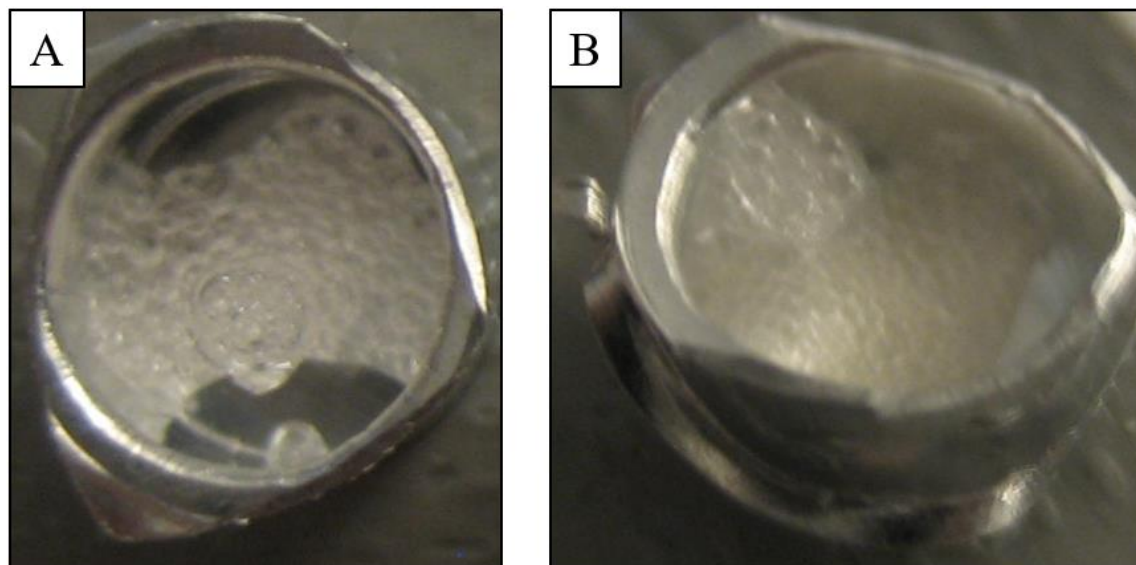


Figure 21. “Pillar” shape of sample in DSC pan after testing, in the PS160 condition (A; Sample ID #8 in Appendix A) and in the CS160 condition (B; Sample ID #1 in Appendix A).

4.2.2.3 Shape distribution

The distribution of shapes from Study 1 is shown in Figure 22. Most samples belonged to the floor-based shape category, which was comprised of both solvent-containing and solventless samples. The coated walls and pillar shape categories were comprised only of solvent-containing samples. The outlier was a single solventless sample.

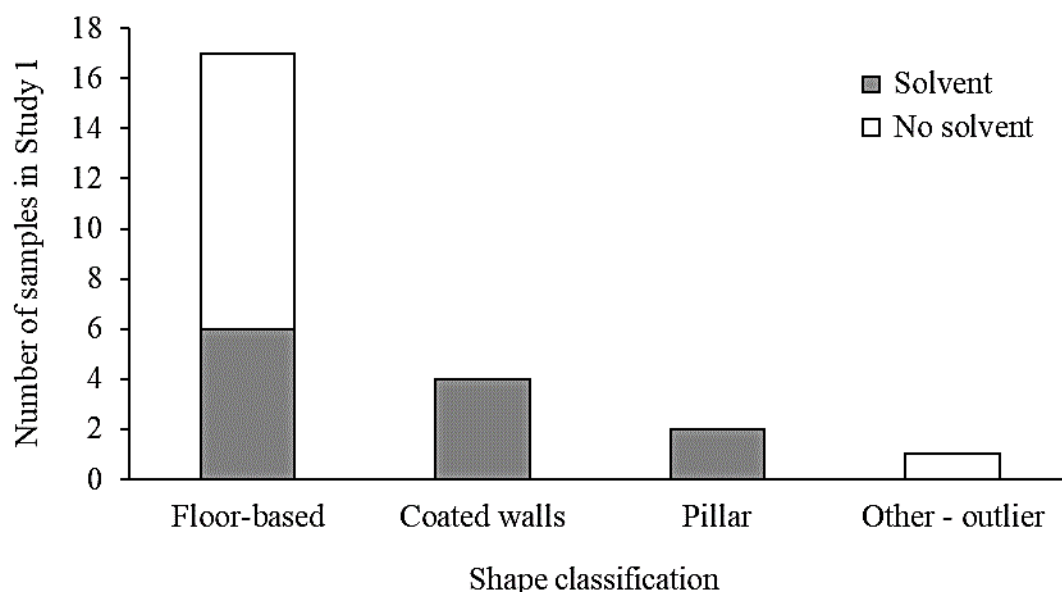


Figure 22. Stacked bar chart of the total number of samples belonging to each shape category in Study 1; solventless samples are distinguished from solvent-containing samples. Both solventless and solvent-containing samples are represented in the floor-based shape category. Aside from the outlier, all solventless samples have a floor-based shape. Only solvent-containing samples were seen to have a coated walls or pillar shape.

4.2.2.4 Glass transition temperatures of samples with different shapes

Glass transition temperatures from first and second heating of differently-shaped solvent-containing samples are summarized in Figure 23. Analysis was performed on solvent-containing samples because they were represented in all three of the main shape types whereas solventless samples were not present in two of those categories.

It can be seen from Figure 23 that samples with the pillar and coated walls shapes have significantly higher T_g values measured from second heating than do samples with a floor-based shape. This trend is present despite measured T_g values from first heating of floor-based shaped samples having been significantly greater than those of pillar-shaped samples and not significantly different from those of samples with the coated walls shape.

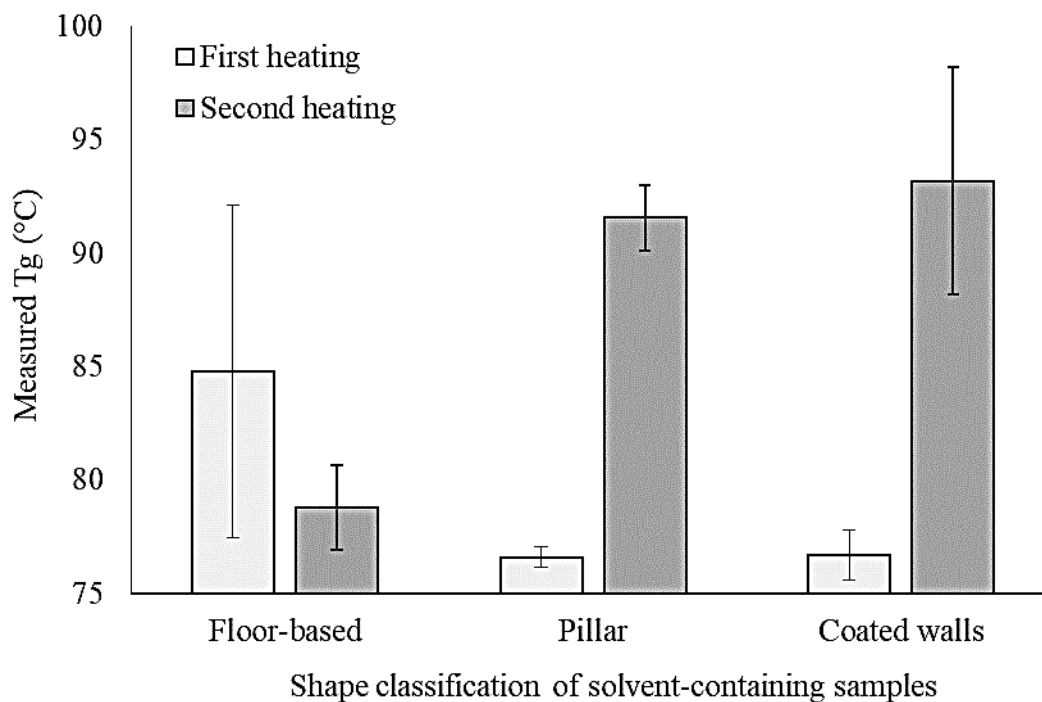


Figure 23. Comparison of measured glass transition temperatures from first and second heating in solvent-containing samples with different shape classifications. Samples with pillar and coated walls shapes have a significantly greater T_g measured from second heating compared to samples with the floor-based shape, despite having had significantly lower or not significantly different T_g when measured from first heating, respectively.

There is a significant increase in measured T_g from first to second heating in pillar-shaped and coated walls-shaped samples but not in samples with the floor-based shape. As seen in Figure 24, the increases in T_g exhibited by the pillar-shaped and coated walls-shaped samples are not significantly different from each other.

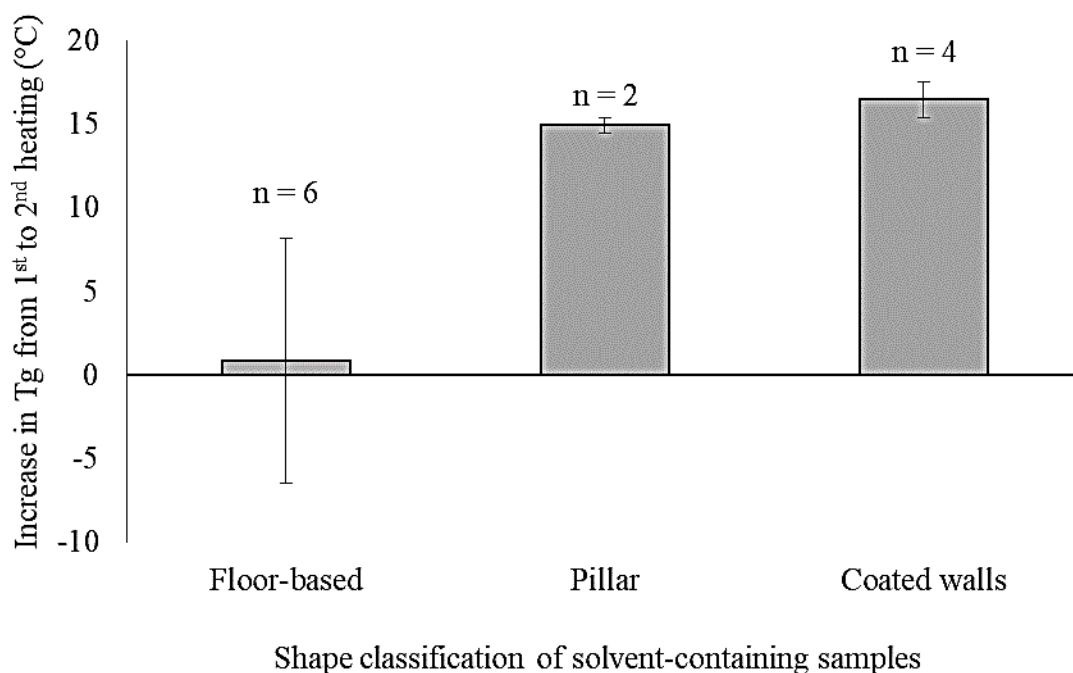


Figure 24. Increase in glass transition temperature from first to second heating of solvent-containing samples with different shape classifications. There is a significant increase in measured Tg from first to second heating in pillar-shaped and coated walls-shaped samples but not in samples with the floor-based shape.

4.2.2.5 Photographs in context of variation in glass transition temperature

These trends can be seen in the context of the variation in measured Tg values mentioned earlier. Figures 25 to 32 show photographs of each experimental condition's samples, indicating where the main deviation in Tg occurred. In many of those cases, two samples have the same shape type and similar Tg values while one sample has a different shape type and Tg value that deviates from the other two.

From the PS160 and CS160 conditions (Figures 25 and 26), the source of Tg variation appears to be the pillar shape, having a higher Tg on second heating than its counterparts with the floor-based shape. In the PS200 and CS200 conditions (Figures 27 and 28), two samples are in the shape of coated walls and one sample has a floor-based shape, with a

lower measured Tg. The remaining conditions (Figures 29 to 32) have floor-based shapes (with the exception of the outlier), without drastic deviations in Tg.

In addition to different shapes, samples are seen to have different degrees of yellowing. In Study 1, yellower samples are seen to have lower Tg values from both first heating and second heating compared to other samples in their experimental condition. Yellowing is seen only in composite samples. No yellowing is seen in the C160 condition. The other composite conditions have yellowing only in one or two of their three samples, not all of them. In one sample (Figure 28), yellowing is seen to occur only one part of the sample; in two other samples, yellowing appears to be greater around bubbles (Figure 28 and 32).

Another factor of potential interest is bubble size in samples. Generally, samples with larger bubbles in their experimental condition are seen to have larger measured Tg values both on first and second heating compared to other samples in their experimental condition.

No correlation is noticed between measured Tg and the number of clumps into which the sample is broken up or the closeness of floor-based shape samples to a round shape.

PS160 – First Sample



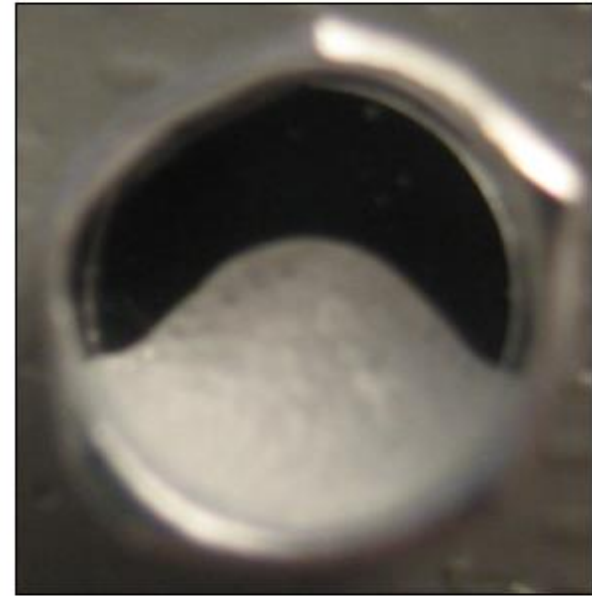
Shape: Floor-based
H1 Tg: 76.92 °C
H2 Tg: 77.57 °C
Sample ID: 7

PS160 – Second Sample



Shape: Pillar
H1 Tg: 76.92 °C
H2 Tg: 90.55 °C
Sample ID: 8

PS160 – Third Sample



Shape: Floor-based
H1 Tg: 75.35 °C
H2 Tg: 77.27 °C
Sample ID: 12

Figure 25. Photographs from the PS160 condition. Although Tg from first heating (H1 Tg) is similar for all samples, Tg from second heating (H2 Tg) is much higher in the pillar-shaped sample compared to the samples with the floor-based shape.

CS160 – First Sample



Shape: Pillar

H1 Tg: 76.28 °C

H2 Tg: 92.58 °C

Sample ID: 1

CS160 – Second Sample



Shape: Floor-based

H1 Tg: 75.88 °C

H2 Tg: 77.90 °C

Sample ID: 2

CS160 – Third Sample



Shape: Floor-based

H1 Tg: 73.97 °C

H2 Tg: 77.7 °C

Sample ID: 9

Figure 26. Photographs from the CS160 condition. The pillar-shaped sample again has a higher Tg from second heating (H2 Tg) than the samples with the floor-based shape. The floor-based shape samples have H2 Tg values very similar to each other despite having had a larger difference in their Tg from first heating (H1 Tg) and one being more yellow than the other.

PS200 – First Sample



Shape: Coated walls
 H1 Tg: 76.26 °C
 H2 Tg: 88.84 °C
 Sample ID: 13

PS200 – Second Sample



Shape: Coated walls
 H1 Tg: 78.03 °C
 H2 Tg: 97.29 °C
 Sample ID: 14

PS200 – Third Sample



Shape: Floor-based
 H1 Tg: 75.52 °C
 H2 Tg: 81.57 °C
 Sample ID: 24

Figure 27. Photographs from the PS200 condition. The samples with the coated walls shape have higher Tg values than the sample with the floor-based shape. The sample with the bubbly coated walls has higher Tg values than the sample with the smooth coated walls.

CS200 – First Sample



Shape: Coated walls
 H1 Tg: 77.02 °C
 H2 Tg: 97.77 °C
 Sample ID: 17

CS200 – Second Sample



Shape: Coated walls
 H1 Tg: 75.45 °C
 H2 Tg: 88.85 °C
 Sample ID: 18

CS200 – Third Sample



Shape: Floor-based
 H1 Tg: 75.26 °C
 H2 Tg: 80.83 °C
 Sample ID: 23

Figure 28. Photographs from the CS200 condition. The samples with the coated walls shape have higher Tg values than the sample with the floor-based shape. The sample with the large-bubbled, white coated walls has higher Tg values than the sample with the smaller-bubbled, yellowed coated walls. The third sample has greatly non-uniform yellowing/browning.

P160 – First Sample



Shape: Floor-based
 H1 Tg: 88.65 °C
 H2 Tg: 87.82 °C
 Sample ID: 5

P160 – Second Sample



Shape: Floor-based
 H1 Tg: 88.43 °C
 H2 Tg: 87.09 °C
 Sample ID: 6

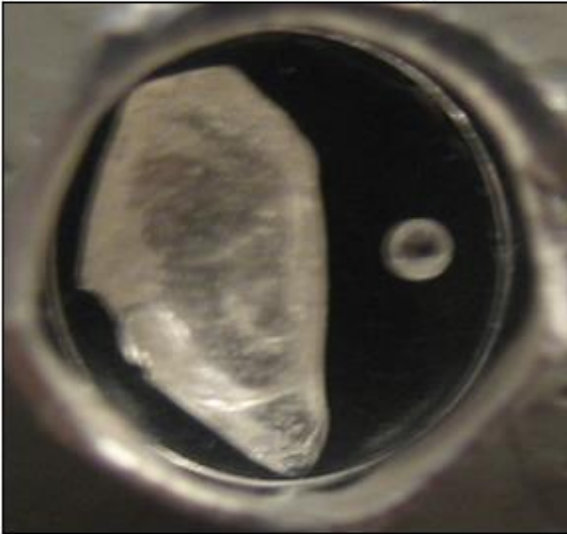
P160 – Third Sample (outlier)



Shape: Other (outlier)
 H1 Tg: 57.29 °C
 H2 Tg: 128.32 °C
 Sample ID: 11

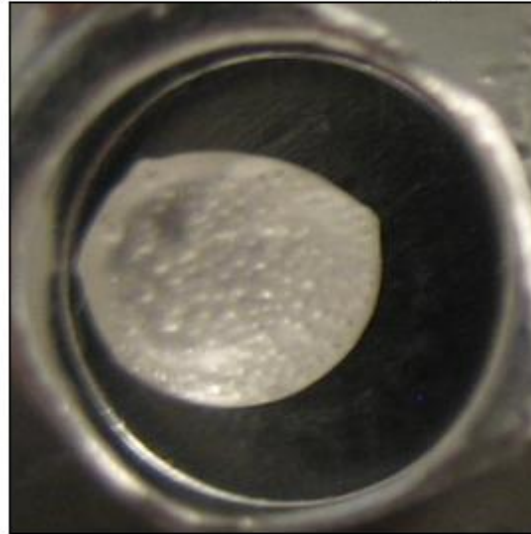
Figure 29. Photographs from the P160 condition. The two floor-based samples have similar Tg values both from first heating (H1 Tg) and from second heating (H2 Tg), despite one being in the form of two clumps instead of one. The outlier, having both Tg values greatly different from the other samples, has a clump located primarily against the pan wall, with very little contact with the pan floor, and only a very small separate clump on the pan floor.

C160 – First Sample



Shape: Floor-based
H1 Tg: 89.45 °C
H2 Tg: 86.9 °C
Sample ID: 3

C160 – Second Sample



Shape: Floor-based
H1 Tg: 89.71 °C
H2 Tg: 89.75 °C
Sample ID: 4

C160 – Third Sample



Shape: Floor-based
H1 Tg: 89.34 °C
H2 Tg: 87.47 °C
Sample ID: 10

Figure 30. Photographs from the C160 condition. All samples have a floor-based shape, similar Tg values from first heating (H1 Tg), and somewhat similar Tg values from second heating (H2 Tg).

P200 – First Sample



Shape: Floor-based
 H1 Tg: 90.19 °C
 H2 Tg: 92.41 °C
 Sample ID: 15

P200 – Second Sample



Shape: Floor-based
 H1 Tg: 90.50 °C
 H2 Tg: 92.17 °C
 Sample ID: 16

P200 – Third Sample



Shape: Floor-based
 H1 Tg: 87.24 °C
 H2 Tg: 88.01 °C
 Sample ID: 22

Figure 31. Photographs from the P200 condition. All samples have a floor-based shape; the large-bubbled samples have larger Tg values than the small-bubbled sample. One of the samples has a small clump on the pan wall in addition to the main clump on the pan floor.

C200 – First Sample



Shape: Floor-based
H1 Tg: 91.74 °C
H2 Tg: 92.45 °C
Sample ID: 19

C200 – Second Sample



Shape: Floor-based
H1 Tg: 95.58 °C
H2 Tg: 91.53 °C
Sample ID: 20

C200 – Third Sample



Shape: Floor-based
H1 Tg: 87.51 °C
H2 Tg: 87.26 °C
Sample ID: 21

Figure 32. Photographs from the C200 condition. All samples have a floor-based shape. Clear samples with large bubbles have higher Tg values than the yellowed sample with small bubbles.

4.2.3 Selective Tg analysis based on visual data

In the previous section it was seen that different sample shapes in DSC pans are associated with different Tg tendencies. Of the three main shapes, only the floor-based shape samples were comprised of both solventless and solvent-containing samples. In this section, experimental conditions are compared only using data from the floor-based shape samples.

The floor-based shape samples in the solventless condition are simply all of the solventless samples other than the outlier; thus, their trends have already been discussed. A comparison of measured Tg from first and second heating using solvent-containing samples with a floor-based shape is shown in Figure 33.

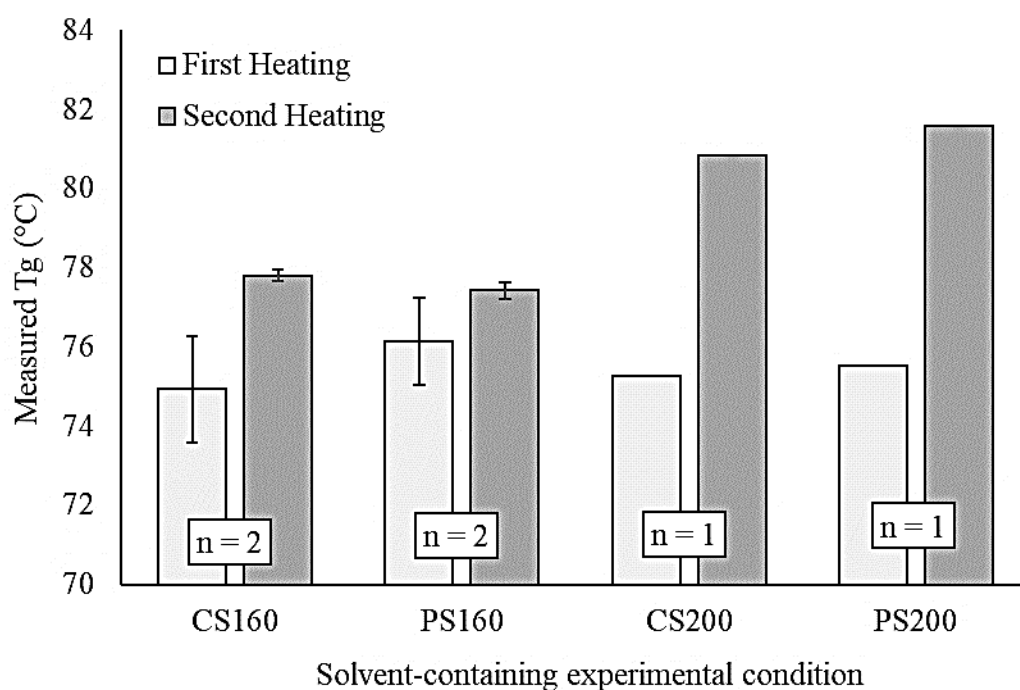


Figure 33. Selective comparison of solvent-containing experimental conditions based on glass transition temperatures from first and second heating using only floor-based-shaped samples. The number of samples in each condition is indicated; only one sample was available in the CS200 and PS200 conditions. C160 but not P160 samples has a significantly greater second heating Tg compared to first heating.

4.2.3.1 Composite vs. PMMA

The CS160 condition is seen to have a significantly higher T_g from second heating than the P160 condition, despite their T_g values from first heating having been not significantly different from each other.

With the CS200 and PS200 conditions, the latter has a higher T_g value from both first and second heating; however, because there is only one sample available in each condition, it cannot be known whether this difference is significant.

The CS160 condition is seen to have a T_g from second heating that is significantly higher than its T_g from first heating. In the PS160 condition, there is no significant difference between the T_g from first heating and the T_g from second heating.

With the CS200 and PS200 conditions, the latter has a greater increase in T_g from first to second heating; however, because there is only one sample available in each condition, it cannot be known whether this difference is significant.

4.2.3.2 160 °C vs. 200 °C

Grouping conditions based on first heating peak temperature, some significant differences can be seen. As shown in Figure 34, with both temperatures, the T_g from second heating is significantly greater than the T_g from first heating for these solvent-containing samples.

However, the T_g from second heating of solvent-containing samples in the 200 °C condition is significantly greater than that of solvent-containing samples in the 160 °C condition, despite their T_g from first heating not having been significantly different. As shown in Figure 35, the solvent-containing samples in the 200 °C condition have a significantly greater average increase in T_g from first to second heating than the solvent-containing samples in the 160 °C condition.

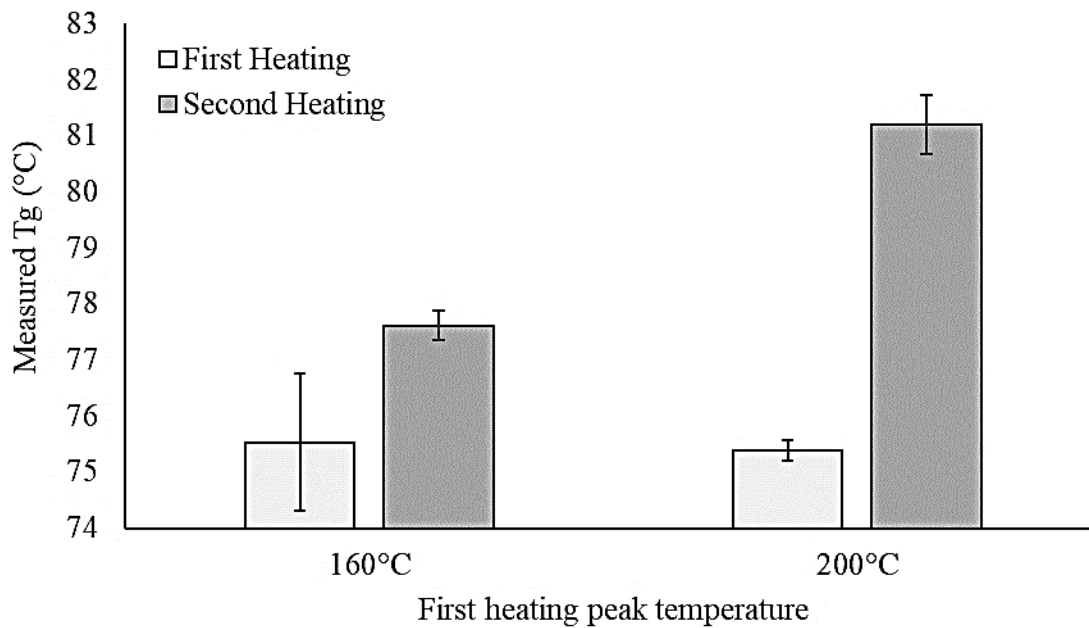


Figure 34. Comparison of first heating peak temperatures based on T_g from first and second heating using only solvent-containing samples with a floor-based shape. Although there is no significant difference between the two sample groups on first heating, the T_g obtained from second heating is significantly greater when measured using a first heating peak temperature of 200 °C compared to 160 °C.

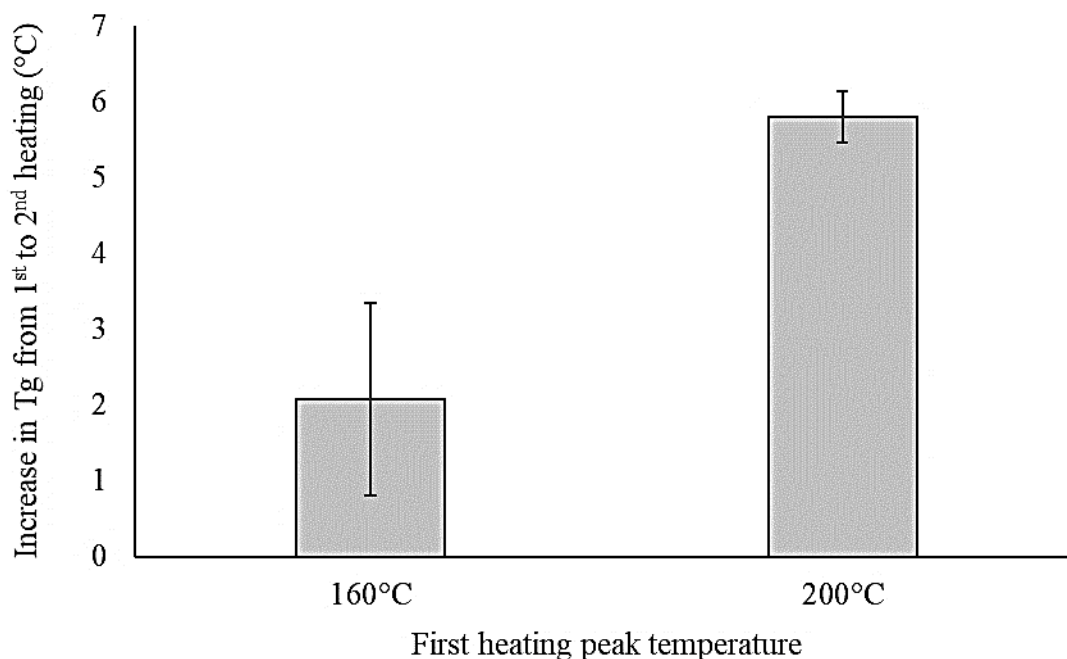


Figure 35. Comparison of first heating peak temperatures based on increase in Tg from first to second heating using only solvent-containing samples with a floor-based shape. Samples subjected to a first heating peak temperature of 200 °C have a significantly greater increase in Tg from first to second heating compared to samples subjected to a first heating peak temperature of 160 °C.

4.3 Study 2

Given that Study 1 samples tended not to cover the DSC pan floor entirely, in Study 2 the effects of larger masses of sample per pan are investigated. Also investigated in Study 2 were the effects of grinding time during sample preparation on measured Tg and cellulose particle characteristics. Results of this second study are comprised of glass transition temperature (Tg) comparisons from DSC data, photographic comparisons of samples after DSC testing, analyses that combine DSC data with photographic data, and FE-SEM imaging of cellulose powders subjected to different grinding times.

4.3.1 Differential scanning calorimetry

In this section, results relating to the effects of grinding time and mass of sample in DSC pan on measured Tg, and variations in measured Tg are presented, both for solventless

and solvent-containing PMMA samples. Comparisons of grinding time are presented using only 10 mg samples. Comparisons of sample mass are presented using only 30-minute ground samples. Unlike in Study 1, Study 2 involved DSC testing with only PMMA samples (no composite samples) and using the same first heating peak of 200 °C for all samples.

4.3.1.1 Effect of grinding time on measured glass transition temperature

In solventless samples, T_g generally appears to generally increase with increasing grinding time, as seen in Figure 36.

From first heating in solventless samples, significant differences are seen between all grinding time conditions except directly successive conditions. For example, there is no significant difference between the 3-minute and 15-minute conditions, but there are significant differences between the 3-minute condition and the 30- and 60-minute conditions.

From second heating in solventless samples, significant differences are seen between all conditions except between 15-minute and 30-minute conditions, and between the 15-minute and 60-minute conditions.

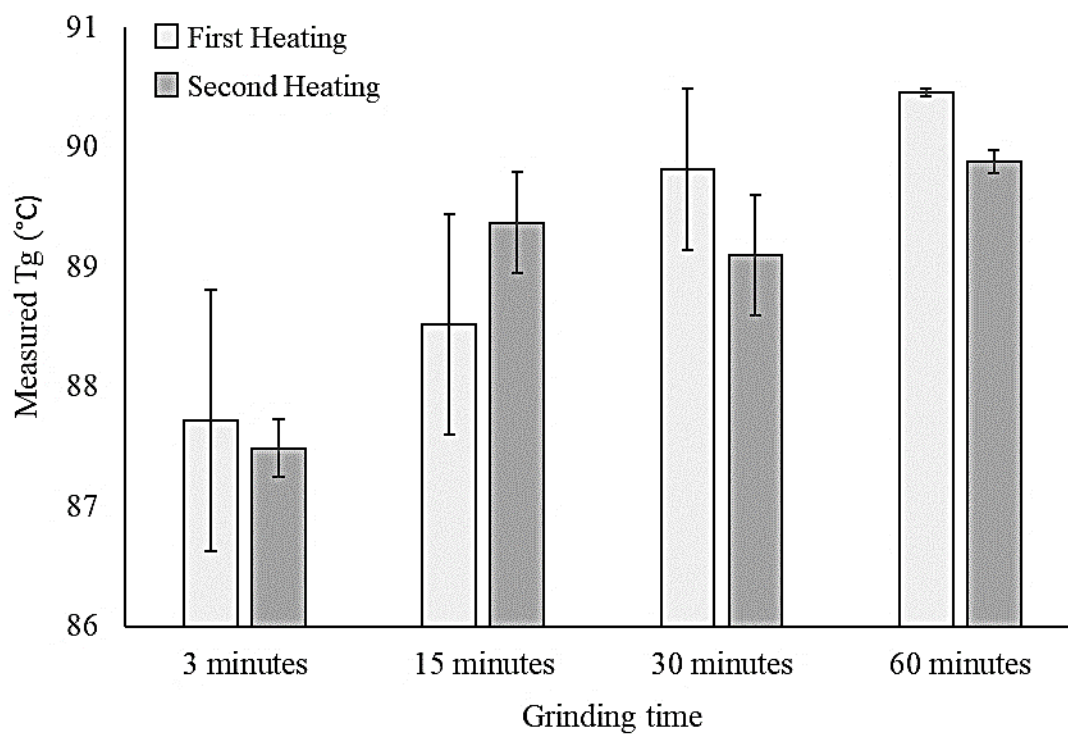


Figure 36. Effect of grinding time on measured T_g in solventless, 10 mg samples. A general trend of increased T_g with increasing grinding time is seen; see text.

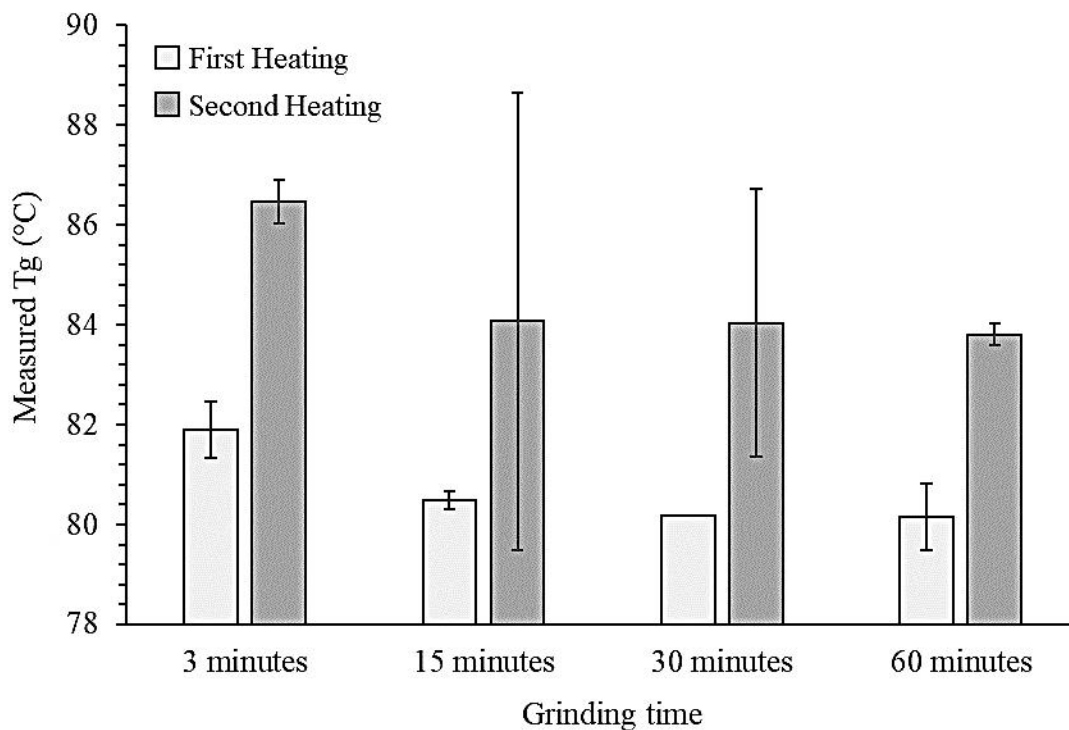


Figure 37. Effect of grinding time on measured Tg in solvent-containing, 10 mg samples. In contrast to the solventless samples (Figure 36), a general trend of decreasing Tg with increasing grinding time is seen; see text. The error bar in the first heating 30-minute condition is too small to be seen.

Whereas Tg appeared to generally increase with grinding time in the solventless samples, the opposite general trend is seen in the solvent-containing samples, which have a Tg that generally decreases with increasing grinding time as shown in Figure 37.

From first heating in solvent-containing samples, significant differences are seen in all combinations between the first three grinding time conditions (3 minutes, 15 minutes, and 30 minutes). The maximal grinding time condition (60 minutes) is only significantly different from the minimum grinding time condition (3 minutes) in comparisons based on Tg measured from first heating of solvent-containing samples.

From second heating in solvent-containing samples, significant differences are seen only between the maximal grinding time (60 minutes) and the minimum grinding time (3 minutes).

4.3.1.1.1 Effect of grinding time on variation in measured glass transition temperature

For solventless samples, it can be seen from error bars that the 60-minute condition has the smallest variation in T_g .

For solvent-containing samples, it can be seen from error bars that the 60-minute condition has the smallest variation in T_g from second heating but not from first heating. In the latter category, the 30-minute condition has the lowest variation in T_g .

However, as can be seen from Figure 38, even in the category of solvent-containing samples with T_g measured from first heating (PS - Heat 1), the variation in T_g of the 60-minute condition is small enough to allow for significant differences in T_g to be seen among all categories of the 60-minute condition, which is not true for any of the other grinding time conditions.

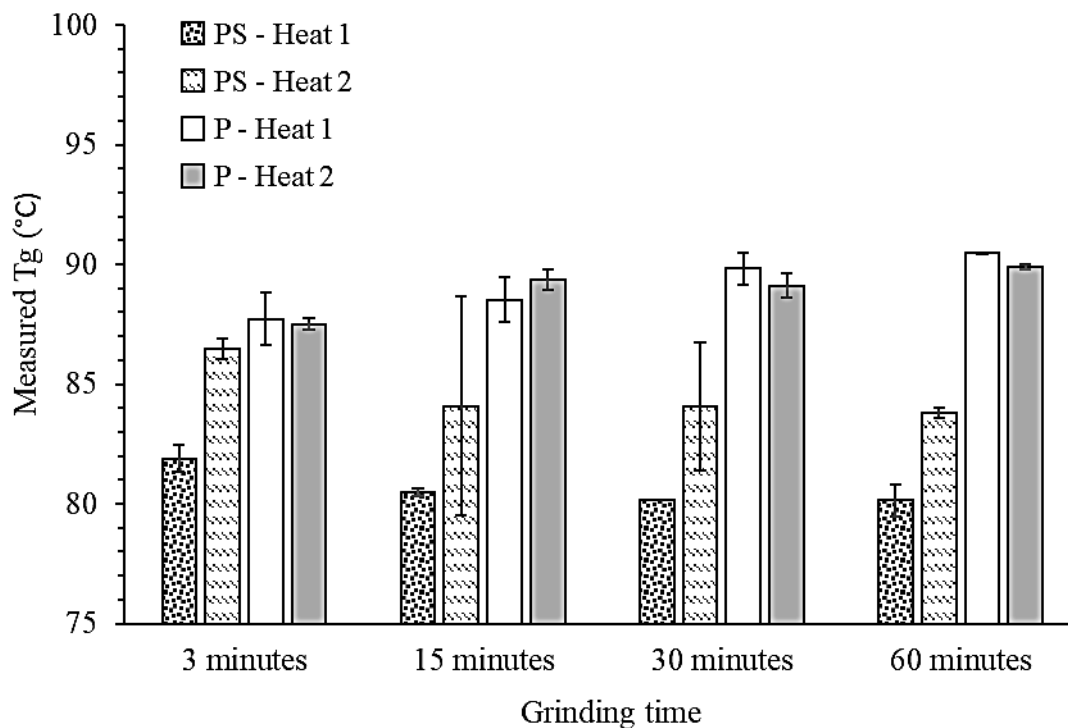


Figure 38. Effect of grinding time on measured glass transition temperature in 10 mg samples. Variation, as seen with error bars, is least with 60 minutes of grinding time.

4.3.1.2 Effect of mass of sample in DSC pan

A summary of the effect of sample mass in the DSC pan on measured glass transition temperature, from first and second heating, is given in Figure 39.

Most comparisons in this section will be made between the 10 mg and 15 mg conditions. The 4 mg condition, which was used for all samples in Study 1, is in this study comprised only of one solventless and one solvent-containing sample; therefore, no commentary on significant differences involving the 4 mg condition can be made. However, the solvent-containing 4 mg sample can be seen to have a measured Tg from second heating that appears much higher than any of the other measured Tg values. The 4 mg sample will be discussed more in the visual analysis results section.

Comparing the 10 mg and 15 mg conditions, a significant difference can be seen in the Tg from first heating; in solventless samples, the 15 mg condition has the significantly higher measured Tg values but, in the solvent-containing samples, it's the 10 mg condition that has the significantly higher measured Tg values. No significant differences are seen between the 10 mg and 15 mg condition when Tg measured from second heating is compared.

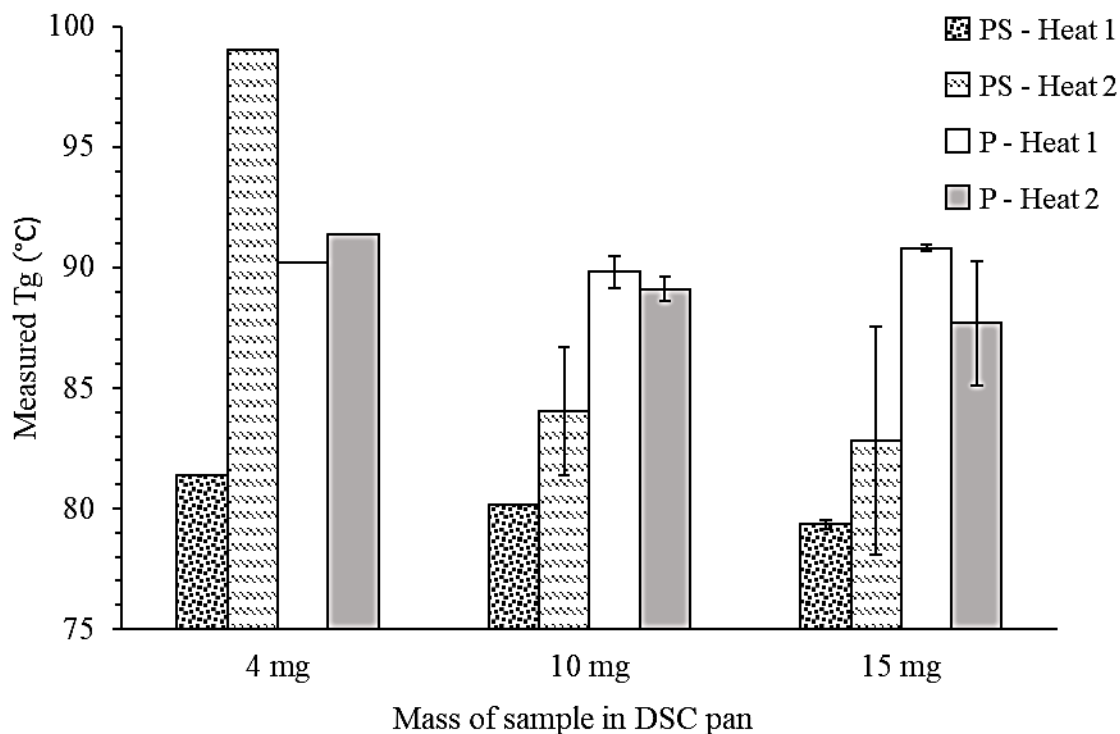


Figure 39. Effect of sample mass in DSC pan on measured glass transition temperature using samples subjected to 30 minutes of grinding time. The 4 mg condition has no error bars because only one solvent-containing and solventless sample was used in that condition. The other conditions had two of each kind of sample. In the 10 mg condition, one error bar is too small to be seen. Variation as shown by error bars is generally lower in the 10 mg condition than in the 15 mg condition.

4.3.1.2.1 Effect of mass of sample in DSC pan on Tg variation

For solvent-containing samples, it can be seen from error bars that the 10 mg condition has less variation in Tg compared to the 15 mg condition.

For solventless samples, it can be seen from error bars that the 10 mg condition has less variation in Tg from second heating but not from first heating. In the latter category, the 15 mg condition has the lower variation in Tg.

However, 10 mg condition allows for significant differences to be seen between solventless samples and their solvent-containing counterparts both based on Tg from first and second heating, which is not true for the 15 mg condition.

4.3.2 Visual analysis of samples after DSC testing

In this section, new shapes are added to the shape classification and shape-related trends are discussed.

4.3.2.1 Classification of additional shapes

Although some of the shapes from Study 1 were seen again in Study 2, namely the floor-based shape and pillar, some new shapes were also seen. The following classifications are proposed for these new shapes:

- **Capsule**, pictured in Figure 40. As the name suggests, this shape is hollow on the inside. When first viewed, this shape can make the pan appear full; however, the roof of the sample can be broken by gentle pressing to reveal the hollowness underneath.
- **Vertical half**, pictured in Figure 41A. With this shape, the pan appears half full but vertically, not horizontally. The top of the sample is flat from touching the lid.

Two new shapes, with the following descriptions, are more difficult to classify because only one of each type was available:

- **Seemingly full**, pictured in in Figure 41B. The one sample seen with this shape appeared to fill its DSC pan and was did not break when pressed with a finger.

Further prodding with a push pin revealed only a small hollow area (not pictured) and it was unclear whether it was pre-existing or caused by the push pin.

- **Capsule + vertical half**, pictured in Figure 42. This sample was found to have a vertical half shape inside a capsule shape.

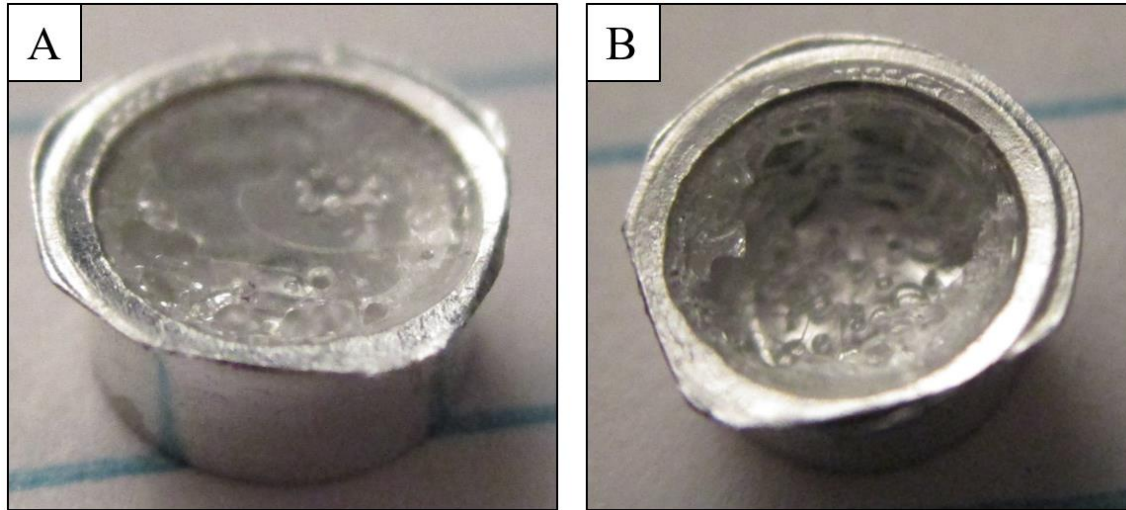


Figure 40. Example of the “capsule” sample shape, intact (A) and after the top was pushed in to reveal the hollow center (B); shown sample is Sample ID #13B.

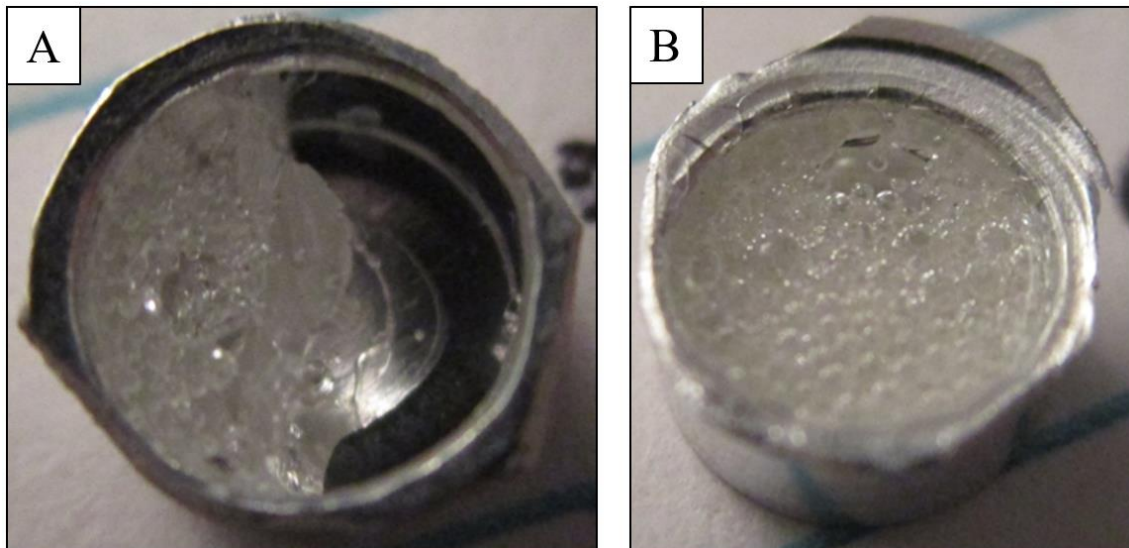


Figure 41. Examples of the “vertical half” (A; Sample ID #7B) and “seemingly full” (B; Sample ID #25B) sample shape.

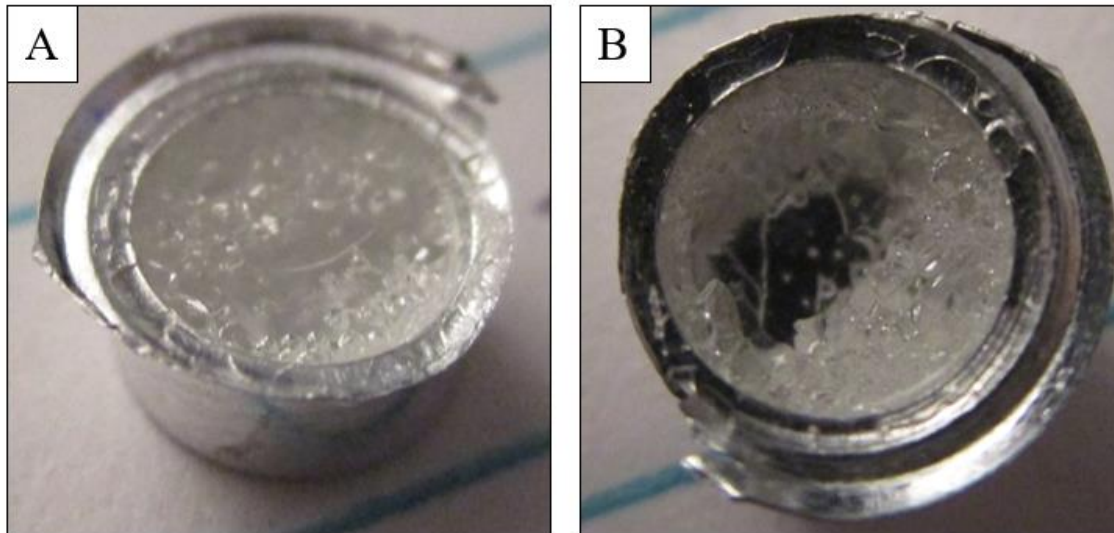


Figure 42. A sample with both a capsule and vertical half shape, intact (A) and after the top was pushed in to reveal the hollow half inside (B); shown sample is Sample ID #24B.

4.3.2.2 Shape Distribution and Properties

The distribution of shapes from Study 2 is shown in Figure 43.

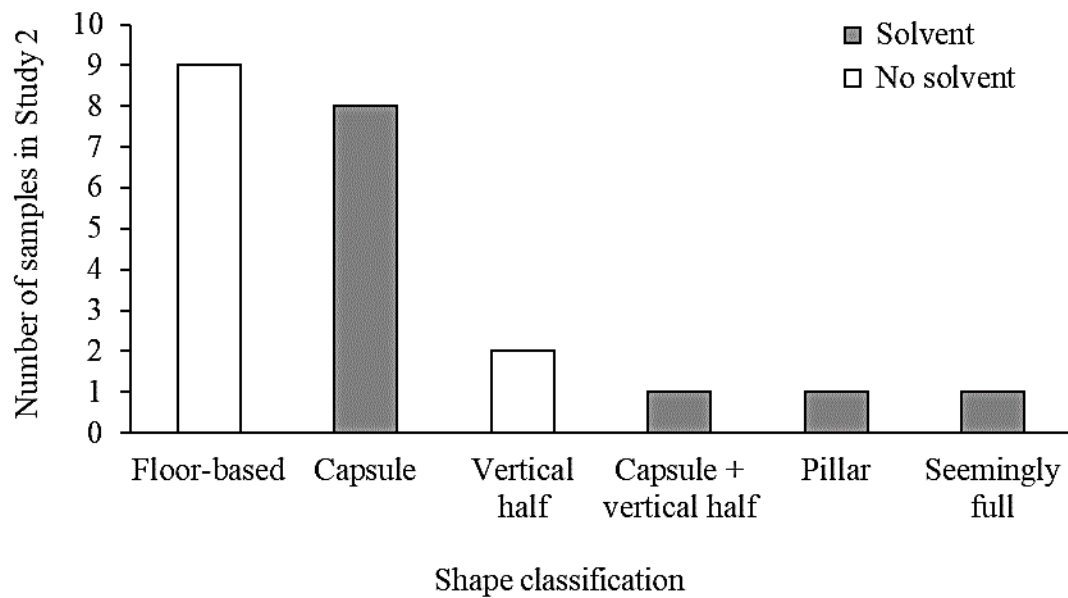


Figure 43. Shape distribution in Study 2. Most solventless samples have a floor-based shape. Most solvent-containing samples have a capsule shape.

In this study it is clearly seen that solvent-containing samples have different shapes from solventless samples. An additional finding is that shape is associated with mass of sample in the DSC pan; the following is a summary of the occurrence of shapes in Study 2 for the investigated pan loadings.

4 mg: floor-based, pillar

10 mg: floor-based, capsule

15 mg: vertical half, capsule + vertical half, seemingly full

If results from Study 1 were also added to this list, then the 4 mg condition would also have the coated walls shape and the shape of the outlier sample.

4.3.2.3 Additional visual data

In the process of documenting sample shapes in DSC pans, leakage from some pans was noted. These leakages varied in their extent, as shown in Figure 44.

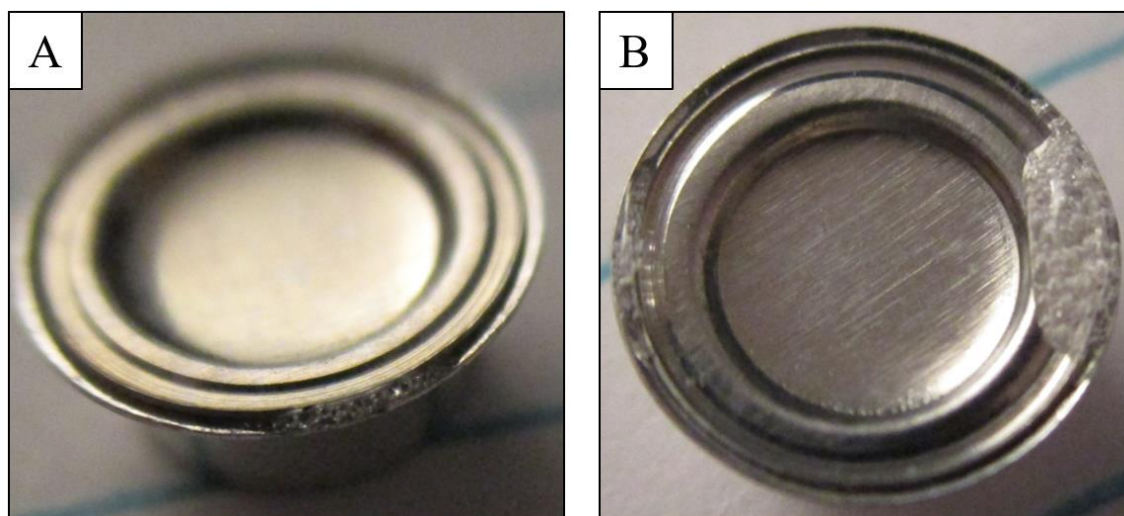


Figure 44. Examples of small (A; Sample ID #22B) and large (B; Sample ID #24B) leakage from DSC pans.

4.3.2.4 Photographs in context of variation in glass transition temperature

As stated in the previous section on DSC analyses, the highest measured T_g value was obtained from the 4 mg condition. The solventless and solvent-containing samples of the 4 mg condition are shown in Figure 45. The solventless sample has a floor-based shape and very little change in T_g from first to second heating. The solvent-containing sample, however, has a pillar shape and a large increase in T_g from first to second heating. The solvent-containing sample has a much higher T_g from second heating than the solventless sample despite having initially had a much lower T_g from first heating.

P200, 4 mg, 30 minutes of grinding



Shape: Floor-based
 H1 T_g: 90.21 °C
 H2 T_g: 91.37 °C
 Sample ID: 4B

PS200, 4mg, 30 minutes of grinding



Shape: Pillar
 H1 T_g: 81.40°C
 H2 T_g: 99.02 °C
 Sample ID: 23B

Figure 45. Photographs of the 4 mg condition, without solvent (left) and with solvent (right). The sample with the pillar shape has a much larger T_g from second heating than the sample with the floor-based shape, despite the former having had a much smaller T_g from first heating than the latter.

At least four samples (Sample ID #13B, 21B, 22B, and 24B) exhibited leakage. In each case of known leakage, greater leakage was associated with greater measured Tg on second heating. For example, the samples 13B and 14B (Figure 46) belong to the 15-minute ground, solvent-containing, 10 mg sample condition; sample 13B was found to have noticeable leakage whereas sample 14B was not. Although their Tg values measured from first heating were within a degree of each other, sample 13B with the leakage ended up having a substantially larger measured Tg value from second heating than did the sample without the leakage. This variation in Tg can be seen as the largest error bar in Figure 38, in the 15-minute condition.



Figure 46. Samples 13B (left of vertical line) and 14B (right of vertical line), which comprise the 15-minute ground, solvent-containing, 10 mg condition. For sample

13B, the leakage (top left), intact sample (top center), and pressed-in-roof sample (bottom left) are shown. For sample 14B, the intact sample (top right) and pressed-in-roof sample (bottom right) are shown. Despite similar Tg values from first heating, sample 13B with the leakage has higher Tg from second heating.

Samples 21B and 22B (Figure 47), which also exhibited leakage, belonged to the same condition: 10 mg, 30-minute ground, with solvent. Both samples have mild leakage, as seen by the bubbles along the lids; however, the leakage is greater in sample 21B than in sample 22B. Despite the two samples having identical Tg values as measured from first heating, sample 21B with the greater leakage has somewhat higher Tg as measured after second heating. This variation in Tg can be seen as the second-largest error bar in Figure 38, in the 30-minute condition.



Shape: Capsule
Heat 1 Tg: 80.18
Heat 2 Tg: 85.93
Sample ID: 21B

Shape: Capsule
Heat 1 Tg: 80.18
Heat 2 Tg: 82.15
Sample ID: 22B

Figure 47. Samples 21B (left) and 22B (right), which comprise the 30-minute ground, solvent-containing, 10 mg condition. Both have mild leakage, but the leakage is greater in sample 21B. Despite identical Tg values from first heating, sample 21B with the greater leakage has somewhat higher Tg after second heating.

The last sample known to have leakage, sample 24B, differed from its partner sample, 25B, both in its great leakage (pictured in Figure 44B) and different shape. The shape of sample 24B was a combination of capsule and vertical half as shown in Figure 42, whereas sample 25 had a seemingly full shape as shown in Figure 41B. These samples belonged to the 15 mg, 30-minute ground, solvent-containing condition. Their T_g from first heating was within a degree of each other but their T_g from second heating was over 6 °C apart from each other, with the leakage-having sample having the larger T_g value. This variation in T_g can be seen as the largest error bar in Figure 39, in the 15 mg condition.

4.3.3 Field Emission Scanning Electron Microscopy

Whereas DSC testing was performed only on PMMA samples, FE-SEM imaging was performed only on cellulose powders. Resulting FE-SEM images are presented in Figures 49 and 50. Powder particles appear clump-like, with a low aspect ratio. Smallest particle size appears to decrease, and particle uniformity appears to increase, with increased grinding time until a plateau after 30 minutes of grinding. An estimate of the smallest particle size with 60 minutes of grinding is $3\mu\text{m} \times 3\mu\text{m} \times 600\text{ nm}$ (Figure 48).

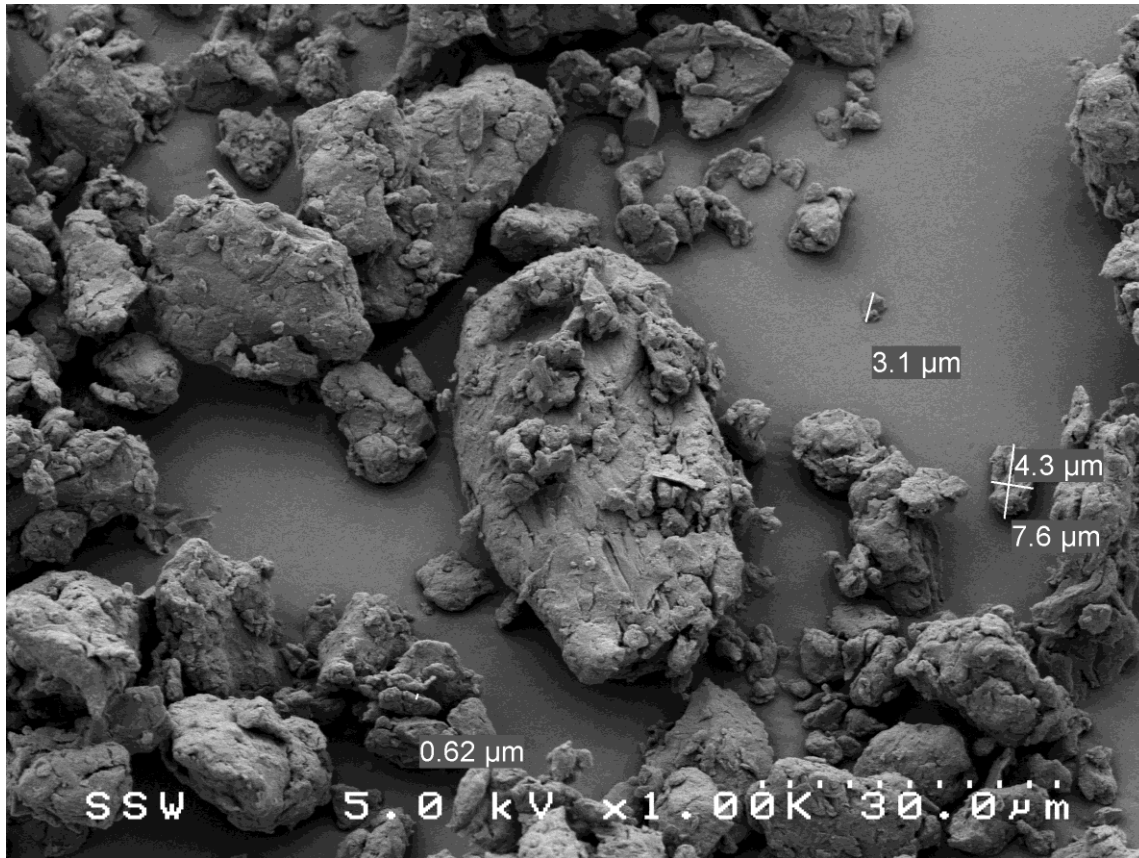


Figure 48. FE-SEM image of the 60-minute ground cellulose powder with indicated dimensions. Only microscale, low aspect ratio particles are seen.

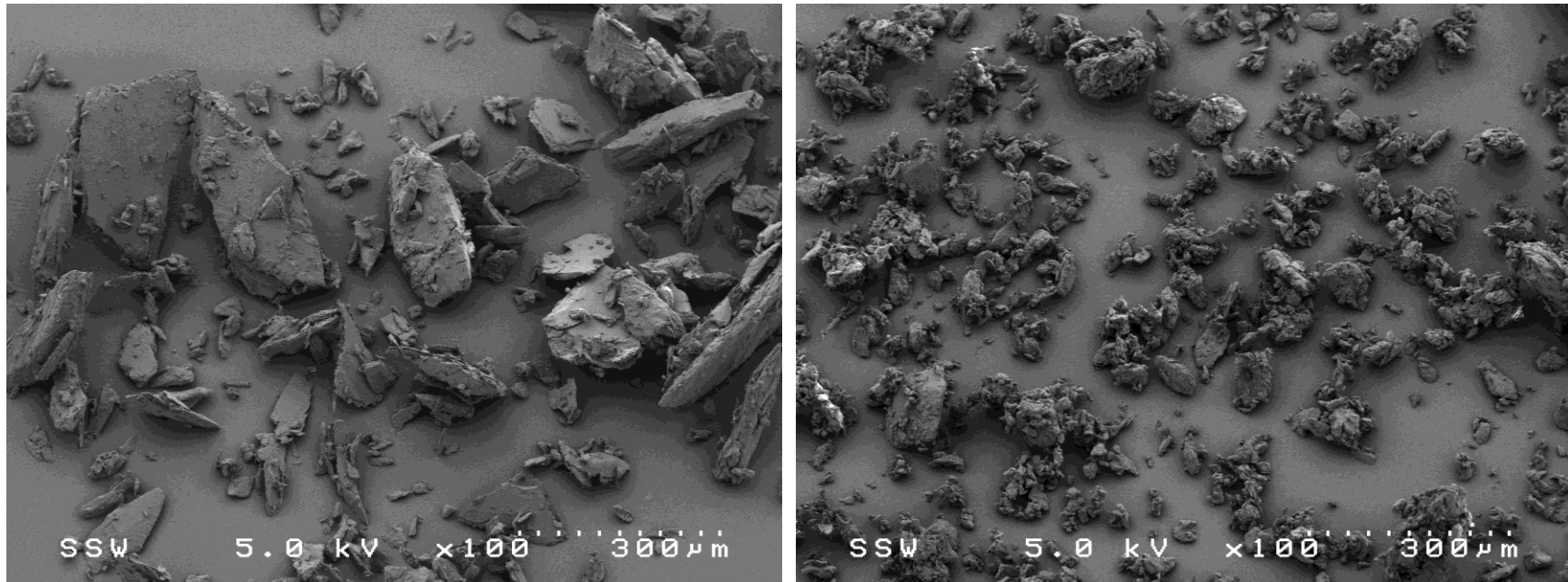


Figure 49. FE-SEM image of cellulose powder after mortar-and-pestle grinding for 3 minutes (left) and 15 minutes (right). A noticeable decrease in particle size and greater particle uniformity is seen with 15 minutes of grinding compared to 3 minutes of grinding.

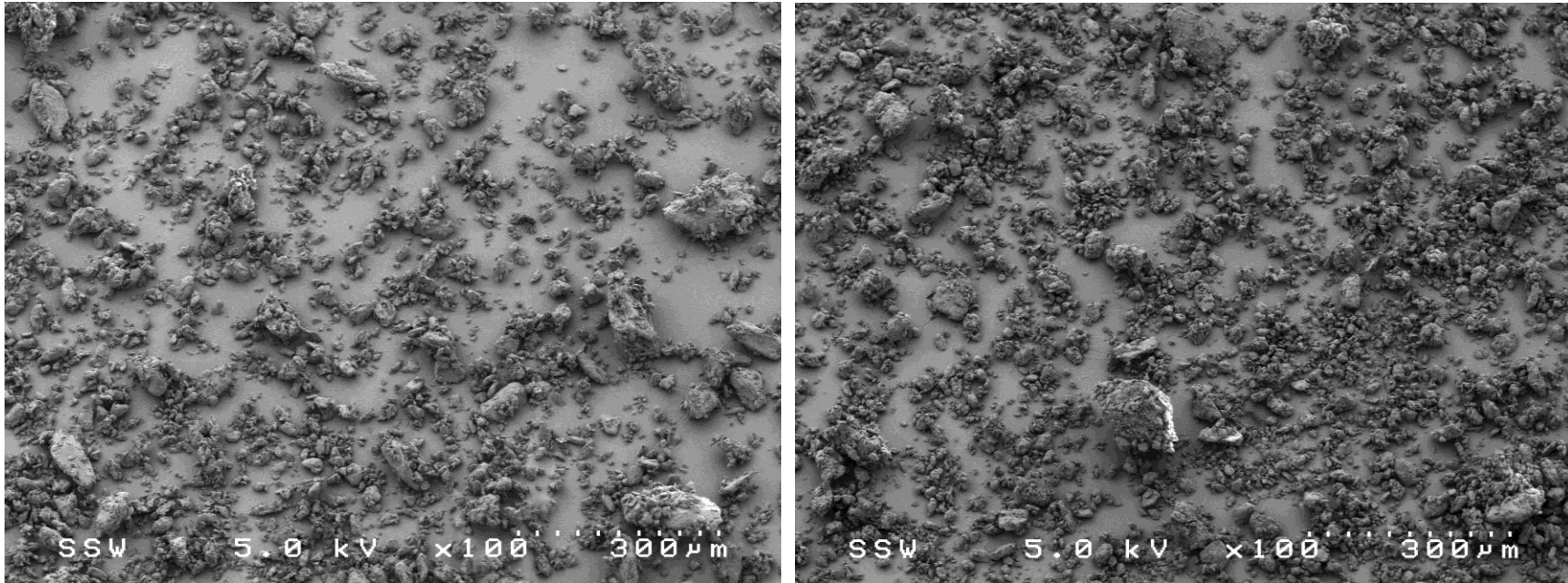


Figure 50. FE-SEM image of cellulose powder after mortar-and-pestle grinding for 30 minutes (left) and 60 minutes (right). Although these greater grinding times have smaller particles and greater particle uniformity compared to the smaller grinding times (Figure 49), a plateau appears to have been reached after 30 minutes of grinding.

4.4 Study 3

This study is essentially a repetition of Study 1 with modifications based on Study 2 that were intended to reduce variation in measured T_g within experimental conditions. Results of this study are, like in Study 1, comprised of T_g comparisons from DSC data, photographic comparisons of samples after DSC testing, and analyses that combine DSC data with photographic data.

4.4.1 Differential scanning calorimetry

Like in Study 1, this section presents comparisons based on the following measurements: T_g measured from the first heating scan, T_g measured from the second heating scan, and increases in T_g from the first to the second heating scan. Comparisons are also presented based on the following factors: presence of solvent vs. absence of solvent; composite vs. PMMA; and a first heating peak temperature of 200 °C vs. 160 °C.

4.4.1.1 Glass transition temperature from first heating

A summary of the measured T_g values from first heating for the different experimental conditions is given in Figure 51. No significant differences are seen between the 160 °C and 200 °C conditions, which is expected because these T_g values are from first heating, before the samples were exposed to those peak temperatures. Because these conditions are thus identical in the case of first heating T_g, their results have been grouped and summarized in Figure 52.

4.4.1.1.1 Solvent vs. no solvent

As previously found, T_g measured from the first heating scan is seen to be greater in the solventless materials than in the solvent-containing materials.

4.4.1.1.2 Composite vs. PMMA

No significant differences are seen between all composite and all PMMA materials based on T_g from first heating, neither in the solventless nor in the solvent-containing condition. However, composite material designated for the 200 °C first heating peak

temperature have a significantly lower Tg as measured from first heating than the PMMA material designated for that same first heating peak temperature.

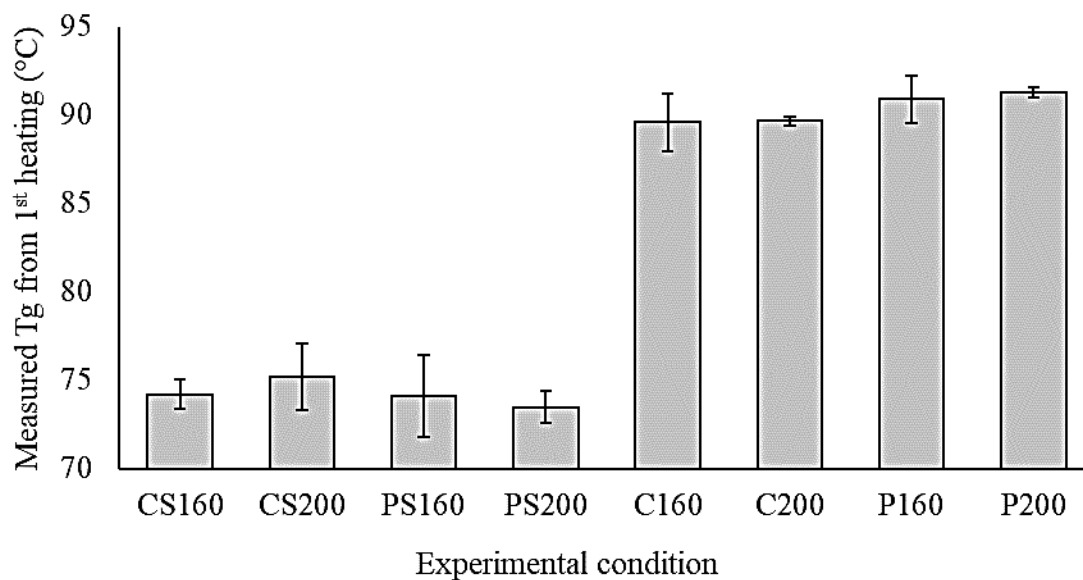


Figure 51. Comparison of experimental conditions based on Tg measured from the first heating scan. No significant difference is seen between samples designated for the different first heating peak temperatures, as expected because these results are from before the first heating peak temperature has been reached. Error bars are relatively small.

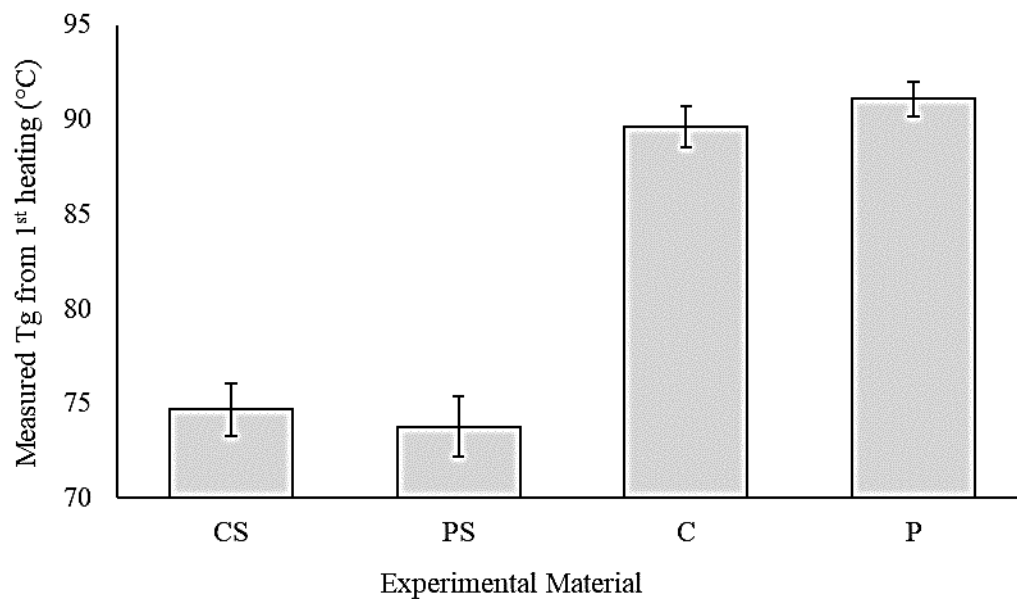


Figure 52. Comparison of Study 3 experimental materials based on T_g measured from the first heating scan. Solventless samples have a significantly greater T_g than solvent-containing samples; no significant difference is seen between equivalent composite and PMMA samples.

4.4.1.2 Glass transition temperature from second heating

A summary of the measured T_g values from second heating for the different experimental conditions is given in Figure 53.

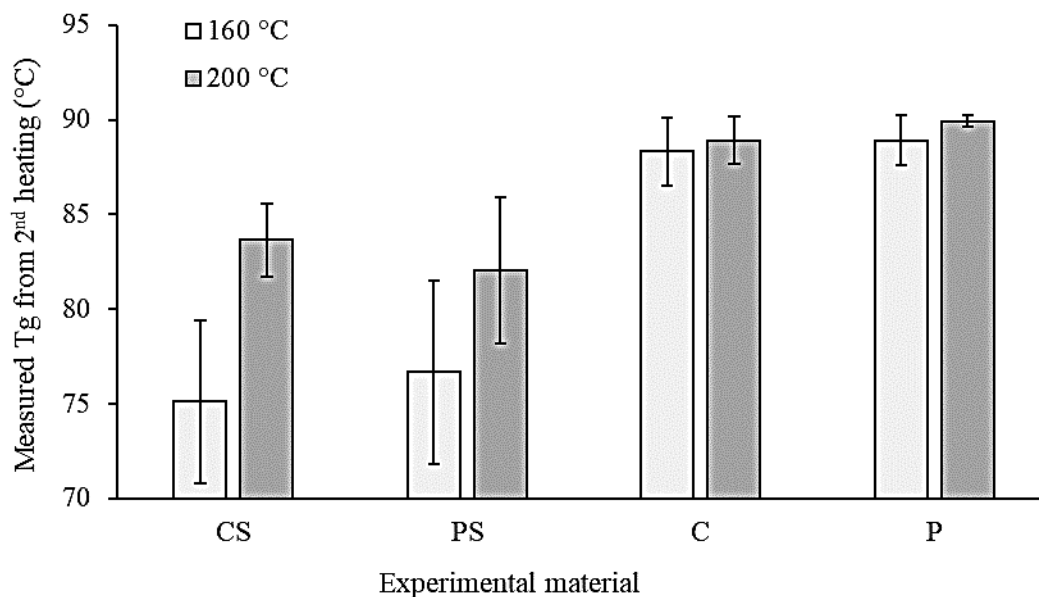


Figure 53. Comparison of Study 3 experimental materials based on Tg measured from the second heating scan, after a first heating peak of either 160 °C or 200 °C. A significant difference between the 200 °C and the 160 °C condition is seen among the solvent-containing composite samples. No such difference is seen among the solvent-containing PMMA samples or among the solventless samples.

4.4.1.2.1 Solvent vs. no solvent

Unlike in Study 1, a significant difference is seen between the solventless and solvent-containing samples based on Tg from second heating, with solventless samples having higher Tg values. Like in Study 1, however, the standard deviations are significantly greater in the solvent-containing conditions than in the solventless conditions.

4.4.1.2.2 Composite vs. PMMA

As in the results from Study 1, no significant differences in Tg measured from second heating are seen between the composite and PMMA samples if compared within the same first heating peak temperature condition. If comparing between the two different first heating peak temperature conditions, however, a significant difference is seen between the CS200 and the PS160 conditions, with the former having a significantly greater Tg measured from second heating.

4.4.1.2.3 160 °C vs. 200 °C

In the solvent-containing condition, the composite has a significantly greater measured T_g after a first heating peak temperature of 200 °C than after a first heating peak temperature of 160 °C. The same is not true for the solvent-containing PMMA material.

With solventless composite and PMMA materials, no significances are seen between the 160 °C and 200 °C conditions in terms of T_g measured from second heating.

4.4.1.3 Increase in glass transition temperature from first to second heating

A summary of the increase in measured T_g from first to second heating for the different experimental conditions is given in Figure 54.

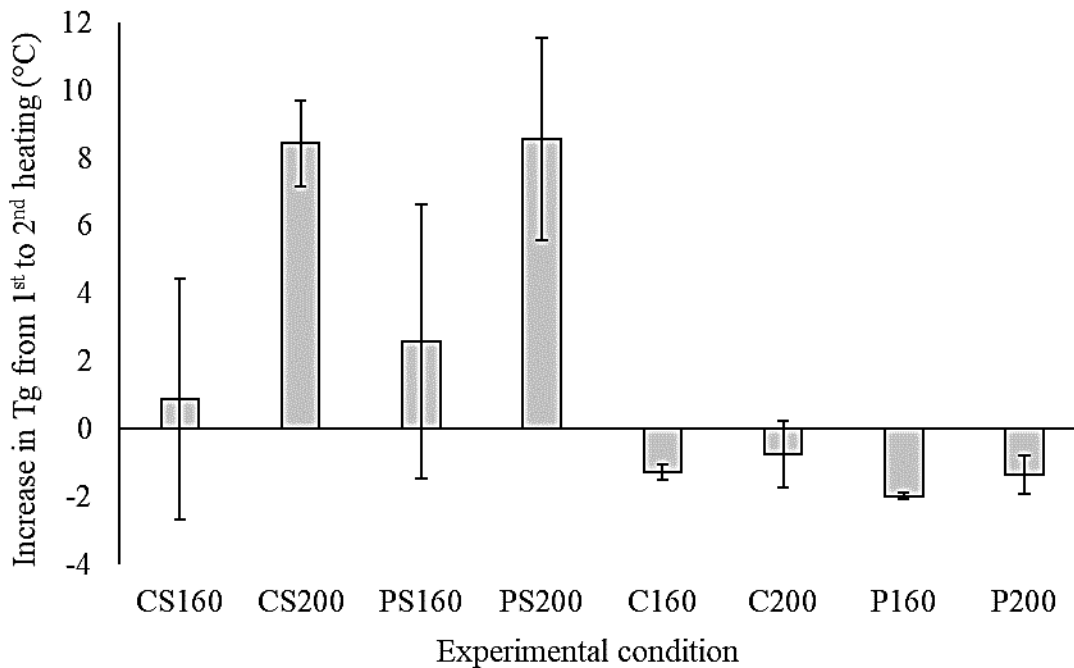


Figure 54. Comparison of differences between T_g measured from the second heating scan and T_g measured from the first heating scan. The increase in T_g from first to second heating is significantly greater in the 200 °C condition than in the 160 °C

condition for solvent-containing composite samples but not for solvent-containing PMMA samples. See text.

4.4.1.3.1 Solvent vs. no solvent

A significant difference in Tg increase from first to second heating is seen between the solventless samples and the solvent-containing samples in the 200 °C condition, with the latter having the larger increase. A significantly greater increase is also seen for the PS160 condition compared to the P160 condition; this finding was not seen in Study 1. Unlike in Study 1, no significant difference is seen between the CS160 and P160 conditions. As in Study 1, significantly more variation in Tg increase from first to second heating is seen in solvent-containing samples compared to solventless samples.

When all solvent-containing samples are grouped and compared with a group of all solventless samples (Figure 55), solvent-containing samples can be seen to have a significant increase in Tg from first to second heating whereas solventless samples can be seen to have a significant decrease from first to second heating. However, unlike in Study 1, in which all solvent-containing samples exhibited an increase in Tg from first to second heating, in Study 2 some samples (two in the CS160 and one in the PS160 condition) exhibited a slight decrease in Tg from first to second heating.



Figure 55. Comparison of solvent-containing and solventless samples based on differences between Tg measured from first heating and from second heating. Solvent-containing samples had a significant increase in Tg whereas solventless samples had a significant decrease in Tg from first to second heating.

4.4.1.3.2 Composite vs. PMMA

No significant difference is seen in Tg increase from first to second heating between composite and PMMA samples in the solvent-containing samples if comparing within the same temperature condition. However, if comparing between temperature conditions, the increase in Tg from first to second heating is seen to be significantly greater in the CS200 condition compared to the PS160 condition, and in the PS200 condition compared to the CS160 condition.

In the solventless samples, the P160 condition has a significantly smaller increase (or rather, a larger decrease) in Tg from first to second heating than both solventless composite samples. No significant differences are seen among the P200 condition and the solventless composite samples.

4.4.1.3.3 160 °C vs. 200 °C

In the solventless samples, no significant difference between the two first heating peak temperature conditions are seen based on increase in Tg from first heating to second heating, unless the significant difference between C200 and P160 is included.

In the solvent-containing samples, the CS200 condition has a significantly greater increase in Tg from first to second heating than CS160, as well as PS160. There is no significant difference in increase in Tg from first to second heating between the PS200 condition and the PS160 condition.

4.4.1.4 Effect of first heating peak temperature on composite evaluation using a fixed reference value

It was previously shown (Figures 51 and 53) that no significant differences in Tg are seen between the currently discussed composite material and PMMA exposed to the same

conditions (such as presence/absence of solvent and the same first heating peak temperature in DSC testing), neither as measured from first nor second heating. However, if the composite material is instead compared to a fixed value, such as to a supplier's reported T_g value for PMMA, then the same composite material can sometimes appear differently effective depending on the first heating peak temperature used and whether T_g is measured from first or second heating. The numbers on the figures (Figures 56 and 57) illustrating these comparisons are negative because all of the current composite material's measured T_g values are less than the supplier's reported T_g value of 105 °C for PMMA.

4.4.1.4.1 Evaluation based on T_g from first heating

When using T_g from the first heating scan to compare a composite material to a fixed value, as shown in Figure 56, no significant differences are seen between the two first heating peak temperature conditions. Of note, the T_g value obtained from first heating is measured before the material has reached the assigned first heating peak temperature.

A difference is only seen between the solventless and solvent-containing samples, the former of which are closer in their measured T_g value to the reported PMMA value.

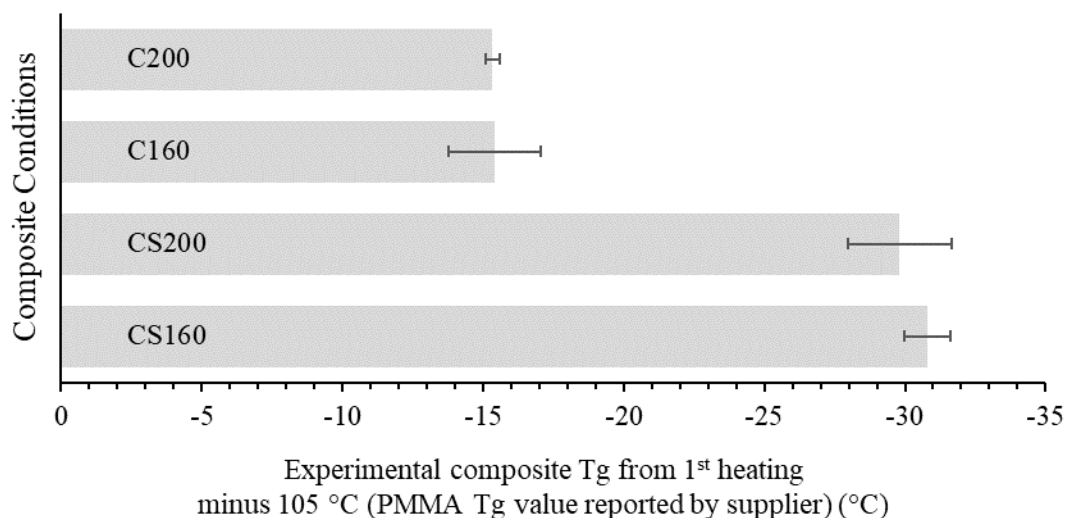


Figure 56. Comparison of PMMA-cellulose composites' glass transition temperatures from first heating relative to a fixed PMMA value. Solventless samples can be seen to be significantly closer in T_g to the fixed T_g value than the solvent-

containing samples. No significant difference between the solvent-containing composite samples designated for the two different first heating peak temperatures is seen if using Tg measured from first heating.

4.4.1.4.2 Evaluation based on Tg from second heating

In the solvent-containing samples, the composite material tested with a first heating peak temperature of 200 °C is seen to have a Tg measured from second heating that is significantly closer to the reported PMMA value than the composite material tested using a first heating peak temperature of 160 °C, as shown in in Figure 57. In other words, when using the second heating scan to measure Tg, the same material can appear significantly different from itself depending on the first heating peak temperature used.

In the solventless samples, no significant difference is seen between the two first heating peak temperature conditions based on Tg from second heating.

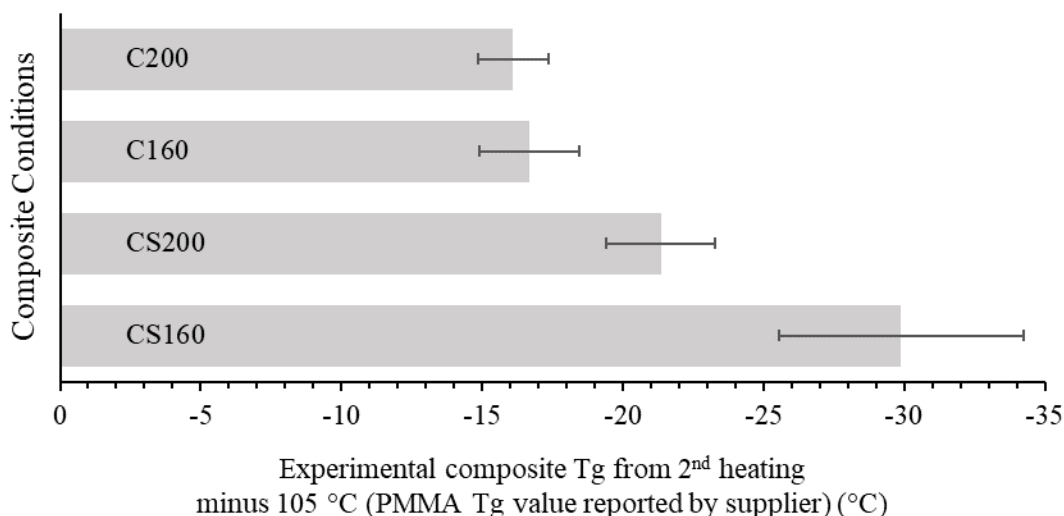


Figure 57. Comparison of PMMA-cellulose composites' glass transition temperatures from second heating relative to a fixed PMMA value. Solventless samples are still significantly closer in Tg to the fixed value than the solvent-containing samples. However, the solvent-containing composite tested using a first heating peak temperature of 200 °C has a significantly closer Tg to the fixed value (by approximately 9 °C) compared to the solvent-containing composite tested using

a first heating peak temperature of 160 °C, despite them both being samples of the same material.

4.4.2 Visual analysis of samples after DSC testing

In this final visual analysis, subtypes of a previous seen shape are identified, shape trends are described and, again, shapes are correlated with measured T_g values.

4.4.2.1 Sample appearance before DSC testing

No correlation was noticed between sample appearance before DSC testing and the samples assumed shape after DSC testing. Photographs of all Study 3 samples before DSC testing are available in Appendix C, alongside photographs after testing.

As mentioned previously, solvent-containing samples tend to be white compared to solventless samples, which are clear. Also, solvent-containing samples are airy and fragile, whereas solventless samples are compact and clear.

4.4.2.2 Distribution and variations of shapes after DSC testing

The main shapes seen in Study 3 were all shapes that were seen in Study 1 and Study 2. All solventless samples had a floor-based shape and, with the exception of one sample, all solvent-containing samples had a capsule shape. The exception in the solvent-containing category was a sample with a coated walls shape.

The capsule-shaped samples in Study 3 had some variations, however. Instead of one hollow compartment, some had two or even three due to inner walls, as shown in Figure 58. Thus, two subtypes of capsule shapes are presented:

- **Single-compartment capsules (SC capsules)**, which are identical to the capsule shapes described previously, with a single inner hollow area.

- **Multi-compartment capsules (MC capsules)**, which are capsule shapes with the inner hollow area divided by one or more walls. Sometimes this division is uneven. During the pressing of the roof to reveal the hollowness of the capsule shape, such walls can be broken. However, it appears these walls can still be detected from the thick line of sample they leave behind on the floor of the pan.

As shown in Figure 59, most capsule shapes seen in Study 3 were of the multi-compartment variety; in contrast, no multi-compartment capsules were seen in Study 2. As shown in Figure 60, samples with single-compartment capsule shapes are seen to have significantly greater increases in T_g from first to second heating than samples with multi-compartment capsule shapes, when compared within their first heating peak temperature category.

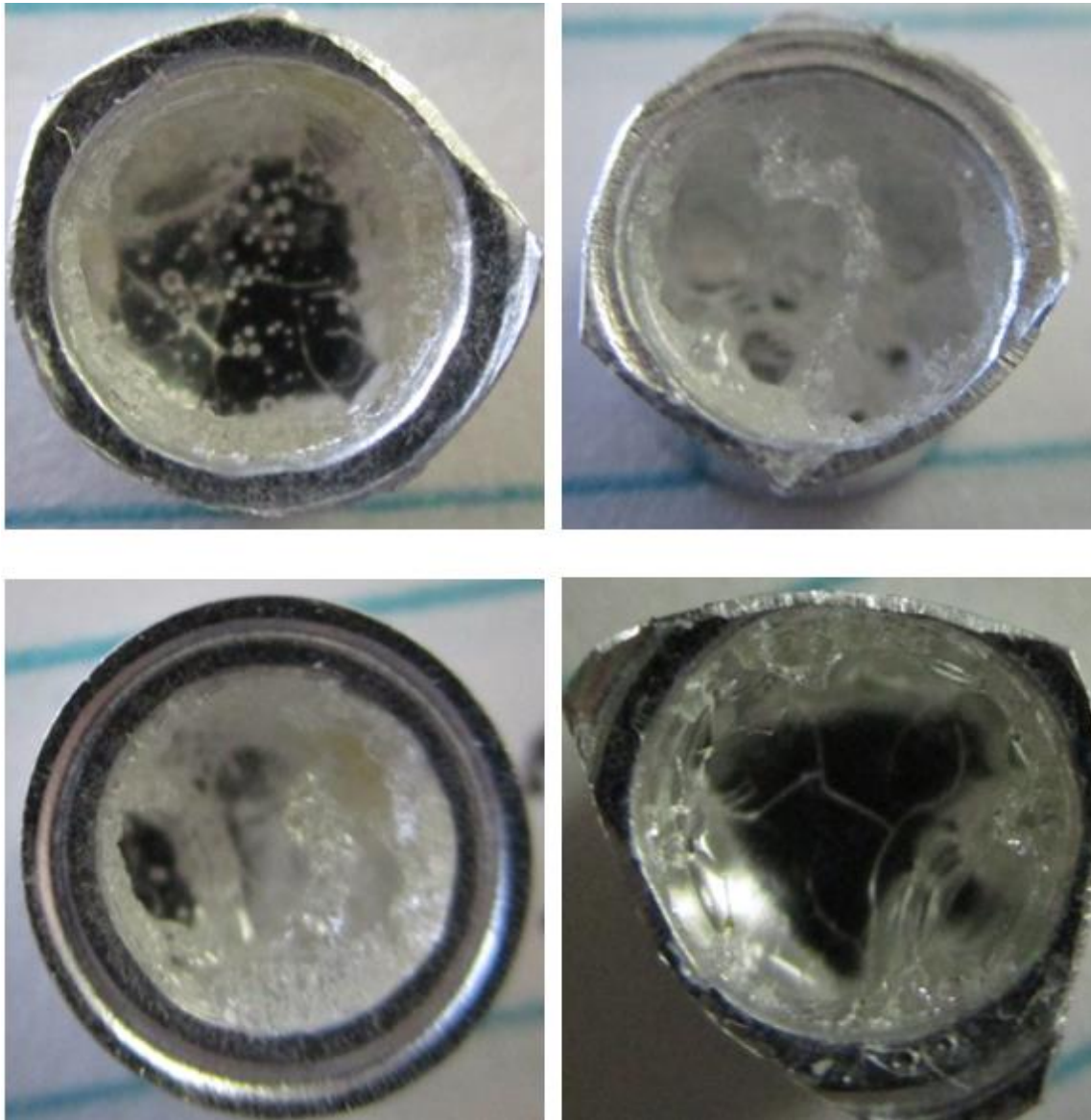


Figure 58. Examples of capsule shapes seen in Study 3: capsule with one single compartment (top left), capsule with two compartments (top right), capsule with three compartments (bottom left), and capsule with two unequal-sized compartments (bottom right). All photos were taken after the roof of the sample was removed by gentle pressing to show the inner hollowness.

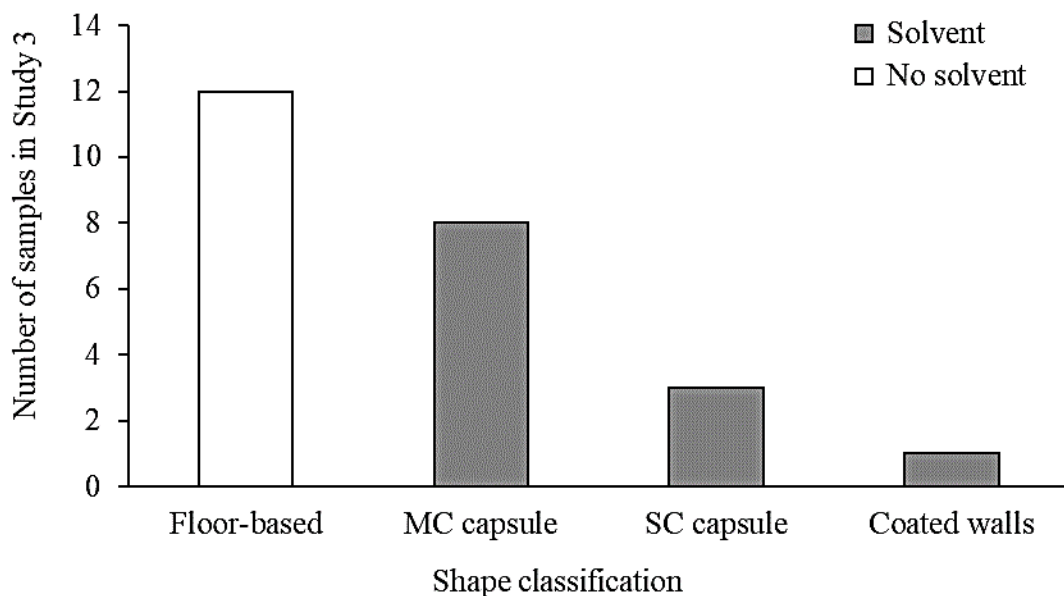


Figure 59. Shape distribution in Study 3. All solventless samples had a floor-based shape. Most solvent-containing samples had a multi-compartment capsule shape.

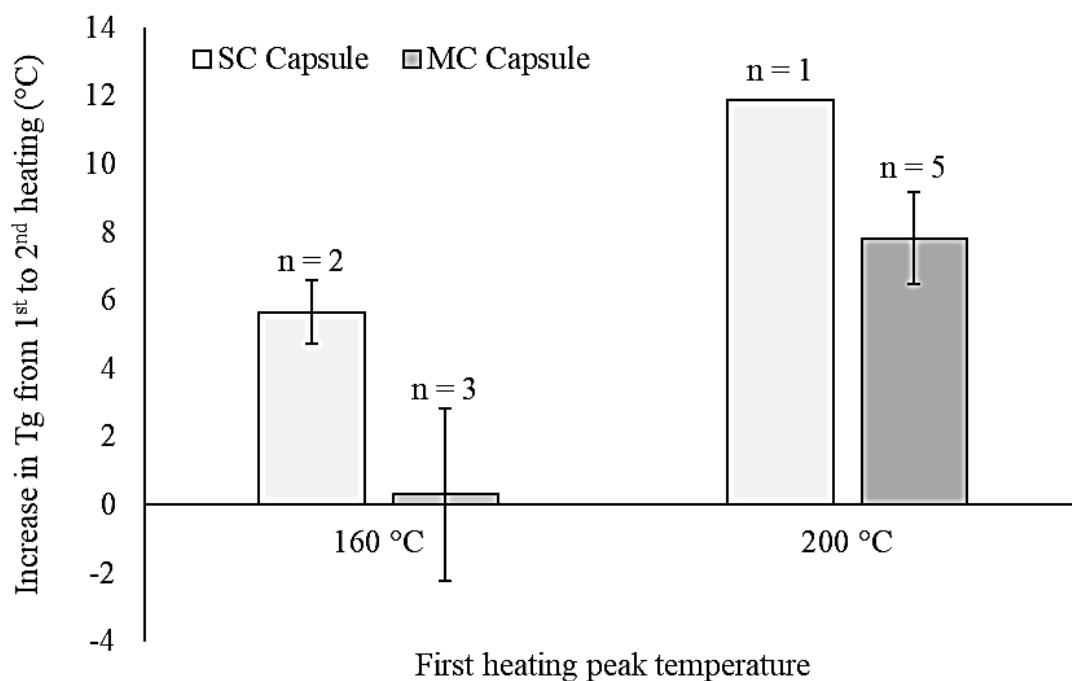


Figure 60. Comparison of the single-compartment and multi-compartment capsule shapes based on increase in Tg measured from the first heating scan to the second heating scan and using a first heating peak temperature of either 160 °C or 200 °C.

The number of samples in each category is indicated. The single-compartment capsule shape is associated with a significantly greater increase in Tg from first to second heating compared to the multi-compartment capsule shape.

4.4.2.3 Visual analysis in context of variation in glass transition temperature

The largest error bars in Figure 53 correspond to the CS160, PS160, and PS200 conditions.

In the CS160 and PS200 conditions, two of the three samples were multi-compartment capsules and one was a single-compartment capsule. In both cases, the Tg on second heating of the single-compartment capsule sample was markedly greater than that of the other two samples.

In the PS160 condition, two samples have a capsule shape and one has a coated walls shape. The two capsule shape samples can be seen to have a higher Tg on second heating than the sample with the coated walls shape. Of these two capsule shape samples, one is a multi-compartment capsule and the other is a single-compartment capsule that had sustained leakage. Although the latter does not have the greater Tg on second heating as would be expected from Study 2, it does have the greater increase in Tg from first to second heating. This latter sample had started from a markedly lower Tg on first heating than the former sample but ended up with a Tg on second heating that was comparable to the former sample. In each case involving single-compartment samples in Study 3, these samples had the highest increase in Tg from first to second heating within the three samples of their experimental condition.

In the CS200 condition, which had a smaller error bar in Figure 53 than the other solvent-containing conditions described above, all three samples were multi-compartment capsules. However, unlike in Study 1 where greater yellowing was associated with lower Tg from first and second heating, in the CS200 condition of Study 3 the two yellow samples had higher Tg values from both first and second heating than did the one non-yellow sample of that condition. Consistent with Study 1, however, is the C200 condition

of Study 3, where greater yellowness was indeed seen to be associated with lower Tg values from first and second heating.

Unlike in Study 1, no association between bubble size and Tg from first and second heating is seen in Study 3.

4.4.3 Selective Tg analysis based on visual data

In Study 3, no shape type was found to be overlapping between the solventless and solvent-containing samples; therefore, these samples were analyzed separately.

Because all of the solventless samples had a floor-based shape, grouping and comparing the floor-based shape solventless samples would yield the same results as already discussed based solely on DSC results.

Regarding solvent-containing samples, the most common shape encountered was the multi-compartment capsule. Samples with this shape are compared in Figure 61.

Regarding Tg measured from first heating, no significant difference is seen between the CS160 and CS200 conditions, as expected because the first heating peak temperature has not yet been reached. Comparing the PS200 and PS160 conditions, the PS160 condition appears to have a higher Tg on first heating than the PS200 condition; however, because only one PS160 sample is available, the significance of this difference is unknown. No significant differences are seen in Tg measured from first heating between the PS200 condition and the composite conditions (CS160 and CS200).

Regarding Tg measured from second heating, the composite appears to have a lower Tg than PMMA when a first heating peak temperature of 160 °C is used, and then a higher Tg than PMMA when a first heating peak temperature of 200 °C is used. The latter difference is statistically significant, whereas the significance of the former difference is unknown because only one sample is available in the PS160 condition.

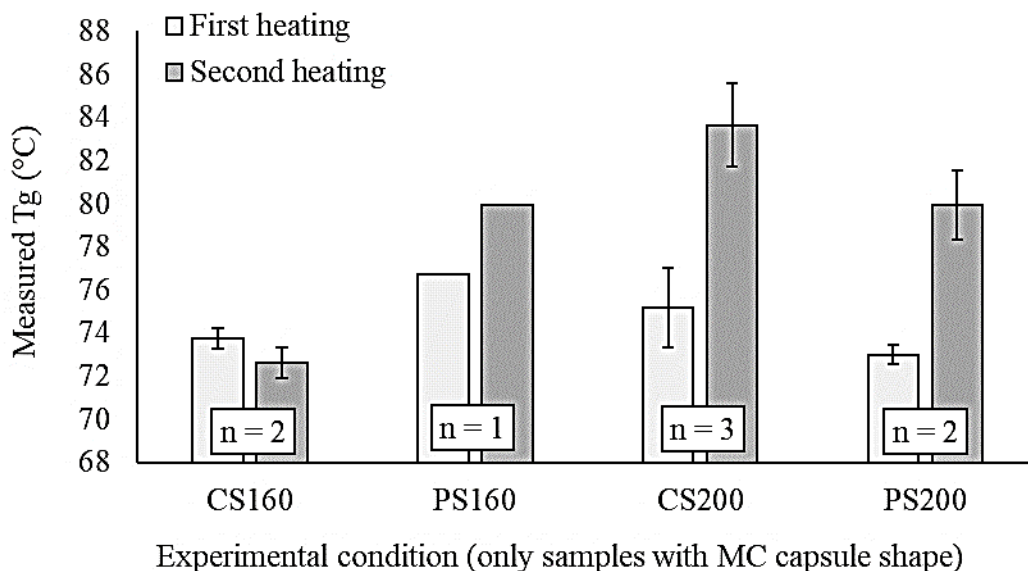


Figure 61. Comparison of solvent-containing experimental conditions based on Tg from first and second heating and using only samples with the multi-compartment capsule shape. Number of samples in each condition is indicated. Composite samples have a significantly greater Tg than PMMA samples as measured from second heating when tested using a first heating peak temperature of 200 °C. See text.

4.5 Open pan heating

This additional study investigated the shapes of a solventless PMMA sample and a solvent-containing composite sample during heating in a DSC pan without a lid.

Before heating, as shown in Figure 62, both samples appear as a pile of fragments; the solventless PMMA sample is clear and the solvent-containing composite sample is white.

Partway through heating, as shown in Figure 63, the solventless PMMA sample appears to be in a more compact form than before heating, whereas the solvent-containing sample appears to have expanded to now take up more of the DSC pan.

Finally, at the end of heating, as shown in Figure 64, both samples are seen to have a concave shape, despite one having solvent and the other not. The shapes do not fit well into the shape classification described earlier, having too much wall involvement and

concavity for the floor-based shape and too little wall involvement relative to floor involvement for the coated walls shape. Non-uniform yellowness is seen in the composite sample.



Figure 62. Samples before heating. On the left is a sample of neat PMMA without solvent; on the right is a solvent-containing composite sample.



Figure 63. Samples at the same time partway through heating. On the left is neat PMMA without solvent; on the right is the solvent-containing composite. The latter is seen to have expanded.

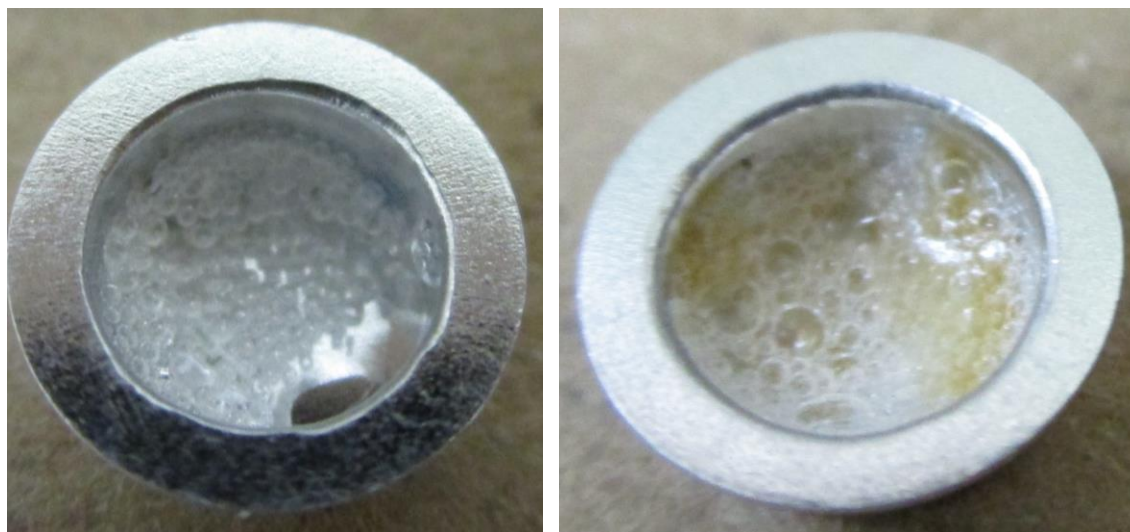


Figure 64. Samples after heating for the same amount of time. On the left is neat PMMA without solvent; on the right is the solvent-containing composite. Both samples have a concave shape. Such a shape was not seen in the current work's DSC samples, which were sealed hermetic lids. These samples are too concave for the floor-based shape and do not have as much wall contact as the coated walls shape.

Chapter 5

5 Discussion

Overall, the samples made by mortar-and-pestle grinding were found to be microscale with low aspect ratio, first heating peak temperature was found to have a greater influence on some experimental conditions than others, no significant differences between composites and PMMA samples were found, and visual analysis allowed for the identification of sample shapes after DSC testing that are associated with various T_g trends from first to second heating.

5.1 Evaluation of mortar-and-pestle grinding

The use of a mortar and pestle has been found unsuitable for PMMA/cellulose nanocomposite preparation in the current work. Much of the advantages of nanocellulose comes from its great aspect ratio [32], and FE-SEM imaging has shown that of mortar-and-pestle-ground cellulose powder consists of low aspect ratio of particles. Furthermore, FE-SEM imaging has shown that resulting powder particles are microscale, not nanoscale, even after one hour of mortar-and-pestle grinding. Nevertheless, this is not to say that mortar-and-pestle grinding is unsuitable for all nanocomposite preparation, because in a recent study involving nanocomposites of high molecular weight polyethylene and graphene nanoplatelets, mixing by mortar and pestle followed by compression moulding was found to be sufficient for nanocomposite preparation [77].

5.2 Influences on glass transition temperature

The influence of DSC measurement technique and of various sample features on measured glass transition temperature are discussed.

5.2.1 First heating vs. second heating

Standard deviations of T_g values obtained from the first heating scan were generally less than those from the second heating scan, especially for solvent-containing samples, suggesting that the first heating scan is a more reliable source of T_g values for such

samples especially. This finding comes in contrast to the finding that PMMA/cellulose studies have generally reported using the second heating scan for their Tg measurements. I question the fairness of using the second heating for solvent-containing composites to describe their Tg, because after some of the solvent is gone during first heating they are no longer the same samples that they were at the beginning of testing. In a hypothetical situation, if a customer were sold a solvent-containing composite with only the second heating Tg written on the label, then they will likely be disappointed when they see the composite becoming rubbery at a lower temperature, which would be more similar to the Tg measured from first heating.

5.2.2 First heating peak temperature

The influence of the first heating peak temperature on Tg values measured from the second heating scan was clearly seen in the solvent-containing samples, especially the composites. Interestingly, there was a significant difference between the two first heating peak temperature conditions based on Tg measured from second heating for solvent-containing composites but not for solvent-containing PMMA samples. Therefore, I question the validity of the assumption of Dong et al., who assumed that the difference in solvent retention between their composites and PMMA samples in their study were negligible [60]. In the current work, composites are seen to have a greater sensitivity to the first heating peak temperature than PMMA samples.

This finding may possibly be due to increased solvent loss in the composite samples. However, this explanation would contradict previous reports and proposed explanations of cellulose being able to impart gas barrier properties and impeding the escape of volatile products of decomposition, increasing thermal stability, which would instead suggest that evaporated solvent would be more trapped in composite samples [49][58]. Increased solvent retention in composites may have been due to tortuosity provided by the cellulose; tortuosity can be thought of as the path length the solvent molecule would need to take to exit the composite sample – the path length is increased because the solvent cannot move through the cellulose particles and has to go around them, which manifests itself as longer diffusion time [78][79]. If greater amounts of solvent were indeed found in the composite samples, then the greater Tg values may be explained by

greater reactions between the cellulose and the solvent at the higher temperatures, or longer high temperature time. This possibility would be similar to the finding that PMMA can react with a certain solvent to result in greater Tg [33].

In any case, the finding of a difference in solvent-containing composite response to higher first heating peak temperature compared to solvent-containing PMMA is especially clear in the selective Tg comparison using only multi-compartment capsule shapes (Figure 61). In this comparison, the solvent-containing composite sample has a lower Tg than solvent-containing PMMA when tested using a first heating peak temperature of 160 °C but the opposite is true when the first heating peak temperature used is 200 °C. However, due to exclusion of the coated-wall-shaped sample and the single-compartment-capsule-shaped samples, the number of compared samples is low in this comparison so it may be that the findings are just coincidental. Further studies would need to be done to determine the importance of grouping samples by shape category.

5.2.3 Sample geometry

A summary of sample shape classification for samples seen in post-DSC visual analysis is given below:

1. **Floor-based shape**, which has most of its contact with the floor of the pan and has a convex shape.
2. **Coated walls shape**, which appears to be climbing up the walls from the pan floor, in most directions. It can be distinguished from the floor-based shape by its lack of convexity and its range of wall contact around the floor and up the wall.
3. **Pillar shape**, which is like a pillar that grew from the pan floor and supports the lid of the pan. This pillar appears to have an approximately circular region of flatness right under the pan lid.
4. **Capsule**, which, as the name suggests, is hollow on the inside. When first viewed, this shape can make the pan appear full; however, the roof of the sample can be broken to reveal the hollowness by gentle pressing. There are two types of capsule shapes: single-compartment capsules and multi-compartment capsules.

- a. **Single-compartment capsules (SC capsules)**, which are identical to the capsule shapes described previously, with a single inner hollow area.
 - b. **Multi-compartment capsules (MC capsules)**, which are capsule shapes with the inner hollow area divided by one or more walls. Sometimes this division is uneven. During the pressing of the roof to reveal the hollowness of the capsule shape, such walls can be broken. However, it appears these walls can still be detected from the thick line of sample they leave behind on the floor of the pan.
5. **Vertical half**, with which the pan appears half full but vertically, not horizontally. The top of the sample is flat from touching the lid.

Two of the shapes, with the following descriptions, are more difficult to classify because only one of each type was available:

1. **Seemingly full**, which appears to fill its DSC pan and does not break when pressed with a finger.
2. **Capsule + vertical half**, which is found to have a vertical half shape inside a capsule shape.

Only solvent-containing samples were found to exhibit the pillar, capsule, coated walls, seemingly full, and capsule + vertical half shapes. Both solvent-containing and solventless samples were seen to exhibit the floor-based shape. The finding of none of the above shapes being exhibited when samples were heated without a lid suggests that these shapes might be more relevant to studies involving hermetic lids, which the current work used.

Generally, highest increases in T_g from first to second heating were found in samples with the pillar, coated walls, and capsule shapes, particularly compared to floor-based shapes. These samples have a smaller proportion of sample along the bottom of the DSC pan and larger amounts of sample touching the walls and lid of the DSC pan. A possible explanation for this trend is that these sample shapes exhibited greater thermal lag than floor-based shapes. In other words, these shapes would take longer to heat up than samples with the floor-based shape and would consequently result in measurements

indicating that the glass transitions took place later during the heating scan (i.e. greater measured T_g). Reasons for this possible heating delay in those samples are discussed below. Of note, shifting of samples during DSC testing has been previously reported; this shifting was suggested to result in altered heat transfer from change in contact between the sample and DSC pan walls, resulting in inaccuracies of the resulting thermal data [80].

5.2.3.1 Sample heights/thicknesses

Sample heights/thicknesses likely affected the T_g results. Heat is transmitted into DSC pans through their bottom via a thermoelectric disk; the walls and lids of DSC pans have no direct contact with a heating source [81]. Therefore, to minimize thermal lag, samples should ideally be thin and in good contact with the bottom of the DSC pan; unideal contact with the bottom of the DSC pan increases thermal lag [82][83]. The temperature within a sample varies proportionally to the square of the sample's thickness; therefore, the thicker the sample, the greater the thermal lag [84]. In the different shapes seen in the current work, sample thickness could also be interpreted as sample height, because it represents the longest distance that the heat has to be transferred, having initially been taken in from the sample's bottom. Greater sample heights were achieved in the pillar, coated walls, and capsule shapes than in the samples with the floor-based shape, resulting in greater required times for heat transfer.

5.2.3.2 Contact with DSC pan walls and lids

Although those taller sample shapes made contact with the walls and lids of the pans, which were made from a relatively highly thermally conductive material (aluminum), it is possible that this contact actually increased thermal lag, through heat loss, rather than decreased it. Heat may have been lost from the walls and lids of the pans due to the purge gas on the outside, constantly flowing past the pans and stealing heat. Thus, in samples with more contact with the pan walls and lids, more heat may have been lost and, consequently, more heat input would have been required for those samples to transition from a brittle to rubbery state, which would be seen on measurements as a higher T_g for those samples.

5.2.3.3 A note on sample thickness and thermal conductivity

Thickness of samples in thermal analysis is particularly important in materials with relatively low thermal conductivity, which the materials in the currently work likely were since they were polymer-based [85]. Given that addition of cellulose has been reported to increase thermal conductivity in at least one polymeric material, it is possible that the composites in the current work had greater thermal conductivity than the PMMA samples [86]. If thermal conductivity is indeed different between composite and PMMA samples, then even in samples with ideally equal thicknesses and shapes, thermal lag would be different between the two categories of samples (being less in the composite samples due to their higher thermal conductivity), resulting in PMMA samples have greater measured T_g values. It may therefore be that a fair DSC test would require determining differences in thermal conductivity in advance and performing DSC testing on slightly thinner PMMA samples than composite samples, to account for differences in thermal conductivity. Thermal conductivity of various samples can be determined by DSC testing based on data from indium melted on its own and indium melted on top of the experimental material [87].

Of note, it is possible that studies on polymer composites and polymer nanocomposites with findings of low improvements in T_g may have had differences in thermal conductivity among their samples interfere with T_g measurement, especially in samples with higher filler loadings. Typically, in PMMA/cellulose nanocomposite studies, lower T_g values in samples with higher filler loadings are attributed to filler agglomeration. If the filler increases thermal conductivity, it may be possible that the increased thermal conductivity rather than filler agglomeration is the main contributor to the reduced T_g values found at those loadings.

5.2.4 Composite vs. PMMA

No significant difference in T_g was found between composites and PMMA, neither with nor without solvent. Given the low aspect ratio of the cellulose particles, as evidenced by FE-SEM, the lack of increase in T_g is expected [15]. However, given that the composites contained microscale cellulose particles, again as evidenced by FE-SEM, and these

particles could have been classified as agglomerates in a PMMA/cellulose nanocomposite study, I question the accuracy of previous PMMA/cellulose nanocomposite studies in their citing of agglomerates as a reason for reduced T_g findings [57][52]. It is possible that the FE-SEM image of cellulose powder on their own was not representative of cellulose particles when ground together with PMMA; however, given that white specks were seen to the naked eye when looking at the composite specimens, it is assumed that at least some microscale cellulose particles were contained.

Unlike in other PMMA/cellulose studies, the current work involved the production of a solvent-containing composite that appeared white, bubbly, and fragile, instead of compact and translucent. This difference could be due to the PMMA chains in the current work being very short, very easily moved by evaporating acetone.

5.2.5 Leakage and yellowing

Greater increases in T_g from first to second heating were generally found for samples involving sample leakage from the DSC pan. This finding may suggest that solvent vapour was released due to the leakage, promoting further solvent evaporation by Le Chatelier's principle, reducing solvent content and its plasticizing effect, and increasing T_g [88].

It is unclear what the meaning of the yellowing in certain samples is. Yellowing is only seen in composite samples, suggesting it involves cellulose. However, some of the highest T_g values the Study 3 of the current work came from samples that were very yellow, casting doubt upon the idea that the yellowing might be due to cellulose degradation. Furthermore, extremely non-uniform yellowing as well as very uniform yellowing has been seen in the current work. Sample heating in open pans resulted in only partial yellowing of the solvent-containing composite sample, despite oxygen being available across the whole open surface of the sample. It is possible that there were multiple types of yellowing due to multiple reasons, such as due to degradation or due to a byproduct of a reaction between cellulose and the solvent. The former would be consistent with Study 1 of the current work where yellower samples were found to have

lower T_g values; the latter would be consistent with Study 3 of the current work, where, as mentioned above, some of the highest T_g values came from yellow samples.

5.3 Study limitations

Some limitations of the current work come from limitations of tools, techniques, approaches, and assumptions.

Despite results being obtained from three samples for each experimental condition, which is on the upper end of the norm for sample repetition in the field of T_g measurement of PMMA/cellulose composites and nanocomposites, variation due to sample shape differences have yielded some T_g comparisons based on fewer than three samples in some conditions. This low number of samples can make conclusions from these comparisons more susceptible to error from over-representation of possibly rare phenomena or findings that are random and coincidental. Due to the limited number of samples, some sample shapes (such as the “seemingly full” shape) were seen only once or a few times; consequently, trends with respect to their associated T_g increases from first to second heating are not as clear as they are for more common shapes (such as the “capsule” shape).

Furthermore, the approach in the current work of correlating sample shape with T_g is just that – a correlational approach. Correlation does not necessarily mean causation. If the sample shapes in reality have no effect on the measured T_g, then selective analysis of one specific shape would simply limit data size without added benefit. In fact, if intrinsic variation in materials makes some materials more likely to assume certain shapes, then a selective analysis of only samples with one of those shapes would involve a selection of samples that are not representative of the entire sample population. Ideally, to determine how or whether sample shape affects T_g, those sample shapes would be randomly assigned.

A limitation of the DSC machine used in the current work with regard to the investigation of sample shapes arising during DSC testing is that it does not permit for the sample to be observed during the heat treatment. Consequently, it cannot be known in the current work

at which time during the DSC heat treatment the different shapes arise, and whether all shapes arise at the same point. If, for example, it is found that this shape only arises during cooling after the final scan, after all of the T_g measurements have been taken, then it might not have much relevance to T_g, other than by possibly being a shape with a form favorable for material with a certain T_g. Of note, the use of a DSC video microscopy technique to visually record a sample during DSC testing has been reported and would have allowed for the monitoring of shape changes throughout testing [89].

Some assumptions were made in this work about the uniformity of the tested material; generally, it was assumed that samples within an experimental material condition were more similar to each other than to samples outside of their experimental material condition. In other words, solvent-containing composite samples were assumed to be more similar to each other than to any solvent-containing PMMA samples or solventless composite or PMMA samples. However, insufficient dispersion of cellulose in composite material may have yielded composite samples that had much lower cellulose content than other composite samples. Consequences of this variation in material composition may include a high variation in T_g, which might be mistaken as being due to some other factors, such as sample shape.

Variation in tested material might also come from the grinding technique, which involves using a mortar and pestle manually. A limitation of this technique is that it relies on the human operator of the mortar and pestle to make sure that all parts of the powder are equally ground by spending equal amounts of time and force on all parts of the powder, which is unlikely to be achieved. Consequently, some parts of the powder are likely to be more thoroughly ground than other parts, which may result in some tested samples having polymer chains with a higher or lower molecular weight or cellulose particles that are larger or smaller in size. In DSC measurement, this variation may reveal itself as different T_g results for different samples, which might be mistaken as being due to some other factors.

Limitations related to material uniformity are partially addressed through the comparison of T_g values from both first and second heating. Samples in experimental conditions for

the two tested first heating peak temperatures were only considered comparable based on T_g values from second heating if there was no significant difference between them based on T_g values from first heating. An assumption was made that there was only negligible influence of thermal history on first heating T_g . If this assumption is incorrect, then samples that were considered equivalent based on T_g from first heating may have actually not been equivalent due to differences in thermal history affecting their T_g . Upon second heating, then, the effect of thermal history would be erased and would no longer mask the difference in T_g , but upon analysis the material would be assumed to have changed from first to second heating, possibly due to change in shape.

Variations in thermal history among samples may have arisen from mortar-and-pestle grinding and from inconsistencies in melt pressing. Grinding involves friction and heat, which can change thermal history [13]. Melt pressing was performed with a melt press that exhibited fluctuations in temperature that were unequal between composite and neat PMMA sample preparation. Additionally, the melt press involved heating specimens across a relatively large surface, and the temperature at different points on the surface may have been different. Finally, the pressure to which different parts of the sample were exposed likely varied due the pressed sample initially having been in the form of a hill and the edges of the sample having remained in powdered form after pressing. All of these sources of variation of thermal history may have made the samples' T_g value obtained from first heating be an inaccurate representation of the sample's T_g . Consequently, conclusions made regarding T_g increase from first to second heating may have been inaccurate.

Even if samples were completely uniform, a limitation of the approach used to compare the influences of first heating peak temperatures (160 °C vs. 200 °C) is that the 200 °C first heating peak temperature was associated with a longer total heating time, due to the heating and cooling rates being equal between the conditions. Therefore, it is possible that some or maybe even all findings related to difference in first heating peak temperature in this work are in actuality findings related to difference in total heating time from the first heating scan.

Chapter 6

6 Conclusions

This work investigated measurement of T_g with different DSC settings as well as the use of post-DSC sample photography to uncover unconsidered potential sources of variation in measured T_g ; the reliability of T_g obtained from the first heating scan and from the heating scan was compared. Additionally, the use of a mortar and pestle for preparing solventless PMMA/cellulose composites was evaluated.

From DSC tests of solventless and solvent-containing PMMA and PMMA/cellulose composite samples using a first heating peak temperature of either 160 °C or 200 °C, it was found that the first heating peak temperature significantly affects T_g measured from second heating of solvent-containing composite samples. Solvent-containing composite samples tested using the 200 °C first heating peak temperature were found to have significantly higher T_g values than those tested using the 160 °C first heating peak temperature. The same was not true for the solvent-containing PMMA samples, for which this effect was not statistically significant. In solventless samples, no variation in T_g in response to differences in assigned first heating peak temperature was found. Thus, variation in first heating peak temperature is concluded to be a potential source of T_g variation among studies of solvent-containing materials that have different first heating peak temperatures.

No significant differences in T_g were found between PMMA and PMMA/cellulose composite samples, neither in the solventless nor in the solvent-containing condition. However, a significantly greater increase in T_g from first to second heating was found in the solvent-containing composite sample compared to solvent-containing PMMA when the first heating peak temperature of 200 °C was used.

Measurement of T_g from first heating was generally found to provide more consistent T_g values among samples within experimental groups than measurement of T_g from second heating. In solventless samples, T_g from first heating and second heating were similar. In solvent-containing samples, T_g from second heating was generally greater and more

varied among samples in the same experimental condition than Tg from first heating. Therefore, Tg from first heating is concluded to be more reliable than Tg from second heating, especially for solvent-containing samples, despite possible variations in thermal history.

From FE-SEM imaging of cellulose powder ground using a mortar and pestle, it was found that mortar-and-pestle grinding up to 60 minutes yields only microscale, low aspect ratio cellulose particles. Therefore, mortar-and-pestle grinding is concluded to be unsuitable for preparation of solventless PMMA/cellulose nanocomposites.

Opening sample pans after DSC testing and visually analyzing samples by eye and with photographs resulted in unexpected sample shapes to be seen. A classification of shapes was proposed, and some shapes were found to be associated with greater increases in Tg from first to second heating. Shape variation was correlated with Tg variation, leading to some explanations for variation and outliers. Selective comparison of Tg values corresponding to samples with only one shape type allowed for findings with less Tg variation within experimental conditions, graphs with smaller error bars, and more statistically significant findings. Thus, the use of post-DSC photography has been concluded to be analytically useful for Tg comparison by providing information about sample shapes, which may be a source of Tg variation within DSC-involving studies.

References

- [1] W. Bolton, "Structure and properties of solids," in *Materials for Engineering*, 2000, p. 85.
- [2] R. Riesen, "The rate dependence and comparability of glass transition temperatures," *Thermochim. Acta*, vol. 93, pp. 213–216, 1985.
- [3] H. F. Giles, E. M. Mount, and J. R. Wagner, "Amorphous Polymers," in *Extrusion: The Definitive Processing Guide and Handbook*, William Andrew, 2004, p. 179.
- [4] Y. Zhang, R. D. Adams, and L. F. M. da Silva, "A Rapid Method of Measuring the Glass Transition Temperature Using a Novel Dynamic Mechanical Analysis Method," *J. Adhes.*, vol. 89, no. 10, pp. 785–806, 2013.
- [5] J. Tanaka and K. Wolter, "Glass," in *Engineering Dielectrics Volume IIa Electrical Properties of Solid Insulating Materials: Molecular Structure and Electrical Behavior*, R. M. Eichhorn, Ed. ASTM International, 1983, p. 552.
- [6] J. He, W. Liu, and Y.-X. Huang, "Simultaneous Determination of Glass Transition Temperatures of Several Polymers," *PLoS One*, vol. 11, no. 3, p. e0151454, 2016.
- [7] M. Mohammadi, H. fazli, M. karevan, and J. Davoodi, "The glass transition temperature of PMMA: A molecular dynamics study and comparison of various determination methods," *Eur. Polym. J.*, vol. 91, no. March, pp. 121–133, 2017.
- [8] E. Erbas Kiziltas, A. Kiziltas, S. C. Bollin, and D. J. Gardner, "Preparation and characterization of transparent PMMA-cellulose-based nanocomposites," *Carbohydr. Polym.*, vol. 127, pp. 381–389, 2015.
- [9] N. M. Barkoula, B. Alcock, N. O. Cabrera, and T. Peijs, "Fatigue properties of highly oriented polypropylene tapes and all-polypropylene composites," *Polym. Polym. Compos.*, vol. 16, no. 2, pp. 101–113, 2008.

- [10] K. H. Liao, S. Kobayashi, H. Kim, A. A. Abdala, and C. W. Macosko, "Influence of functionalized graphene sheets on modulus and glass transition of PMMA," *Macromolecules*, vol. 47, no. 21, pp. 7674–7676, 2014.
- [11] H. G. Brittain and R. D. Bruce, "Differential Scanning Calorimetry," in *Modern Instrumental Analysis*, S. Ahuja and N. Jespersen, Eds. 2006, pp. 74–75.
- [12] H. Lobo, "Practical uses of differential scanning calorimetry for plastics," in *Handbook of Plastics Analysis*, 2003, p. 83.
- [13] ASTM International, "ASTM E1356 Standard Test Method for Assignment of the Glass Transition Temperatures by Differential Scanning Calorimetry." pp. 1–4, 2014.
- [14] O. A. Serenko, V. I. Roldughin, A. A. Askadskii, E. S. Serkova, P. V. Strashnov, and Z. B. Shifrina, "The effect of size and concentration of nanoparticles on the glass transition temperature of polymer nanocomposites," *RSC Adv.*, vol. 7, no. 79, pp. 50113–50120, 2017.
- [15] M. Eriksson, H. Goossens, and T. Peijs, "Influence of drying procedure on glass transition temperature of PMMA based nanocomposites," *Nanocomposites*, vol. 1, no. 1, pp. 36–45, 2015.
- [16] O. V. Mazurin, "Problems of compatibility of the values of glass transition temperatures published in the world literature," *Glas. Phys. Chem.*, vol. 33, no. 1, pp. 22–36, 2007.
- [17] U. Ali, K. J. B. A. Karim, and N. A. Buang, "A Review of the Properties and Applications of Poly (Methyl Methacrylate) (PMMA)," *Polym. Rev.*, vol. 55, no. 4, pp. 678–705, 2015.
- [18] S. Rebouillat and F. Pla, "State of the Art Manufacturing and Engineering of Nanocellulose: A Review of Available Data and Industrial Applications," *J. Biomater. Nanobiotechnol.*, vol. 4, pp. 165–188, 2013.

- [19] R. J. Moon, G. T. Schueneman, and J. Simonsen, "Overview of Cellulose Nanomaterials, Their Capabilities and Applications," *JOM*, vol. 68, no. 9, pp. 2383–2394, 2016.
- [20] P. K. Vallittu, "A review of methods used to reinforce polymethyl methacrylate resin.," *J. Prosthodont.*, vol. 4, no. 3, pp. 183–7, 1995.
- [21] D. K. Platt, "Polymethyl Methacrylate (PMMA)," in *Engineering and High Performance Plastics Market Report: A Rapra Market Report*, iSmithers Rapra Publishing, 2003, p. 45.
- [22] S. A. Kedzior, L. Graham, C. Moorlag, B. M. Dooley, and E. D. Cranston, "Poly(methyl methacrylate)-grafted cellulose nanocrystals: One-step synthesis, nanocomposite preparation, and characterization," *Can. J. Chem. Eng.*, vol. 94, 2016.
- [23] G. A. Mahmoud, D. E. Hegazy, and H. Kamal, "In-vitro release of ketoprofen behavior loaded in polyvinyl alcohol/acrylamide hydrogels prepared by gamma irradiation," *Arab J. Nucl. Sci. Appl.*, vol. 47, no. 1, pp. 28–40, 2014.
- [24] A. F. Miles, "Preparation and Characterization of (Monomethyl Itaconate)-(Methyl Methacrylate) and of (Itaconic Anhydride)-(Methyl Methacrylate) Copolymers," vol. 27, no. 2, pp. 165–170, 1991.
- [25] T. Yu, F. Sun, M. Lu, and Y. Li, "Water absorption and hygrothermal aging behavior of short ramie fiber reinforced poly(lactic acid) composites," *Polym. Compos.*, 2016.
- [26] C. M. Roland, "Constraints on Local Segmental Motion in Poly(vinylethylene) Networks," *Macromolecules*, vol. 27, no. 15, pp. 4242–4247, 1994.
- [27] H. Cruz and Y. Son, "Effect of Aspect Ratio on Electrical, Rheological and Glass Transition Properties of PC/MWCNT Nanocomposites," *J. Nanosci. Nanotechnol.*, vol. 18, no. 2, pp. 943–950, 2018.

- [28] V. Khoshkava and M. R. Kamal, "Effect of surface energy on dispersion and mechanical properties of polymer/nano-crystalline cellulose nano-composites," *Biomacromolecules*, vol. 14, no. 9, pp. 3155–3163, 2013.
- [29] N. L. Garcia de Rodriguez, W. Thielemans, and A. Dufresne, "Sisal cellulose whiskers reinforced polyvinyl acetate nanocomposites," *Cellulose*, vol. 13, no. 3, pp. 261–270, 2006.
- [30] Y. P. Handa, S. Capowski, and M. O'Neill, "Compressed-gas-induced plasticization of polymers," *Thermochim. Acta*, vol. 226, pp. 177–185, 1993.
- [31] J. Tarrío-Saavedra, J. López-Beceiro, S. Naya, C. Gracia, and R. Artiaga, "Controversial effects of fumed silica on the curing and thermomechanical properties of epoxy composites," *Express Polym. Lett.*, vol. 4, no. 6, pp. 382–395, 2010.
- [32] H.-M. Ng, L. T. Sin, S.-T. Bee, T.-T. Tee, and A. R. Rahmat, "Review of Nanocellulose Polymer Composite Characteristics and Challenges," *Polym. Plast. Technol. Eng.*, vol. 56, no. 7, pp. 687–731, 2017.
- [33] N. Patra, A. C. Barone, and M. Salerno, "Solvent effects on the thermal and mechanical properties of poly(methyl methacrylate) casted from concentrated solutions," *Adv. Polym. Technol.*, vol. 30, no. 1, pp. 12–20, 2011.
- [34] J. Perlich, V. Ko, E. Metwalli, L. Schulz, R. Georgii, and P. Mu, "Solvent Content in Thin Spin-Coated Polystyrene Homopolymer Films," *Macromol.*, vol. 42, pp. 337–344, 2009.
- [35] R. A. Pethrick, "Characterization of Polymers," in *Characterization and Analysis of Polymers*, John Wiley & Sons, 2008, p. 14.
- [36] K. Kobayashi, S. Nakayama, and T. Niwa, "A New Estimation Method of Thermal History in Cross-Linked Polyethylene," *Int. J. Polym. Mater.*, vol. 21, no. 3–4, pp. 147–156, 1993.

- [37] ASTM International, "ASTM D3418 Standard Test Method for Transition Temperatures and Enthalpies of Fusion and Crystallization of Polymers by Differential Scanning." pp. 1–7, 2015.
- [38] J. D. Menczel, L. Judovits, R. B. Prime, H. E. Bair, and M. Reading, "Differential Scanning Calorimetry," in *Thermal Analysis of Polymers: Fundamentals and Applications*, John Wiley & Sons, 2014.
- [39] I. W. Gilmour and J. N. Hay, "Determination of the specific heat of polystyrene by d.s.c.," *Polymer*, vol. 18, no. 3, pp. 281–285, 1977.
- [40] J. Hong, D. Radojčić, M. Ionescu, Z. S. Petrović, and E. Eastwood, "Advanced materials from corn: isosorbide-based epoxy resins," *Polym. Chem.*, vol. 5, no. 18, pp. 5360–5368, 2014.
- [41] C. Y. Zahra and A. M. Zahra, "The Perkin-Elmer 1020 series thermal analysis system," *Thermochim. Acta*, vol. 276, no. 1–2, pp. 161–174, 1996.
- [42] J. H. Flynn, "Thermal analysis kinetics-problems, pitfalls and how to deal with them," *J. Therm. Anal.*, vol. 34, pp. 367–381, 1988.
- [43] O. Bäumchen, J. D. McGraw, J. A. Forrest, and K. Dalnoki-Veress, "Reduced glass transition temperatures in thin polymer films: Surface effect or artifact?," *Phys. Rev. Lett.*, vol. 109, no. 5, pp. 1–5, 2012.
- [44] R. K. Wunderlich *et al.*, "Thermophysical properties of a Fe-Cr-Mo alloy in the solid and liquid phase," *Steel Res. Int.*, vol. 83, no. 1, pp. 43–54, 2012.
- [45] B. P. Rodrigues and E. D. Zanotto, "Evaluation of the guided random parameterization method for critical cooling rate calculations," *J. Non. Cryst. Solids*, vol. 358, no. 18–19, pp. 2626–2634, 2012.
- [46] S. Sohn, A. Alizadeh, and H. Marand, "On the multiple melting behavior of bisphenol-A polycarbonate," *Polymer*, vol. 41, no. 25, pp. 8879–8886, 2000.

- [47] C. T. Moynihan, A. J. Easteal, and J. Wilder, "Dependence of the glass transition temperature on heating and cooling rate," *J. Phys. Chem.*, vol. 78, no. 26, pp. 2673–2677, 1974.
- [48] K. Israkarn and S. Charoenrein, "Influence of annealing temperature on Tg' of cooked rice stick noodles," *Int. J. Food Prop.*, vol. 9, no. 4, pp. 759–766, 2006.
- [49] F. Deng, M.-C. Li, X. Ge, Y. Zhang, and U. R. Cho, "Cellulose nanocrystals/poly(methyl methacrylate) nanocomposite films: Effect of preparation method and loading on the optical, thermal, mechanical, and gas barrier properties," *Polym. Compos.*, pp. 1–10, 2015.
- [50] S. Sain, D. Ray, and A. Mukhopadhyay, "Improved Mechanical and Moisture Resistance Property of In Situ Polymerized Transparent PMMA/Cellulose Composites," *Polymer Composites*, pp. 1748–1758, 2015.
- [51] S. Sain *et al.*, "Synthesis and characterization of PMMA-cellulose nanocomposites by in situ polymerization technique," *J. Appl. Polym. Sci.*, vol. 126, pp. E127–E134, 2012.
- [52] K. Littunen, U. Hippi, T. Saarinen, and J. Seppälä, "Network formation of nanofibrillated cellulose in solution blended poly(methyl methacrylate) composites," *Carbohydr. Polym.*, vol. 91, no. 1, pp. 183–190, 2013.
- [53] T. Huang, K. Kuboyama, H. Fukuzumi, and T. Ougizawa, "PMMA/TEMPO-oxidized cellulose nanofiber nanocomposite with improved mechanical properties, high transparency and tunable birefringence," *Cellulose*, vol. 25, no. 4, pp. 2393–2403, 2018.
- [54] V. P. Anju and S. K. Narayanankutty, "Impact of Bis-(3-triethoxysilylpropyl)tetrasulphide on the properties of PMMA/Cellulose composite," *Polymer*, vol. 119, pp. 224–237, 2017.
- [55] G. Han, S. Huan, J. Han, Z. Zhang, and Q. Wu, "Effect of acid hydrolysis conditions on the properties of cellulose nanoparticle-reinforced

- polymethylmethacrylate composites,” *Materials*, vol. 7, no. 1, pp. 16–29, 2014.
- [56] H. Liu, D. Liu, F. Yao, and Q. Wu, “Fabrication and properties of transparent polymethylmethacrylate/cellulose nanocrystals composites,” *Bioresour. Technol.*, vol. 101, no. 14, pp. 5685–5692, 2010.
- [57] H. Dong, K. E. Strawhecker, J. F. Snyder, J. A. Orlicki, R. S. Reiner, and A. W. Rudie, “Cellulose nanocrystals as a reinforcing material for electrospun poly(methyl methacrylate) fibers: Formation, properties and nanomechanical characterization,” *Carbohydr. Polym.*, vol. 87, no. 4, pp. 2488–2495, 2012.
- [58] F. Fahma, N. Hori, T. Iwata, and A. Takemura, “The morphology and properties of poly(methyl methacrylate)-cellulose nanocomposites prepared by immersion precipitation method,” *J. Appl. Polym. Sci.*, vol. 128, no. 3, pp. 1563–1568, 2013.
- [59] S. Sain *et al.*, “A comparative study of polymethylmethacrylate/cellulose nanocomposites prepared by in situ polymerization and ex situ dispersion techniques,” *J. Reinf. Plast. Compos.*, vol. 32, no. 3, pp. 147–159, 2013.
- [60] H. Dong *et al.*, “Highly Transparent and Toughened Poly(methyl methacrylate) Nanocomposite Films Containing Networks of Cellulose Nanofibrils,” *ACS Appl. Mater. Interfaces*, vol. 7, no. 45, pp. 25464–25472, 2015.
- [61] M. Banerjee, S. Sain, A. Mukhopadhyay, S. Sengupta, T. Kar, and D. Ray, “Surface treatment of cellulose fibers with methylmethacrylate for enhanced properties of in situ polymerized PMMA/cellulose composites,” *J. Appl. Polym. Sci.*, vol. 131, no. 2, pp. 1–9, 2014.
- [62] A. Dufresne, “Thermal properties,” in *Nanocellulose: From nature to high performance tailored materials*, Walter de Gruyter GmbH, 2012, p. 282.
- [63] A. Watanabe, T. S. Morita, and Y. Ozaki, “Temperature-dependent changes in hydrogen bonds in cellulose I α studied by infrared spectroscopy in combination with correlation spectroscopy: comparison with cellulose I β ,” *Biomacromolecules*, pp. 2969–2975, 2007.

- [64] V. P. Anju and S. K. Narayanankutty, "Impact of Bis-(3-triethoxysilylpropyl) tetrasulphide on the properties of PMMA/Cellulose composite," *Polymer*, vol. 119, pp. 224–237, 2017.
- [65] M. Avella, M. E. Errico, and E. Martuscelli, "Novel PMMA/CaCO₃ Nanocomposites Abrasion Resistant Prepared by an in Situ Polymerization Process," *Nano Lett.*, vol. 1, no. 4, pp. 213–217, 2001.
- [66] T. N. Tran *et al.*, "Transparent and flexible amorphous cellulose-acrylic hybrids," *Chem. Eng. J.*, vol. 287, pp. 196–204, 2016.
- [67] M. Cheng, Z. Qin, S. Hu, H. Yu, and M. Zhu, "Use of electrospinning to directly fabricate three-dimensional nanofiber stacks of cellulose acetate under high relative humidity condition," *Cellulose*, vol. 24, no. 1, pp. 219–229, 2017.
- [68] K. A. Connors, S. D. Dyer, and S. E. Belanger, "Advancing the quality of environmental microplastic research," *Environ. Toxicol. Chem.*, vol. 36, no. 7, pp. 1697–1703, 2017.
- [69] A. J. Eagle, L. P. Olander, K. L. Locklier, J. B. Heffernan, and E. S. Bernhardt, "Fertilizer Management and Environmental Factors Drive N₂O and NO₃ Losses in Corn: A Meta-Analysis," *Soil Sci. Soc. Am. J.*, vol. 81, no. 5, pp. 1191–1202, 2017.
- [70] D. Angerame and M. De Biasi, "Do Nanofilled/Nanohybrid Composites Allow for Better Clinical Performance of Direct Restorations Than Traditional Microhybrid Composites? A Systematic Review," *Oper. Dent.*, 2018.
- [71] M. H. Keshavarz, K. Esmaeilpour, and H. Taghizadeh, "A new approach for assessment of glass transition temperature of acrylic and methacrylic polymers from structure of their monomers without using any computer codes," *J. Therm. Anal. Calorim.*, vol. 126, no. 3, pp. 1787–1796, 2016.
- [72] S. Affolter, A. Ritter, and M. Schmid, "Interlaboratory Tests on Polymers by Differential Scanning Calorimetry (DSC): Determination of Glass Transition

- Temperature (T_g),” *Macromol. Mater. Eng.*, vol. 286, no. 10, pp. 606–610, 2001.
- [73] D. Turnbull and M. H. Cohen, “Free-volume model of the amorphous phase: Glass transition,” *J. Chem. Phys.*, vol. 34, no. 1, pp. 120–125, 1961.
- [74] S. Bao *et al.*, “Sensitive and reliable detection of glass transition of polymers by fluorescent probes based on AIE luminogens,” *Polym. Chem.*, vol. 6, no. 18, pp. 3537–3542, 2015.
- [75] Z. Qiu *et al.*, “A Simple and Sensitive Method for an Important Physical Parameter: Reliable Measurement of Glass Transition Temperature by AIEgens,” *Macromolecules*, vol. 50, no. 19, pp. 7620–7627, 2017.
- [76] S. E. Root, M. A. Alkhadra, D. Rodriguez, A. D. Printz, and D. J. Lipomi, “Measuring the Glass Transition Temperature of Conjugated Polymer Films with Ultraviolet-Visible Spectroscopy,” *Chem. Mater.*, vol. 29, no. 7, pp. 2646–2654, 2017.
- [77] M. H. Al-Saleh, “Electrical and electromagnetic interference shielding characteristics of GNP/UHMWPE composites,” *J. Phys. D. Appl. Phys.*, vol. 49, no. 19, 2016.
- [78] A. Dufresne, “Barrier properties,” in *Nanocellulose: From nature to high performance tailored materials*, Walter de Gruyter GmbH, 2012, p. 379.
- [79] S. S. Nair, J. Zhu, Y. Deng, and A. J. Ragauskas, “High performance green barriers based on nanocellulose,” *Sustain. Chem. Process.*, vol. 2, no. 1, pp. 1–7, 2014.
- [80] K. R. Tate, “Extrusion and Orientation of Higher Molecular Weight Polyethylenes,” University of Toronto, 1992.
- [81] “DSC Q Series Getting Started Guide.” TA Instruments, p. 14, 2004.
- [82] L. M. L. Nollet, “Differential scanning calorimetry,” in *Handbook of Food*

Analysis: Methods and instruments in applied food analysis, Volume 3, CRC Press, 2004, p. 1840.

- [83] R. Svoboda, “How to determine activation energy of glass transition,” *J. Therm. Anal. Calorim.*, vol. 118, no. 3, pp. 1721–1732, 2014.
- [84] P. Skoglund and A. Fransson, “Temperature Distribution in Polymer Samples During DSC-Scan,” *J. Therm. Anal.*, vol. 49, no. 2, pp. 999–1005, 1997.
- [85] S. X. Xu, Y. Li, and Y. P. Feng, “Study of temperature profile and specific heat capacity in temperature modulated DSC with a low sample heat diffusivity,” *Thermochim. Acta*, vol. 360, no. 2, pp. 131–140, 2000.
- [86] Y. Shimazaki *et al.*, “Excellent thermal conductivity of transparent cellulose nanofiber/epoxy resin nanocomposites,” *Biomacromolecules*, vol. 8, no. 9, pp. 2976–2978, 2007.
- [87] G. Hakvoort, L. L. van Reijen, and A. J. Aartsen, “Measurement of the thermal conductivity of solid substances by DSC,” *Thermochim. Acta*, vol. 93, pp. 317–320, 1985.
- [88] F. R. Foulkes, “Chemical Equilibrium (II),” in *Physical Chemistry for Engineering and Applied Sciences*, CRC Press, 2012, pp. 14–12.
- [89] K. D. Beyer, C. S. Pearson, and D. S. Henningfield, “Solid/Liquid Phase Diagram of the Ammonium Sulfate/Glutaric Acid/ Water System,” *J. Phys. Chem. A*, vol. 117, pp. 3630–3641, 2013.

Appendices

This section includes obtained glass transition temperature values for each sample, descriptions of sample shapes, as well as photographs of samples in their DSC pans after testing (as well as, in the case of Appendix C, before testing).

Appendix A: Data from Study 1

Table A4. Glass transition temperatures and shapes from Study 1.

Sample ID	Condition	Tg from 1 st heating (°C)	Tg from 2 nd heating (°C)	Shape Classification
1	CS160	76.28	92.58	Pillar
2	CS160	75.88	77.9	Floor-based
9	CS160	73.97	77.7	Floor-based
7	PS160	76.92	77.57	Floor-based
8	PS160	76.92	90.55	Pillar
12	PS160	75.35	77.27	Floor-based
17	CS200	77.02	97.77	Coated walls
18	CS200	75.49	88.85	Coated walls
23	CS200	75.26	80.83	Floor-based
13	PS200	76.26	88.84	Coated walls
14	PS200	78.03	97.29	Coated walls
24	PS200	75.52	81.57	Floor-based
3	C160	89.45	86.9	Floor-based
4	C160	89.71	89.75	Floor-based
10	C160	89.34	87.47	Floor-based
5	P160	88.65	87.82	Floor-based
6	P160	88.43	87.09	Floor-based
11	P160	57.29	128.32	Other – outlier
19	C200	91.74	92.45	Floor-based
20	C200	95.58	91.53	Floor-based
21	C200	87.51	87.26	Floor-based
15	P200	90.19	92.41	Floor-based
16	P200	90.5	92.17	Floor-based
22	P200	87.24	88.01	Floor-based

Appendix B: Data from Study 2

Table A5. Glass transition temperatures and shapes from Study 2.

Sample ID	Grinding Time (min)	Condition	Mass (mg)	Tg from 1 st heating (°C)	Tg from 2 nd heating (°C)	Shape Classification
4B	30	P200	4	90.21	91.37	Floor-based
5B	30	P200	10	89.34	88.75	Floor-based
6B	30	P200	10	90.29	89.46	Floor-based
7B	30	P200	15	90.9	85.88	Vertical half
8B	30	P200	15	90.74	89.53	Vertical half
9B	60	P200	10	90.44	89.81	Floor-based
10B	60	P200	10	90.48	89.95	Floor-based
11B	3	PS200	10	81.49	86.77	Capsule
12B	3	PS200	10	82.3	86.16	Capsule
13B	15	PS200	10	80.61	87.32	Capsule
14B	15	PS200	10	80.37	80.84	Capsule
15B	15	P200	10	87.87	89.67	Floor-based
16B	15	P200	10	89.17	89.07	Floor-based
17B	60	PS200	10	80.63	83.65	Capsule
18B	60	PS200	10	79.68	83.96	Capsule
19B	3	P200	10	86.95	87.66	Floor-based
20B	3	P200	10	88.49	87.32	Floor-based
21B	30	PS200	10	80.18	85.93	Capsule
22B	30	PS200	10	80.18	82.15	Capsule
23B	30	PS200	4	81.4	99.02	Pillar
24B	30	PS200	15	79.49	86.16	Vertical half Capsule
25B	30	PS200	15	79.23	79.49	Seemingly full



Figure 65. Photograph of Sample 4B. This sample has a floor-based shape.



Figure 66. Photograph of Sample 5B. This sample has a floor-based shape.



Figure 67. Photograph of Sample 6B. This sample has a floor-based shape.



Figure 68. Photograph of Sample 7B. This sample has a “vertical half” shape.

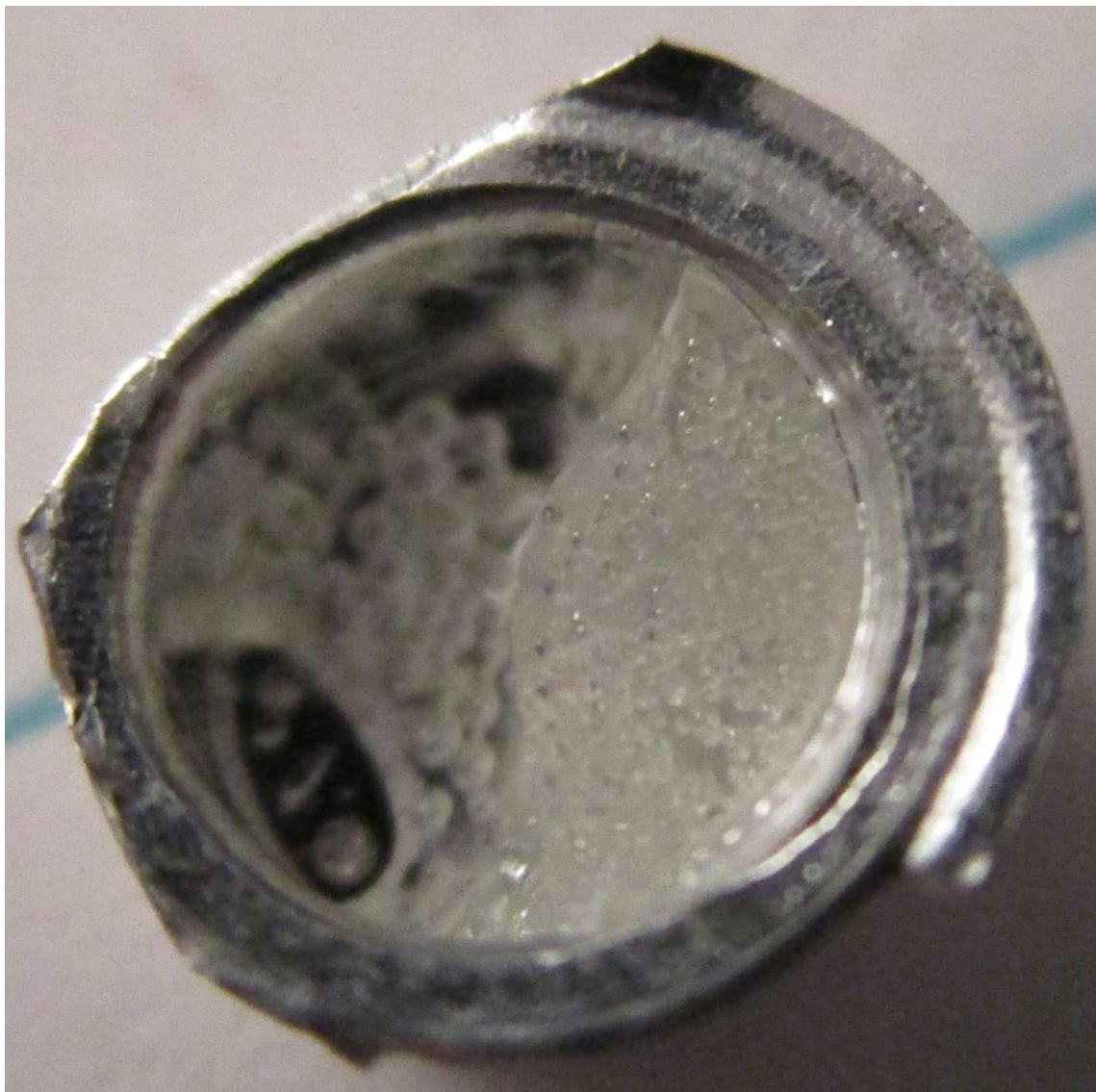


Figure 69. Photograph of Sample 8B. This sample has a “vertical half” shape.



Figure 70. Photograph of Sample 9B. This sample has a floor-based shape.



Figure 71. Photograph of Sample 10B. This sample has a floor-based shape.



Figure 72. Photograph of Sample 11B, with its roof pushed in to reveal a hollow center. This sample has a capsule shape.



Figure 73. Photographs of Sample 12B, showing intact structure (top) and structure after pressing in roof to reveal hollow center (bottom). This sample has a capsule shape.



Figure 74. Photographs of Sample 13B, showing pan leakage (top left), intact structure (top right), and structure after pressing in roof to reveal hollow center (bottom). This sample has a capsule shape.



Figure 75. Photographs of Sample 14B, showing intact structure (top) and structure after pressing in roof to reveal hollow center (bottom). This sample has a capsule shape.



Figure 76. Photograph of Sample 15B. This sample has a floor-based shape.

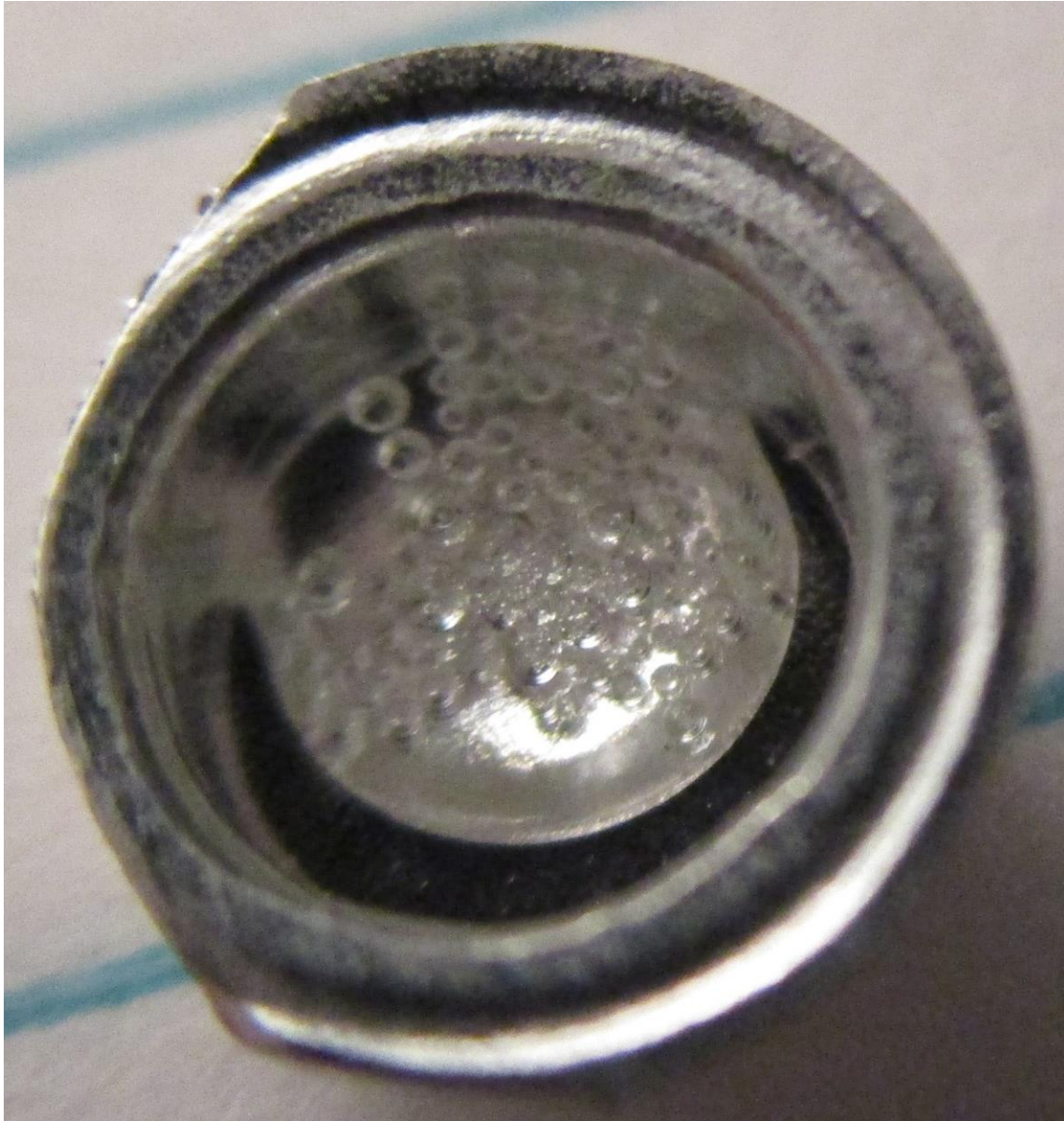


Figure 77. Photograph of Sample 16B. This sample has a floor-based shape.



Figure 78. Photographs of Sample 17B, showing intact structure (top) and structure after pressing in roof to reveal hollow center (bottom). This sample has a capsule shape.

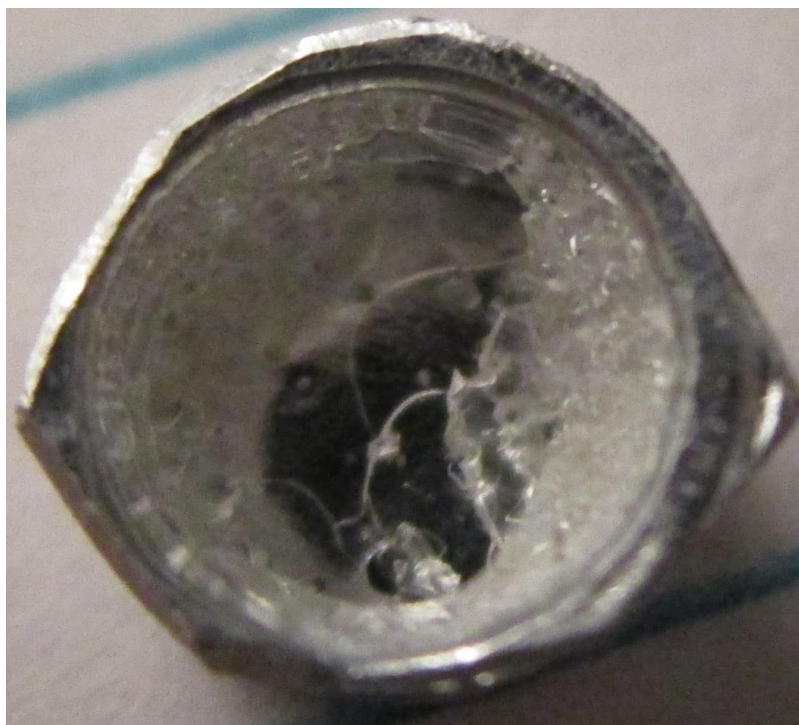


Figure 79. Photographs of Sample 18B, showing intact structure (top) and structure after pressing in roof to reveal hollow center (bottom). This sample has a capsule shape.



Figure 80. Photograph of Sample 19B. This sample has a floor-based shape.



Figure 81. Photograph of Sample 20B. This sample has a floor-based shape.



Figure 82. Photographs of Sample 21B, showing pan leakage (top left), intact structure (top right), and structure after pressing in roof to reveal hollow center (bottom). This sample has a capsule shape.



Figure 83. Photographs of Sample 22B, showing pan leakage (top left), intact structure (top right), and structure after pressing in roof to reveal hollow center (bottom). This sample has a capsule shape.



Figure 84. Photograph of Sample 23B, which has a pillar shape.



Figure 85. Photographs of Sample 24B, showing pan leakage (top left), intact structure (top right), and structure after pressing in roof to reveal hollow center (bottom). This sample appears to have both a “capsule” and “vertical half” shape.



Figure 86. Photograph of Sample 25B, which has a “seemingly full” shape.

Appendix C: Data from Study 3

Table A6. Glass transition temperatures from Study 3. “MC Capsule” means multi-compartment capsule. “SC Capsule” means single compartment capsule.

Sample ID	Condition	Tg from 1 st heating (°C)	Tg from 2 nd heating (°C)	Shape Classification
1C	CS160	73.44	72.11	MC Capsule
2C	CS160	75.06	80.06	SC Capsule
3C	CS160	74.11	73.13	MC Capsule
4C	PS160	76.74	79.97	MC Capsule
5C	PS160	72.64	78.95	SC Capsule
6C	PS160	72.84	71.12	Coated walls
7C	C160	90.93	89.58	Floor-based
8C	C160	90.07	89.07	Floor-based
9C	C160	87.74	86.28	Floor-based
10C	P160	91.47	89.58	Floor-based
11C	P160	91.84	89.76	Floor-based
12C	P160	89.35	87.38	Floor-based
13C	CS200	74.04	81.52	MC Capsule
14C	CS200	74.19	84.06	MC Capsule
15C	CS200	77.33	85.32	MC Capsule
16C	PS200	74.42	86.3	SC Capsule
17C	PS200	72.68	78.78	MC Capsule
18C	PS200	73.33	81.05	MC Capsule
19C	C200	89.87	89.84	Floor-based
20C	C200	89.74	89.38	Floor-based
21C	C200	89.36	87.48	Floor-based
22C	P200	91.63	89.66	Floor-based
23C	P200	91.03	89.87	Floor-based
24C	P200	91.18	90.26	Floor-based



Figure 87. Photographs of Sample 1C, after originally being put into the DSC pan (left), after testing when the lid was removed (center), and after pressing in the roof of the structure to reveal the hollowness inside (right). This sample has a multi-compartment capsule shape.



Figure 88. Photographs of Sample 2C, after originally being put into the DSC pan (left), after testing when the lid was removed (center), and after pressing in the roof of the structure to reveal the hollowness inside (right). This sample has a single compartment capsule shape.



Figure 89. Photographs of Sample 3C, after originally being put into the DSC pan (left), after testing when the lid was removed (center), and after pressing in the roof of the structure to reveal the hollowness inside (right). This sample has a multi-compartment capsule shape.



Figure 90. Photographs of Sample 4C, after originally being put into the DSC pan (left), after testing when the lid was removed (center), and after pressing in the roof of the structure to reveal the hollowness inside (right). This sample has a multi-compartment capsule shape.

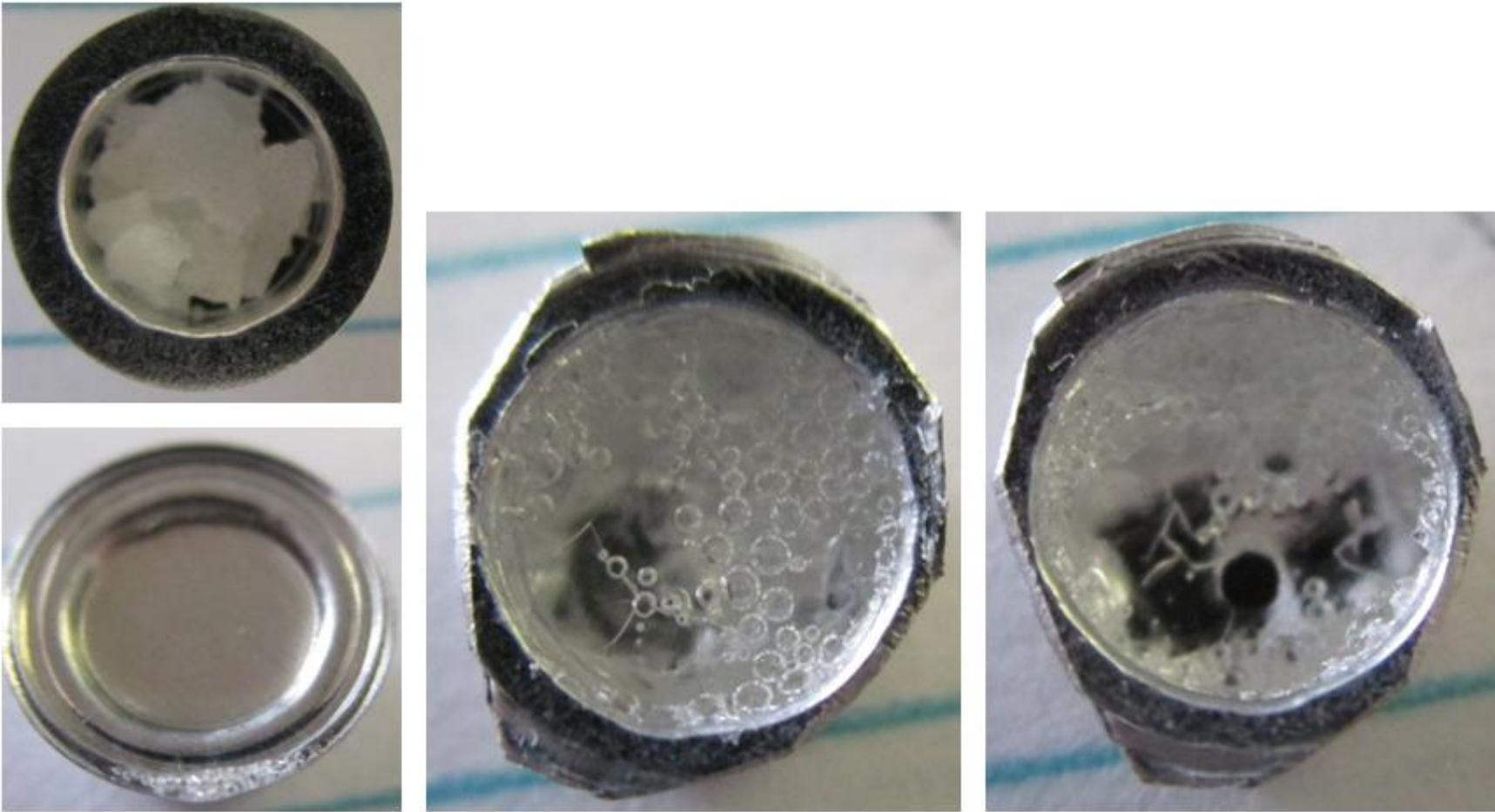


Figure 91. Photographs of Sample 5C, after originally being put into the DSC pan (left top), after testing before the lid was removed – leakage is seen (left bottom), after the lid was removed (center), and after pressing in the roof of the structure to reveal the hollowness inside (right). This sample has a single compartment capsule shape.

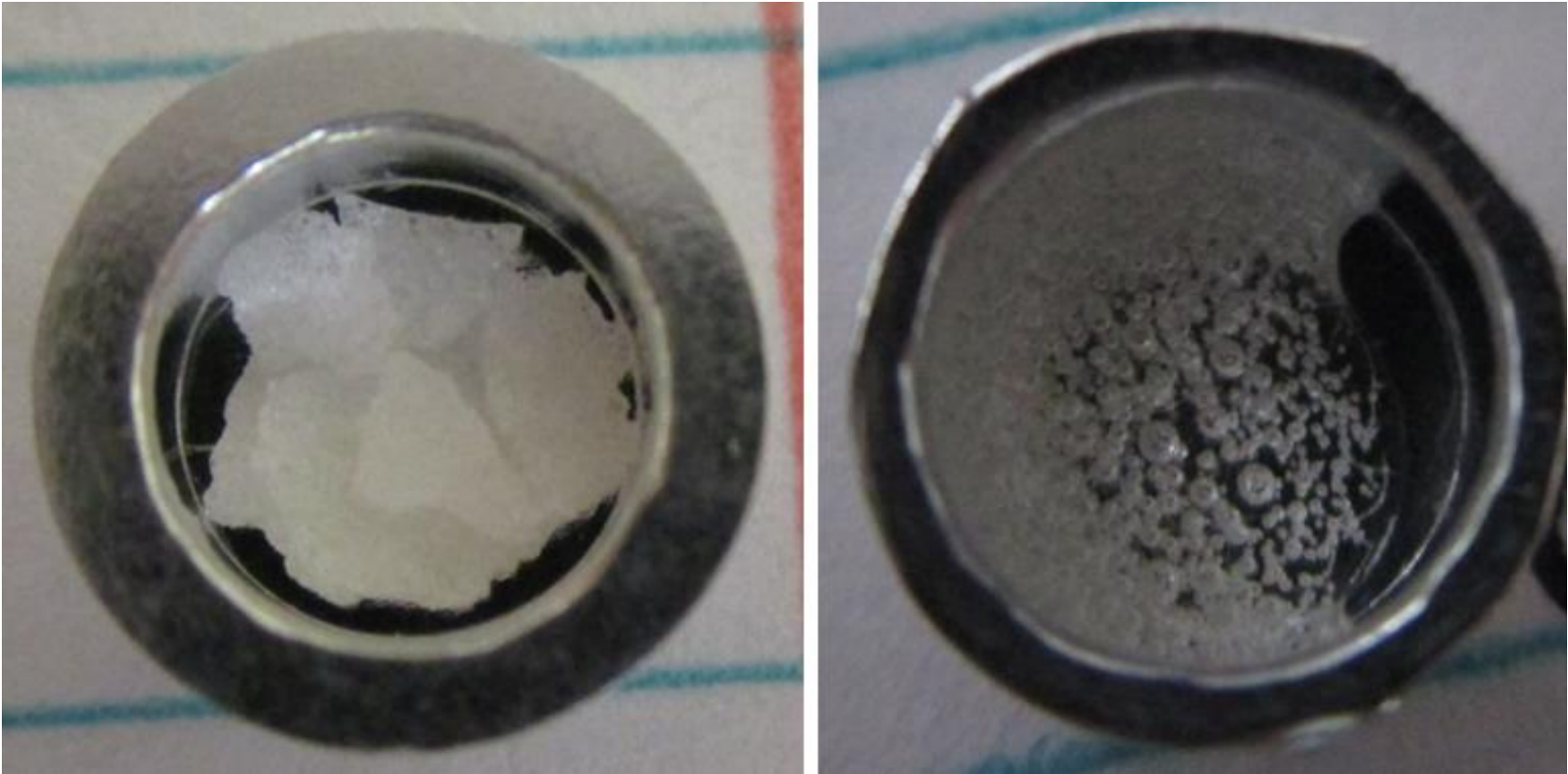


Figure 92. Photographs of Sample 6C, after originally being put into the DSC pan (left) and after testing when the lid was removed (right). This sample has a coated walls shape.



Figure 93. Photographs of Sample 7C, after originally being put into the DSC pan (left) and after testing when the lid was removed (right). This sample has a floor-based shape.



Figure 94. Photographs of Sample 8C, after originally being put into the DSC pan (left) and after testing when the lid was removed (right). This sample has a floor-based shape.

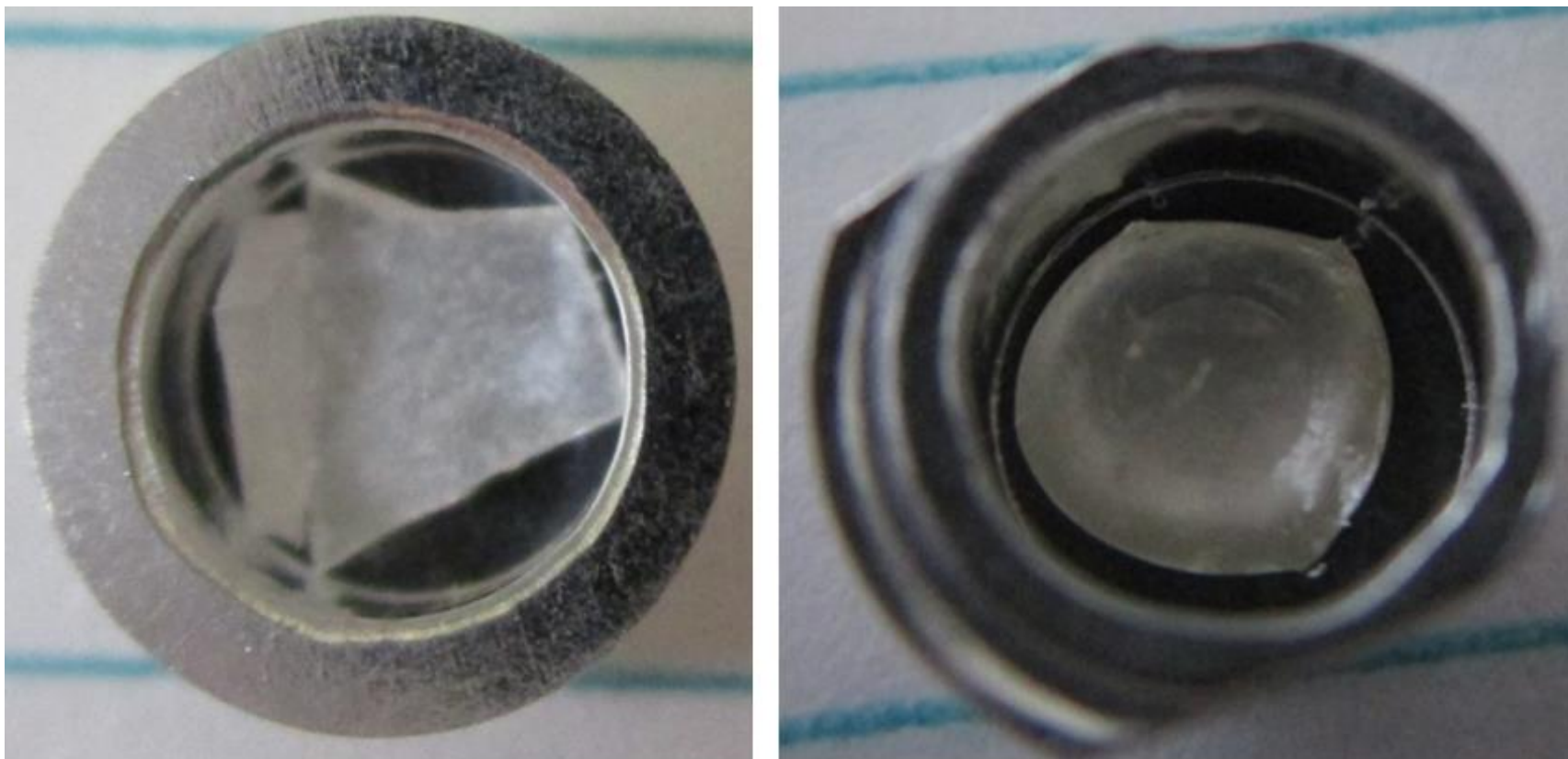


Figure 95. Photographs of Sample 9C, after originally being put into the DSC pan (left) and after testing when the lid was removed (right). This sample has a floor-based shape.

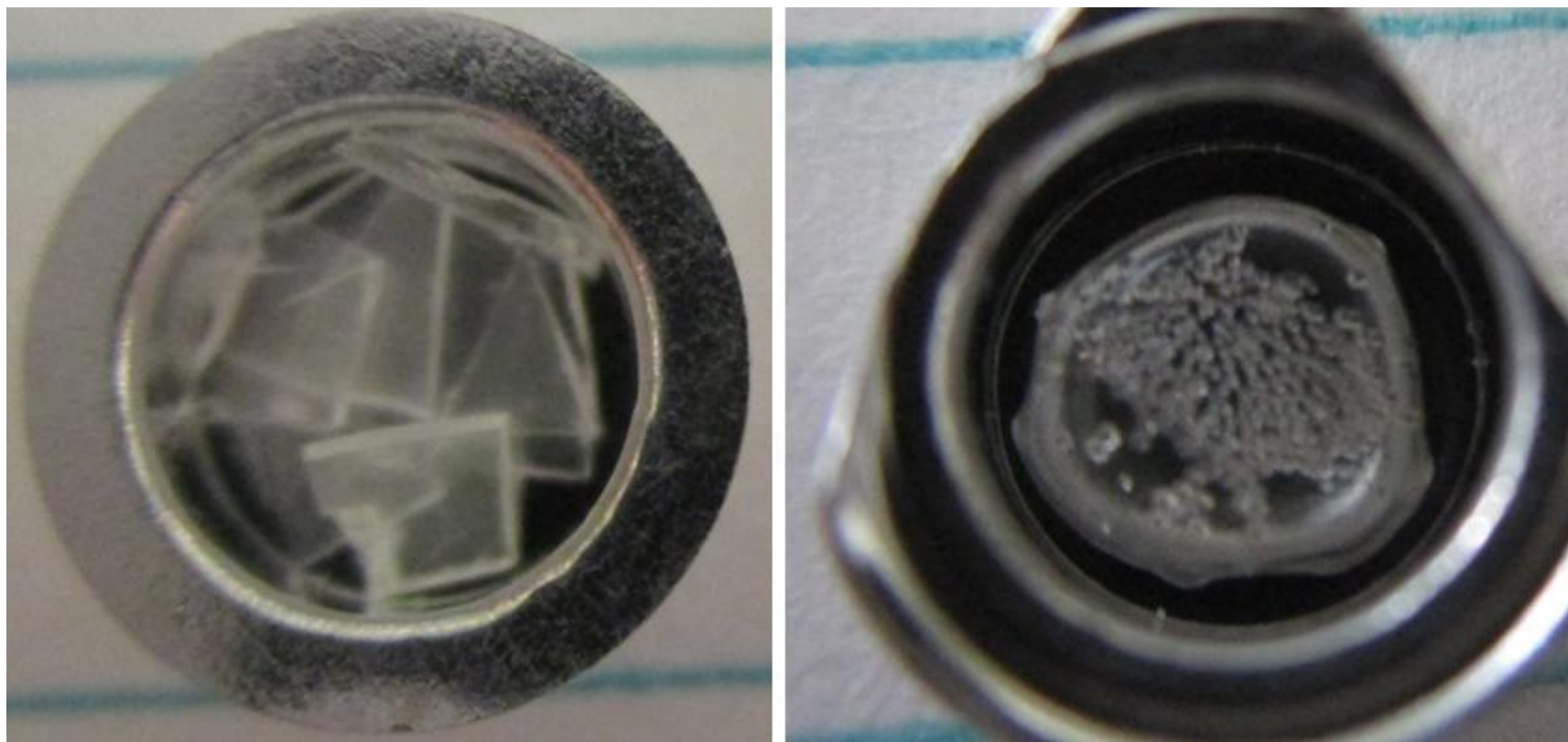


Figure 96. Photographs of Sample 10C, after originally being put into the DSC pan (left) and after testing when the lid was removed (right). This sample has a floor-based shape.

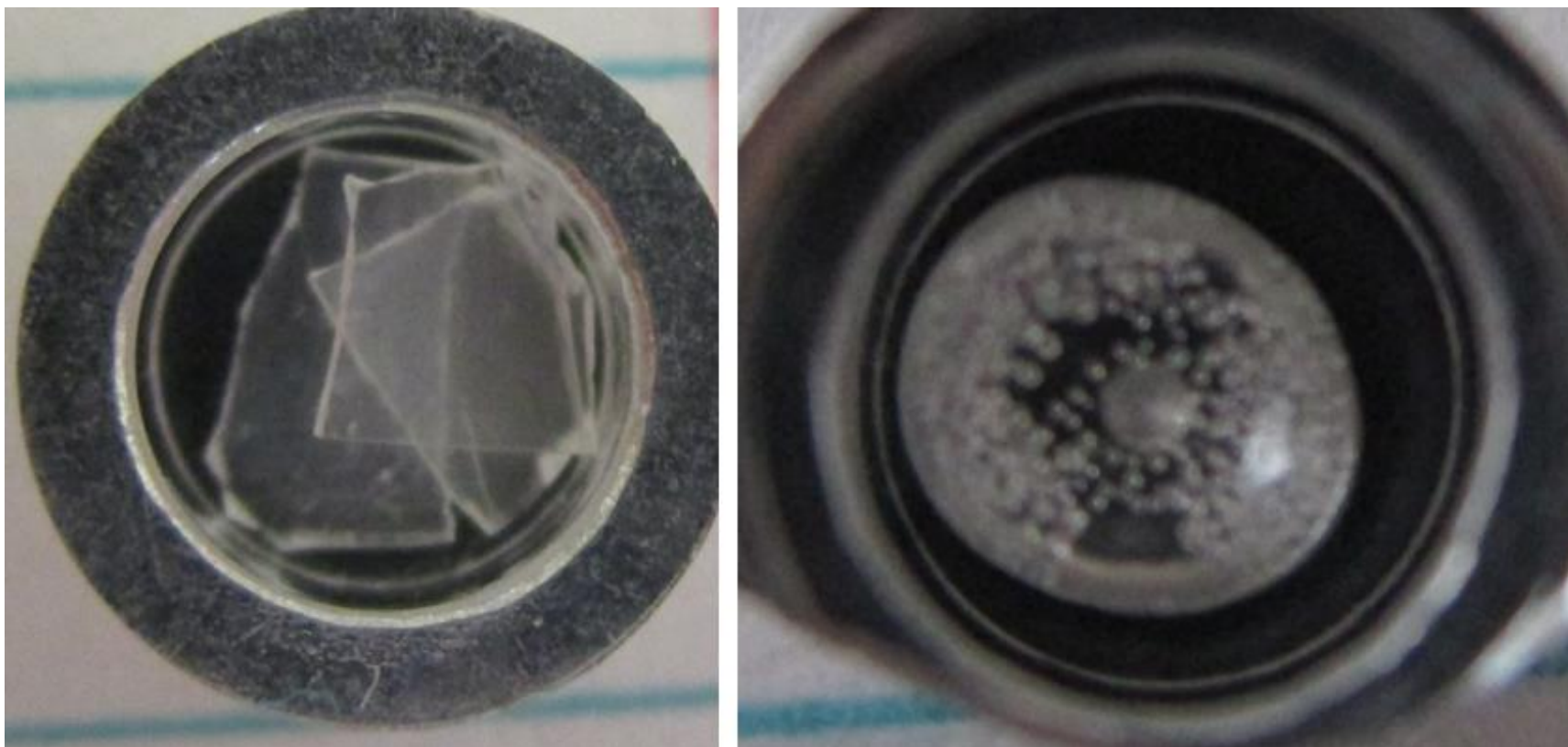


Figure 97. Photographs of Sample 11C, after originally being put into the DSC pan (left) and after testing when the lid was removed (right). This sample has a floor-based shape.



Figure 98. Photographs of Sample 12C, after originally being put into the DSC pan (left) and after testing when the lid was removed (right). This sample has a floor-based shape.



Figure 99. Photographs of Sample 13C, after originally being put into the DSC pan (left top), after testing before the lid was removed – a dent is seen (left bottom), after the lid was removed (center), and after pressing in the roof of the structure to reveal the hollowness inside (right). This sample has a multi-compartment capsule shape.

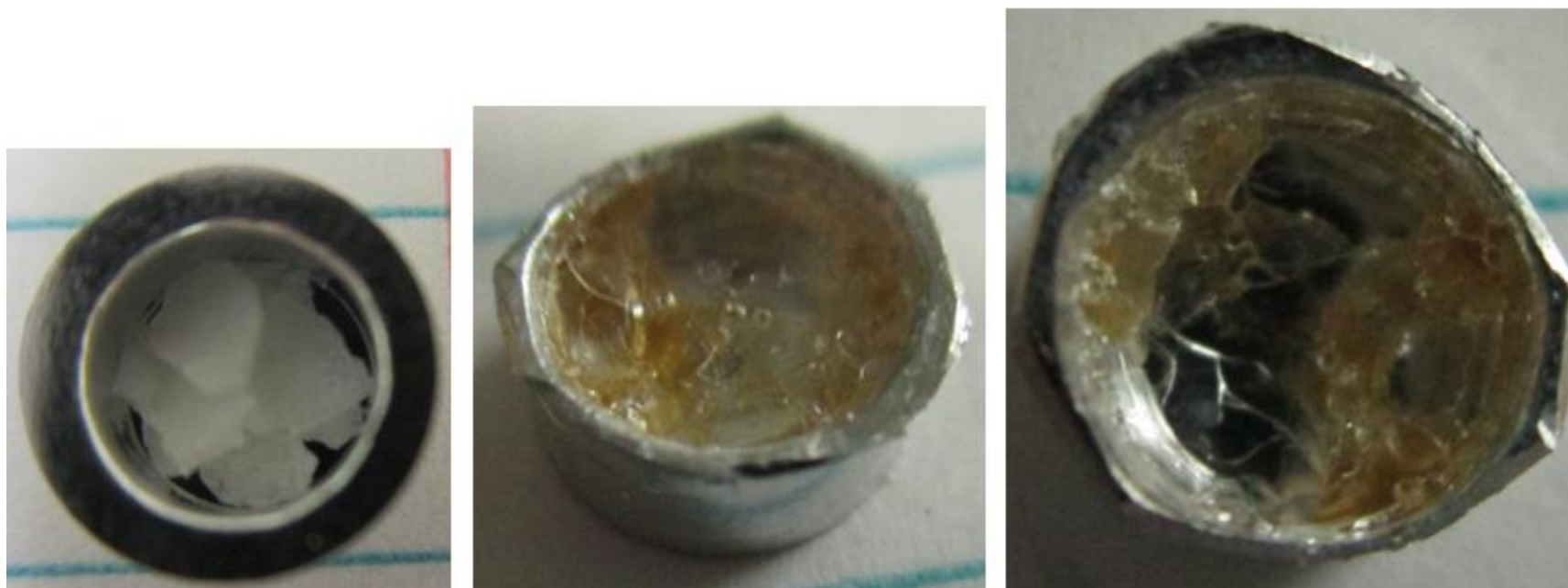


Figure 100. Photographs of Sample 14C, after originally being put into the DSC pan (left), after testing when the lid was removed (center), and after pressing in the roof of the structure to reveal the hollowness inside (right). This sample exhibits yellowing and a multi-compartment capsule shape.



Figure 101. Photographs of Sample 15C, after originally being put into the DSC pan (left), after testing when the lid was removed (center), and after pressing in the roof of the structure to reveal the hollowness inside (right). This sample exhibits yellowing and a multi-compartment capsule shape.



Figure 102. Photographs of Sample 16C, after originally being put into the DSC pan (left), after testing when the lid was removed (center), and after pressing in the roof of the structure to reveal the hollowness inside (right). This sample has a single compartment capsule shape.



Figure 103. Photographs of Sample 17C, after originally being put into the DSC pan (left), after testing when the lid was removed (center), and after pressing in the roof of the structure to reveal the hollowness inside (right). This sample has a multi-compartment capsule shape.



Figure 104. Photographs of Sample 18C, after originally being put into the DSC pan (left), after testing when the lid was removed (center), and after pressing in the roof of the structure to reveal the hollowness inside (right). This sample has a multi-compartment capsule shape.



Figure 105. Photographs of Sample 19C, after originally being put into the DSC pan (left) and after testing when the lid was removed (right). This sample exhibits slight yellowing and a floor-based shape.



Figure 106. Photographs of Sample 20C, after originally being put into the DSC pan (left) and after testing when the lid was removed (right). This sample exhibits slight yellowing and a floor-based shape.



Figure 107. Photographs of Sample 21C, after originally being put into the DSC pan (left) and after testing when the lid was removed (right). This sample exhibits yellowing and a floor-based shape.



Figure 108. Photographs of Sample 22C, after originally being put into the DSC pan (left) and after testing when the lid was removed (right). This sample has a floor-based shape.



Figure 109. Photographs of Sample 23C, after originally being put into the DSC pan (left) and after testing when the lid was removed (right). This sample has a floor-based shape.



Figure 110. Photographs of Sample 24C, after originally being put into the DSC pan (left) and after testing when the lid was removed (right). This sample has a floor-based shape.

Curriculum Vitae

Name: Elena Mamychева

Post-secondary Education and Degrees: University of Western Ontario
London, Ontario, Canada
2010-2014 B.Sc. (Double Major in Physiology & Psychology)

University of Western Ontario
London, Ontario, Canada
2014-2015 General studies

University of Western Ontario
London, Ontario, Canada
2015-2018 M.E.Sc.

Honours and Awards: Western Scholarship of Excellence
2010

Western Scholars Scholarship
2012

Dean's Honour List
2011-2015

Best TA Award
Winter 2018

Related Work Experience Research Assistant (Work Study Program)
University of Western Ontario
2014-2015

Teaching Assistant
University of Western Ontario
2015-2018